MVMA TWO-DIMENSIONAL CRASH VICTIM SIMULATION, VERSION 6

VOLUME 1

The Analytical Model

B. M. Bowman, Research Scientist
R. O. Bennett, Senior Research Associate

Transportation Research Institute
The University of Michigan
2901 Baxter Road
Ann Arbor, Michigan 48109-2150

June 30, 1988

1. Report No.	2. Government Accession No.	3. Recipient's Catalog No.
UMTRI-88-23		

4. Title and Subtitle	5. Report Date
MVMA Two-Dimensional Crash Victim Simulation Version 6. Volume 1.	June 30, 1988
	6. Performing Organization Code

7. Author's)	8. Performing Organization Report No.
B. M. Bowman and R. O. Bennett	UMTRI-88-23

9. Performing Organization Name and Address	10. Work Unit No. (TRAIS)
Transportation Research Institute University of Michigan Huron Parkway and Baxter Road Ann Arbor, Michigan 48109-2150	302743
	11. Contract or Grant No.

12. Sponsoring Agency Name and Address	13. Type of Report and Period Covered
Motor Vehicle Manufacturers Association 320 New Center Building Detroit, Michigan 48202	Final Report
	14. Sponsoring Agency Code

15. Supplementary Notes This report is an update of the report released June 28, 1985, titled "MVMA Two-Dimensional Crash Victim Simulation, Version 5." This report is for Version 6.

16. Abstract

Volume One is intended primarily for the analyst who is interested in the theoretical bases of the MVMA Two-Dimensional Crash Victim Simulation.

This volume contains the detailed formulation of the equations of planar motion of a vehicle occupant in a crash environment. The features of the analytical model include: 1) an eight-mass, fourteen-degree-of-freedom representation of the human body; 2) an extensible multi-joint neck and a flexible shoulder joint; 3) simulation of biodynamic muscle contraction as a time-dependent phenomenon; 4) the modeling of contact between the occupant and the vehicle by means of contact sensing ellipses and lines attached to the body and to the vehicle interior or exterior; 5) non-body links that can be referenced to the occupant links, the vehicle or the inertial frame; 6) specification of material properties for all lines and ellipses in terms of general force-deformation relationships; 7) an airbag model which predicts forces on the occupant by solution of the equations of gas thermodynamics; 8) a three-dimensional belt restraint submodel with up to seven straps (including snorkel), two slip points, belt slip friction, and spoolout; 9) tabular three-degree-of-freedom vehicle accelerations; 10) many features that simplify application in engineering design studies.

Volume Two presents a detailed description of the input data quantities required by the computer model and the normal output produced. Volume Three provides detailed information relating to program design and implementation.

17. Key Words	18. Distribution Statement
Automotive Safety Crash Dynamics Occupant Dynamics Restraint Systems Whole-Body Response	UNLIMITED

19. Security Classif. (of this report)	20. Security Classif. (of this page)	21. No. of Pages
UNCLASSIFIED	UNCLASSIFIED	210 (p. 1 - p. 214.11)

TABLE OF CONTENTS

4/3/87

VOLUME 2   Page

6/30/88

LIST OF FIGURES

LIST OF FIGURES (continued)

Page

viii

LIST OF FIGURES (continued)

Page

LIST OF FIGURES (continued)

Page

LIST OF FIGURES (continued)

LIST OF TABLES

LIST OF TABLES (continued)

Page

Page

Acknowledgements

PART 1. INTRODUCTION TO THE MVMA 2-D CRASH
VICTIM SIMULATION

Since 1966, sophisticated analyses have been developed which can
be used for estimating the dynamic response of a human or an anthro-
pomorphic dummy in a crash environment. The use of such mathematical
models as tools in automotive safety design has been made possible
by modern large-storage, high-speed computers.

The problem of determining occupant dynamics in a crash environ-
ment can be simply stated. A description of a mechanical or bio-
mechanical system, the occupant, is given. A description of a poten-
tially interacting mechanical system, the occupant compartment, is
given. The occupant's position and orientation and their rates of change
are specified for some single instant in time. And finally, the motion
in space of the occupant compartment as a function of time is specified.
It is required to determine the subsequent motion of the occupant and
the forces which describe his interaction with the vehicle interior.

Figure 1 illustrates the relationship between the motion and the
forces. From the initial position and velocity conditions of the occu-
pant relative to a vehicle-fixed reference frame, the instantaneous state
of displacements between body and vehicle elements, and hence the inter-
action forces, may be determined. Further, the instantaneous interaction
forces thus found, together with the motion equations of classical
mechanics, namely Newton's Laws, determine the instantaneous accelera-
tions essentially as $a = F/m$, or $\{a\} = [M]^{-1} \{F\}$ in a vector formulation.
Integration of the accelerations then yields the occupant velocities and
positions at a new time, different from the time at which forces were
determined by an arbitrarily small amount, dt or Δt. New position and

1

velocity conditions having been determined, new deflections can be determined and so forth so that the entire time histories for motion and forces are established. This flow sequence is an appropriate description for all mathematical models which could be used for determining occupant dynamics.

$t = 0$

```
        ┌────────────────────┐
        │  POSITIONS AND     │
        │  VELOCITIES (OF    │     (1)
        │  OCCUPANT AND      │
        │  VEHICLE)          │
        └────────────────────┘
                  │  Geometry
                  ▼
        ┌────────────────────┐
        │   DEFLECTIONS      │     (2)
        └────────────────────┘
                  │  Load-deflection
                  │  properties of
                  │  deformed elements
                  ▼
        ┌────────────────────┐
        │   INTERACTION      │
        │   FORCES           │     (3)
        └────────────────────┘
                  │  Newton's Laws
                  │  (differential equations
                  │  of motion)
                  ▼
        ┌────────────────────┐
        │  ACCELERATIONS     │
        │                    │     (4)
        │  {a} = [M]⁻¹ {F}  │
        └────────────────────┘
```

Integration to $t + \Delta t$

Geometry

Load-deflection properties of deformed elements

Newton's Laws (differential equations of motion)

$$\{a\} = [M]^{-1} \{F\}$$
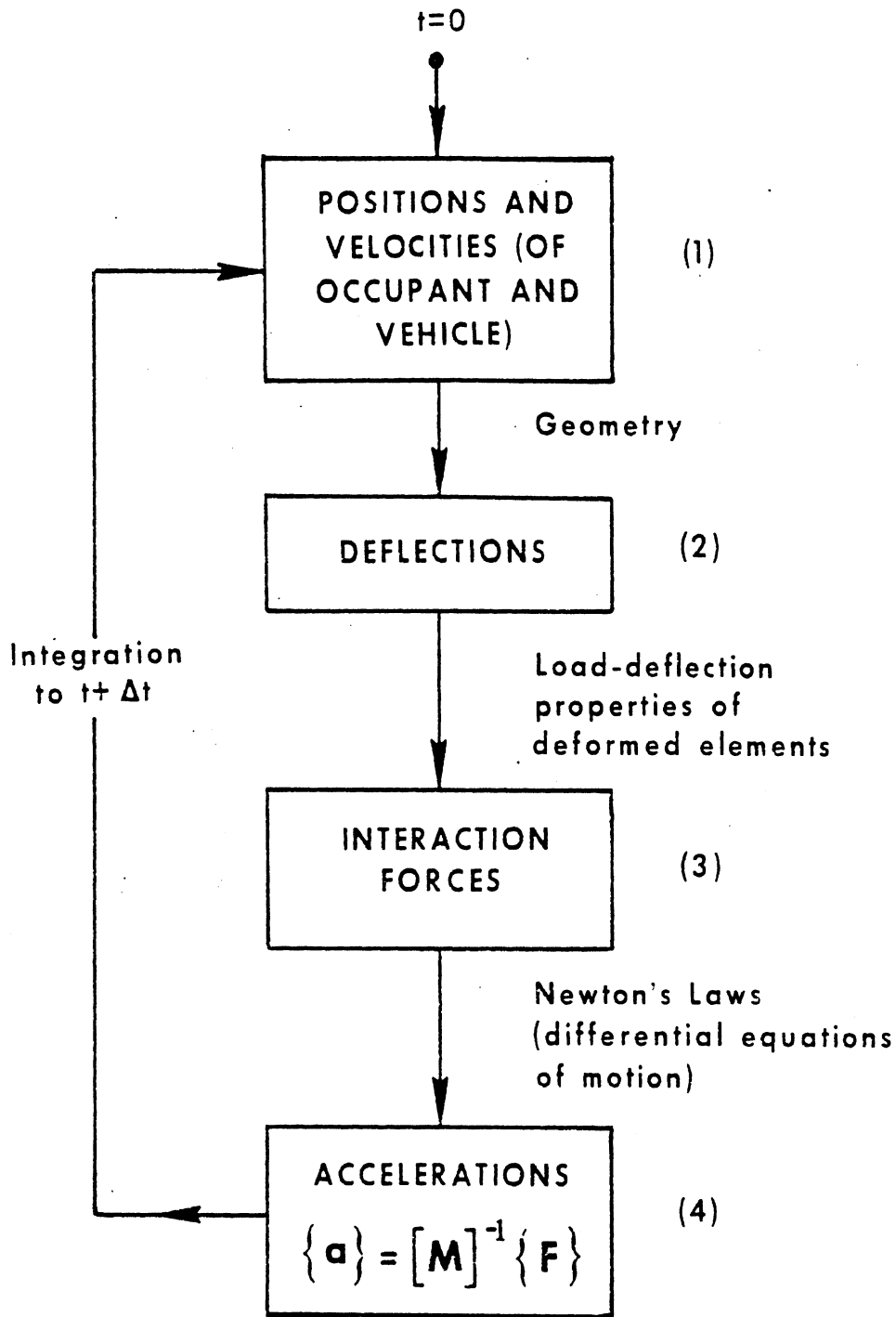
FIGURE 1   Relationship of Position Conditions and Interaction Forces
Within the Framework of an Initial Value Problem

3

The MVMA Two-Dimensional Crash Victim Simulator (Version 1) came into being in 1973 [1]. This model was developed by the Highway Safety Research Institute (HSRI)--now UMTRI-- and was an extension of the MODROS model, released in 1972 by General Motors [2]. The predecessors of MODROS, in turn, were ROS (1971) [3] and Cal 2-D (1966) [4], released by the then Cornell Aeronautical Labs.

Since 1973, the MVMA 2-D model has undergone continuing development at UMTRI. The current release of the computer model (June 1988) is over 42,000 Fortran lines in length and eight times as long as the immediate predecessor of the MVMA 2-D model, MODROS. Versions 2 and 3 were released in January and June of 1974 [5,6], and since 1974 there have been computer tape releases representing several additional stages of model development.

In addition, a "Validation Command Language" program was completed and released in December 1976 [7]. This program performs many post-processing operations on MVMA 2-D generated data and was developed to aid the automotive safety researcher in quantifying comparisons between impact test results and predictions of mathematical simulations.

In April 1977, HSRI released a Tutorial System for the MVMA 2-D model [8]. This consists of a 397-page Self-Study Guide and a 298-page Audio-Visual Program with two hundred 35mm slides and nearly five hours of narration on tape cassettes. The Tutorial System Self-Study Guide is the most detailed document available for aiding the model user in preparation of input data sets.

In 1979 Version 4 of the MVMA 2-D model was released. For various reasons Version 3 continued to be used, however, and Version 4 was not put into use. Nonetheless, this three-volume report still reflects the

1979 update to Version 4 of the 1974 Version 3 documentation.

Material relating to Version 4 in the documentation (mostly in Volume 3) can be ignored. Differences between Version 3 and Version 4 were primarily in program layout and were transparent to the user. Material in Volume 3 (the "programmer's manual") relating to Version 4 should not be confusing since -- with respect to program layout -- Versions 3, 5, and 6 are "subsets" of Version 4.*

Several releases of Version 3 were made from 1979 to 1984. Major modifications to Version 3 in 1985 led to releases of a new version , Version 5, in 1985 and 1986. Versions 5.1, 5.2, 5.3, and 5.4 were released in 1987 and 1988. More recent work has led to the current release, MVMA 2-D CVS, Version 6.** To the user the differences between Version 5 and Version 6 will be transparent except for the many new features in Version 6. Even beyond the new features, however, Version 6 represents a major updating of the model since Version 6 code is ANSI standard Fortran 77 as opposed to the Fortran IV (66) code of all earlier versions of MVMA 2-D CVS. This means that the model can now be installed on almost all computers of sufficient size and run easily with almost any operating system.

The MVMA Two-Dimensional Crash Victim Simulator is a model intended to be used for simulating crash events in which primary occupant motions may be expected to lie in a plane. Thus, it is most useful for simulating front-end and rear-end impacts. With care, however, it can be used for some oblique and side impacts as well. Applications have include simulating anthropomorphic dummy drops onto a hard surface and human fall victims striking yielding and unyielding surfaces. They have included simulating pedestrians struck by a vehicle. Simulations have been made of laboratory tests in which lateral neck response of human subjects was

measured when the head was jerked to the side by a falling weight. The
model has been used to simulate head/neck dynamics of volunteer subjects
in impact sled tests. But use of the MVMA 2-D model need not be restricted
to simulating human or human-analog systems. Diverse applications are pos-
sible if the user is imaginative in utilizing the many features of the
model.

_____

*   A brief description of Version 4 is given here for completeness. The
primary difference between Version 3 and 4 was an extensive reorganization
of the computer model, documented in Volume 3. Version 4 examined the
input data set as a first step and was then able, through automatic gene-
ration of supplementary subroutines, to:

1) assign minimum storage space necessary for the simulation, and

2) make unnecessary the "loading", or "link-editing", of program

     routines which will not be referenced.

Version 5 and Version 6 accomplish the first of these functions for
Output Processor storage (only) through an Output Pre-Processor.

**   See Section 3.2-A.1 for a description of the current release, Version 6.0.

6/30/88

PART 2. ANALYSIS

Following definition of the coordinate systems describing occupant position, the formulation of the equations of motion using Lagrangian techniques is detailed. The addition of forces to the equations of motion is described in general supplemented by specific analyses for vehicle-occupant contact, gravity, joints, and restraint systems.

2.1 COORDINATE SYSTEMS AND GEOMETRY

The basic approach used to describe the crash dynamics has been to define two independent dynamical systems, the occupant and the vehicle, relative to an inertial reference and then to determine the interaction of the systems with appropriate coordinate transformations. In this manner, the position and orientation of the occupant are determined by the inertial coordinates X_2, Z_2, θ_i, $i = 1,2,3, \ldots, 9$ ($\theta_9 = \theta_{neck} = \theta_n$) and the relative coordinates X_s, Z_s, L_n, as shown in Figures 2, 3, and 6. A local coordinate system is fixed to each occupant body segment with the origin coincident with the center of mass of the segment. This is illustrated in Figure 4, which shows, as an example, the positioning of a "foot ellipse" with respect to the coordinate frame fixed to the lower leg. The vehicle position is specified by the inertial coordinates X_v, Z_v, and θ_v as illustrated in Figure 5. The axis system $i_v - k_v$ is assumed to be fixed at any arbitrary point in the vehicle. Belt anchor points are defined relative to this vehicle-fixed axis system. Force-generating contact surfaces may be attached either to the vehicle reference frame or to the inertial frame.

In addition to the nine-segment occupant linkage, an arbitrary number of unlinked, user specified mass elements may be modeled. These elements have various uses (see Section 2.10). Each adds three degrees of freedom to the total system.
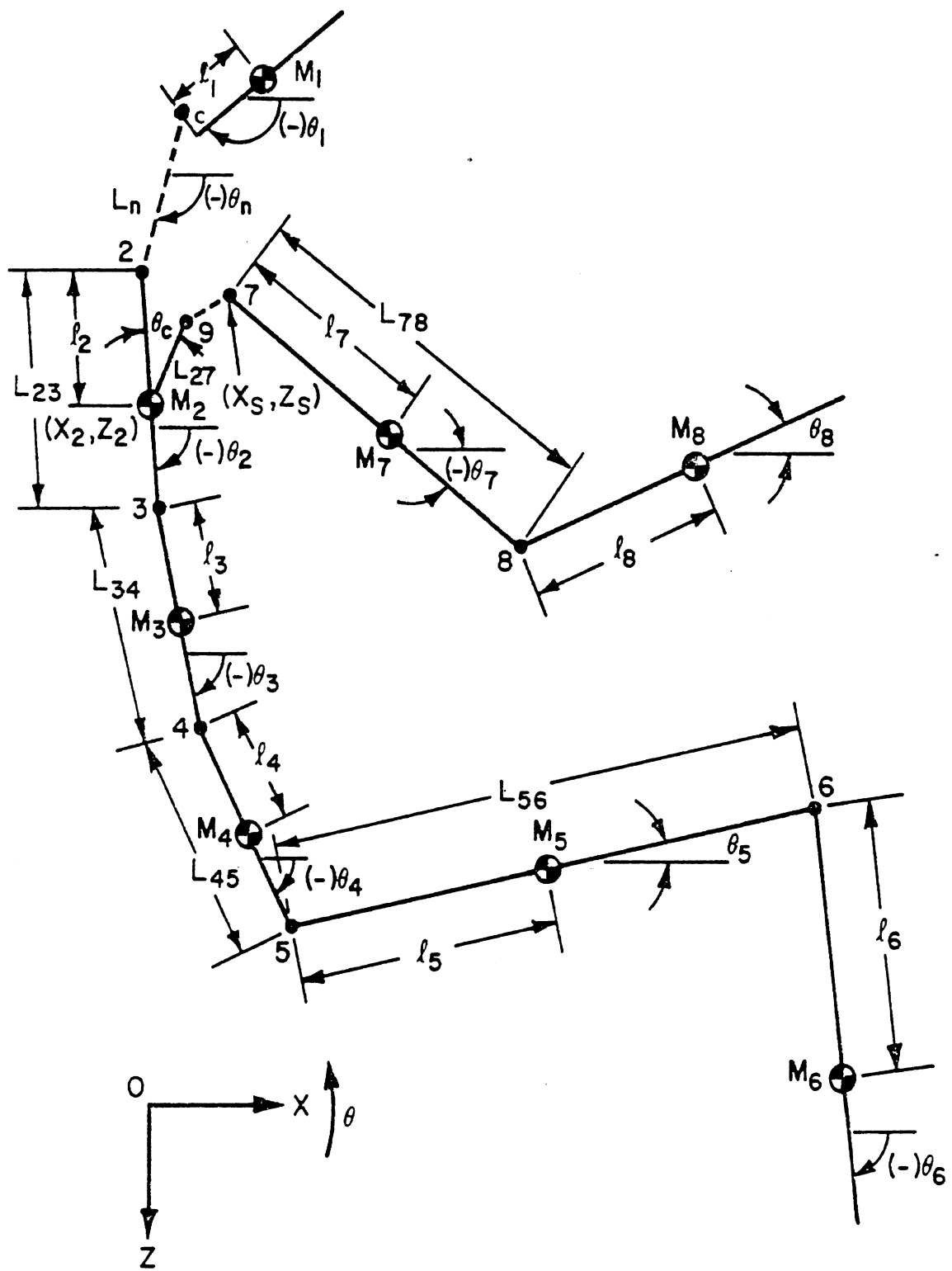
FIGURE 2. Articulated Body Schematic
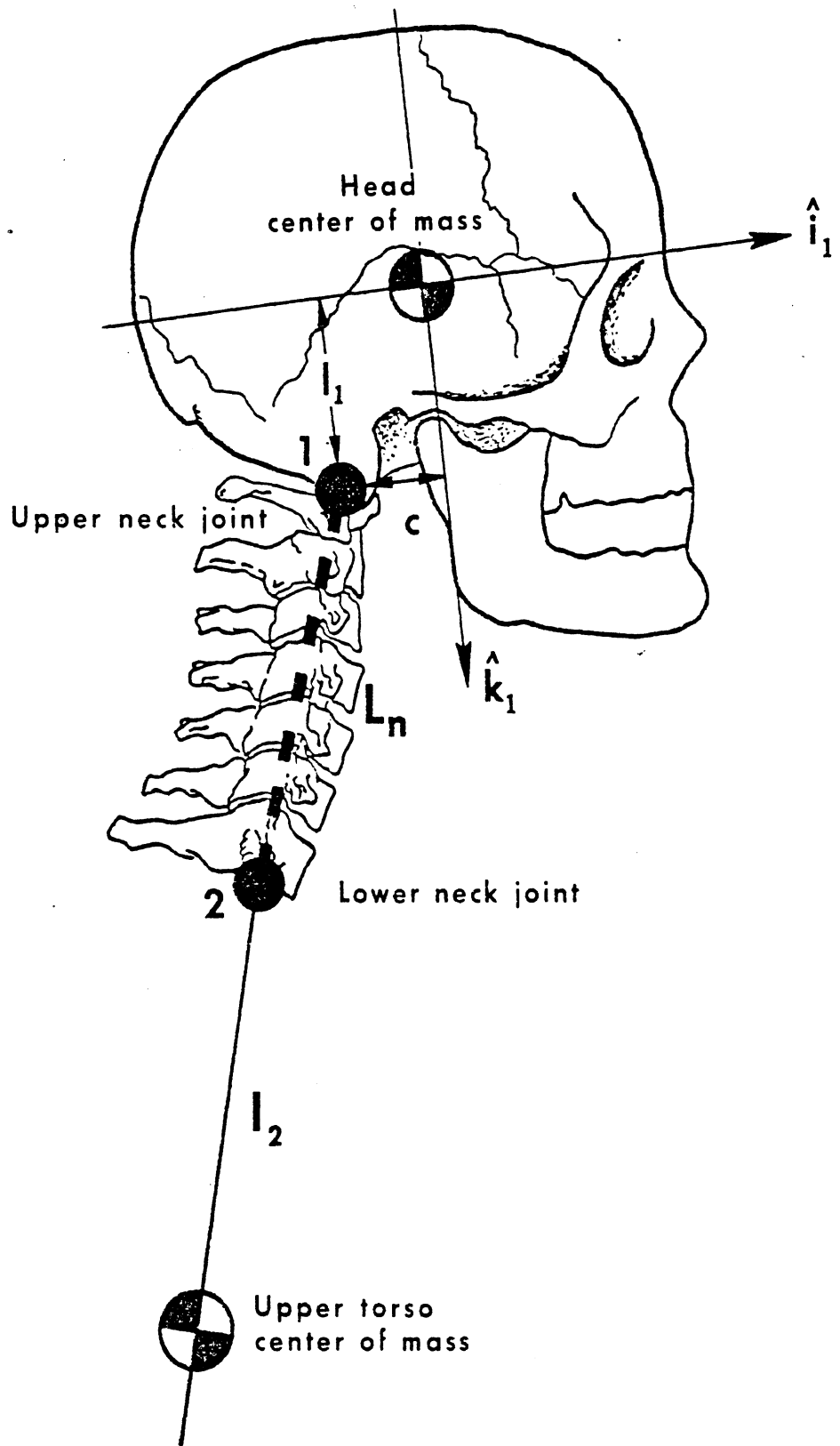
FIGURE 3   MVMA-2D extensible neck geometry

Head　Upper　Middle　Lower　Upper
　　　　torso　torso　torso　legs

x
θ

Upper　　Lower　　　Lower
arms　　arms　　　legs

-z

Anterior

CG
　　　　x
Superior ────●─── Inferior

z

Posterior

semi-axis 2

semi-axis 1
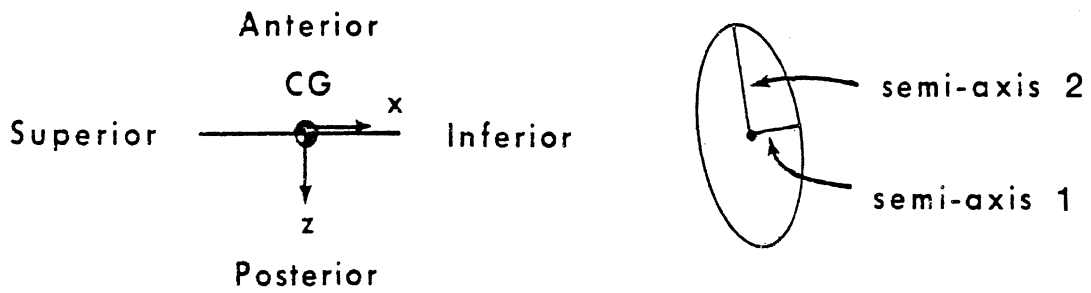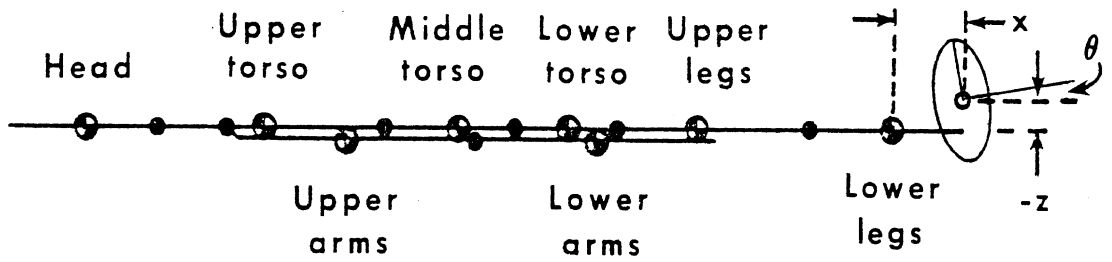
Example for a 'foot' ellipse

FIGURE 4　Body Link Coordinate Systems

　　　6/28/85
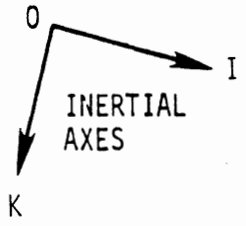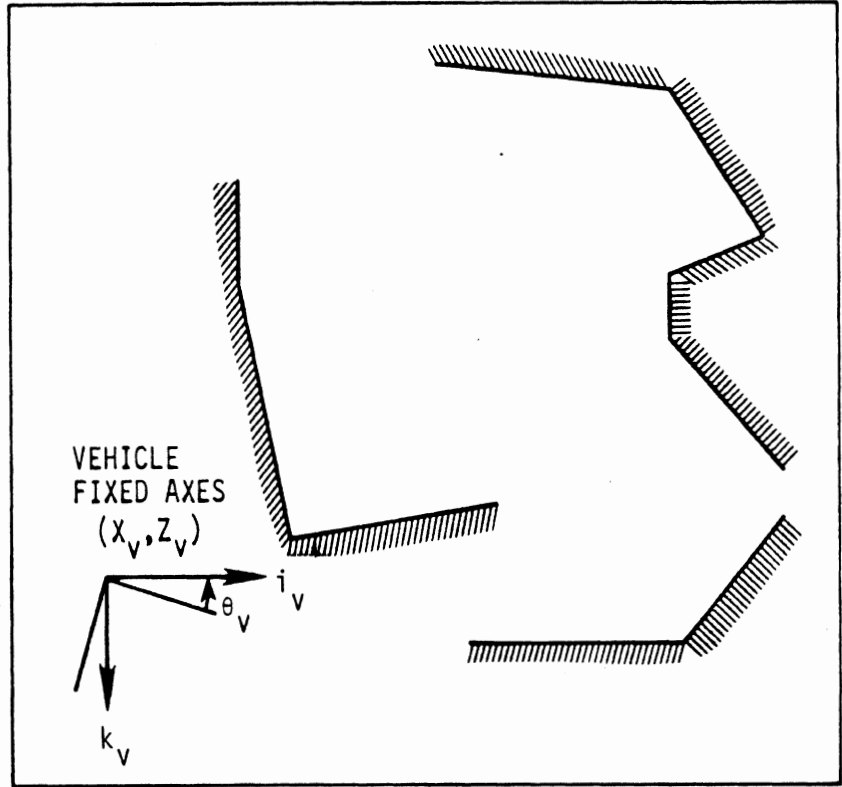
FIGURE 5.   Space and Vehicle Fixed Coordinate Systems

Lower neck joint
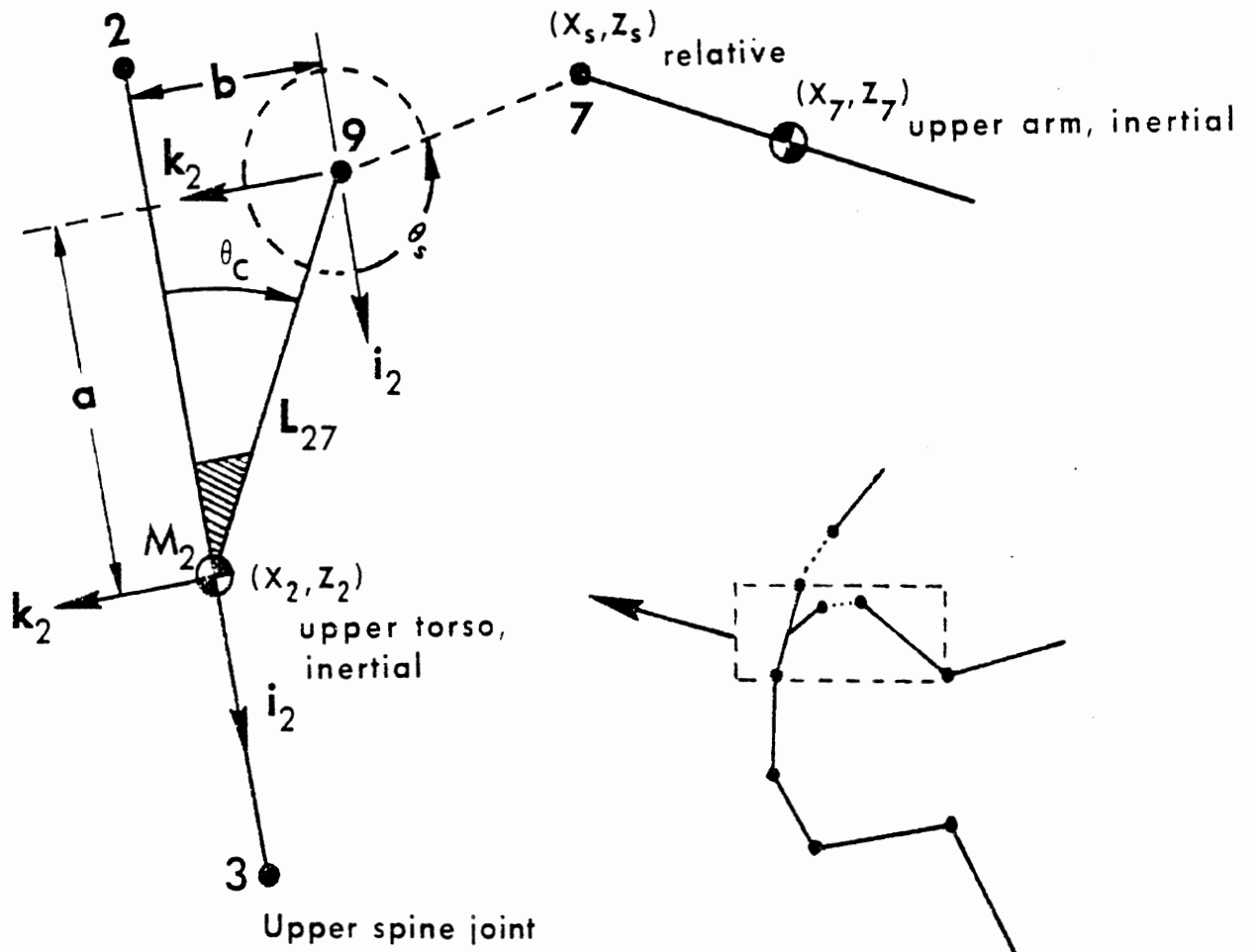
$$\vec{\ell}_{9\to7} = x_s i_2 + z_s k_2$$

$$\theta_C = \text{constant}$$

$$L_{27} = \text{constant}$$

FIGURE 6   Shoulder Joint

12

The positions of the occupant's joints relative to the inertial frame are:

$$\left\{\begin{array}{c} X_2^J \\ Z_2^J \end{array}\right\} = \left\{\begin{array}{c} X_2 \\ Z_2 \end{array}\right\} - \left[\begin{array}{cc} \cos\theta_2 & \sin\theta_2 \\ -\sin\theta_2 & \cos\theta_2 \end{array}\right] \left\{\begin{array}{c} \ell_2 \\ 0 \end{array}\right\}$$

$$\left\{\begin{array}{c} X_1^J \\ Z_1^J \end{array}\right\} = \left\{\begin{array}{c} X_2^J \\ Z_2^J \end{array}\right\} - \left[\begin{array}{cc} \cos\theta_n & \sin\theta_n \\ -\sin\theta_n & \cos\theta_n \end{array}\right] \left\{\begin{array}{c} L_n \\ 0 \end{array}\right\}$$

$$\left\{\begin{array}{c} X_9^J \\ Z_9^J \end{array}\right\} = \left\{\begin{array}{c} X_2 \\ Z_2 \end{array}\right\} - \left[\begin{array}{cc} \cos(\theta_2-\theta_c) & \sin(\theta_2-\theta_c) \\ -\sin(\theta_2-\theta_c) & \cos(\theta_2-\theta_c) \end{array}\right] \left\{\begin{array}{c} L_{27} \\ 0 \end{array}\right\}$$

(1)

$$\left\{\begin{array}{c} X_7^J \\ Z_7^J \end{array}\right\} = \left\{\begin{array}{c} X_9^J \\ Z_9^J \end{array}\right\} + \left[\begin{array}{cc} \cos\theta_2 & \sin\theta_2 \\ -\sin\theta_2 & \cos\theta_2 \end{array}\right] \left\{\begin{array}{c} X_s \\ Z_s \end{array}\right\}$$

$$\left\{\begin{array}{c} X_i^J \\ Z_i^J \end{array}\right\} = \left\{\begin{array}{c} X_{i-1}^J \\ Z_{i-1}^J \end{array}\right\} + \left[\begin{array}{cc} \cos\theta_{i-1} & \sin\theta_{i-1} \\ -\sin\theta_{i-1} & \cos\theta_{i-1} \end{array}\right] \left\{\begin{array}{c} L_{i-1,i} \\ 0 \end{array}\right\},$$

$$i = 3, 4, 5, 6, 8$$

where $L_{i-1,i}$ is the interjoint distance between joints i-1 and i.

The joint velocities in the inertial frame are easily determined from equations (1), where the generalized coordinates X_2, Z_2, θ_1, ... θ_8, θ_n, L_n X_s, and Z_s are time dependent and the quantities ℓ_i, L_{jk}, and θ_c are constants.

The shoulder parameters L_{27} and θ_c are found in terms of the inputted quantities $a = $ ASH and $b = $ BSH (Card 201) as

$$L_{27} = \sqrt{a^2 + b^2}$$

$$\theta_c = \tan^{-1}\frac{b}{a}, \quad L_{27} \neq 0.$$

(2)

The coordinates a and b fix the shoulder joint attachment point on the upper torso. They are defined in the description of input data for the 201-card and illustrated in Figure 6. The point (a,b) serves both as the center of a stop circle for shoulder element stretching and as an equilibrium point to which the shoulder joint (point 7 in Figure 6) tends to return. The stop circle can be thought of as the base of the three-dimensional excursion cone, or "joint sinus," swept out by the clavicle at extreme angulation. (See Reference 9).

The positions, velocities, and accelerations of the centers of mass of the segments relative to inertial space are easily written down:

$$X_1 = X_2 - \ell_2 \cos\theta_2 - L_n \cos\theta_n - \ell_1 \cos\theta_1 - c \sin\theta_1$$

$$Z_1 = Z_2 + \ell_2 \sin\theta_2 + L_n \sin\theta_n + \ell_1 \sin\theta_1 - c \cos\theta_1$$

$$X_2 = X_2$$

$$Z_2 = Z_2$$

$$X_3 = X_2 + (L_{23} - \ell_2)\cos\theta_2 + \ell_3 \cos\theta_3$$

$$Z_3 = Z_2 - (L_{23} - \ell_2)\sin\theta_2 - \ell_3 \sin\theta_3$$

$$X_4 = X_2 + (L_{23} - \ell_2)\cos\theta_2 + L_{34} \cos\theta_3 + \ell_4 \cos\theta_4$$

$$Z_4 = Z_2 - (L_{23} - \ell_2)\sin\theta_2 - L_{34} \sin\theta_3 - \ell_4 \sin\theta_4$$

$$X_5 = X_2 + (L_{23} - \ell_2)\cos\theta_2 + L_{34} \cos\theta_3 + L_{45} \cos\theta_4 + \ell_5 \cos\theta_5$$

$$Z_5 = Z_2 - (L_{23} - \ell_2)\sin\theta_2 - L_{34} \sin\theta_3 - L_{45} \sin\theta_4 - \ell_5 \sin\theta_5$$

(3)

14

$$X_6 = X_2 + (L_{23} - \ell_2)\cos\theta_2 + L_{34}\cos\theta_3 + L_{45}\cos\theta_4 + L_{56}\cos\theta_5 + \ell_6\cos\theta_6$$

$$z_6 = z_2 - (L_{23} - \ell_2)\sin\theta_2 - L_{34}\sin\theta_3 - L_{45}\sin\theta_4 - L_{56}\sin\theta_5 - \ell_6\sin\theta_6$$

$$X_7 = X_2 - L_{27}\cos(\theta_2 - \theta_c) + \ell_7\cos\theta_7 + X_s\cos\theta_2 + z_s\sin\theta_2$$

$$z_7 = z_2 + L_{27}\sin(\theta_2 - \theta_c) - \ell_7\sin\theta_7 - X_s\sin\theta_2 + z_s\cos\theta_2$$

$$X_8 = X_2 - L_{27}\cos(\theta_2 - \theta_c) + L_{78}\cos\theta_7 + \ell_8\cos\theta_8 + X_s\cos\theta_2 + z_s\sin\theta_2$$

$$z_8 = z_2 + L_{27}\sin(\theta_2 - \theta_c) - L_{78}\sin\theta_7 - \ell_8\sin\theta_8 - X_s\sin\theta_2 + z_s\cos\theta_2$$

$$\dot{X}_1 = \dot{X}_2 + \ell_2\dot{\theta}_2\sin\theta_2 + L_m\dot{\theta}_m\sin\theta_m + \ell_1\dot{\theta}_1\sin\theta_1 - \dot{L}_m\cos\theta_m - c\dot{\theta}_1\cos\theta_1$$

$$\dot{z}_1 = \dot{z}_2 + \ell_2\dot{\theta}_2\cos\theta_2 + L_m\dot{\theta}_m\cos\theta_m + \ell_1\dot{\theta}_1\cos\theta_1 + \dot{L}_m\sin\theta_m + c\dot{\theta}_1\sin\theta_1$$

$$\dot{X}_2 = \dot{X}_2$$

$$\dot{z}_2 = \dot{z}_2$$

$$\dot{X}_3 = \dot{X}_2 - (L_{23} - \ell_2)\dot{\theta}_2\sin\theta_2 - \ell_3\dot{\theta}_3\sin\theta_3$$

$$\dot{z}_3 = \dot{z}_2 - (L_{23} - \ell_2)\dot{\theta}_2\cos\theta_2 - \ell_3\dot{\theta}_3\cos\theta_3$$

$$\dot{X}_4 = \dot{X}_2 - (L_{23} - \ell_2)\dot{\theta}_2\sin\theta_2 - L_{34}\dot{\theta}_3\sin\theta_3 - \ell_4\dot{\theta}_4\sin\theta_4$$

$$\dot{z}_4 = \dot{z}_2 - (L_{23} - \ell_2)\dot{\theta}_2\cos\theta_2 - L_{34}\dot{\theta}_3\cos\theta_3 - \ell_4\dot{\theta}_4\cos\theta_4$$

$$\dot{X}_5 = \dot{X}_2 - (L_{23} - \ell_2)\dot{\theta}_2\sin\theta_2 - L_{34}\dot{\theta}_3\sin\theta_3 - L_{45}\dot{\theta}_4\sin\theta_4 - \ell_5\dot{\theta}_5\sin\theta_5$$

$$\dot{z}_5 = \dot{z}_2 - (L_{23} - \ell_2)\dot{\theta}_2\cos\theta_2 - L_{34}\dot{\theta}_3\cos\theta_3 - L_{45}\dot{\theta}_4\cos\theta_4 - \ell_5\dot{\theta}_5\cos\theta_5$$

$$\dot{X}_6 = \dot{X}_2 - (L_{23} - \ell_2)\dot{\theta}_2\sin\theta_2 - L_{34}\dot{\theta}_3\sin\theta_3 - L_{45}\dot{\theta}_4\sin\theta_4$$
$$\qquad - L_{56}\dot{\theta}_5\sin\theta_5 - \ell_6\dot{\theta}_6\sin\theta_6$$

$$\dot{z}_6 = \dot{z}_2 - (L_{23} - \ell_2)\dot{\theta}_2\cos\theta_2 - L_{34}\dot{\theta}_3\cos\theta_3 - L_{45}\dot{\theta}_4\cos\theta_4 \qquad (4)$$
$$\qquad - L_{56}\dot{\theta}_5\cos\theta_5 - \ell_6\dot{\theta}_6\cos\theta_6$$

$$\dot{X}_7 = \dot{X}_2 + L_{27}\dot{\theta}_2\sin(\theta_2 - \theta_c) + \dot{X}_s\cos\theta_2 + \dot{z}_s\sin\theta_2 - \ell_7\dot{\theta}_7\sin\theta_7$$
$$\qquad - X_s\dot{\theta}_2\sin\theta_2 + z_s\dot{\theta}_2\cos\theta_2$$

$$\dot{z}_7 = \dot{z}_2 + L_{27}\dot{\theta}_2\cos(\theta_2 - \theta_c) - \dot{X}_s\sin\theta_2 + \dot{z}_s\cos\theta_2 - \ell_7\dot{\theta}_7\cos\theta_7$$
$$\qquad - X_s\dot{\theta}_2\cos\theta_2 - z_s\dot{\theta}_2\sin\theta_2$$

$$\dot{X}_8 = \dot{X}_2 + L_{27}\dot{\theta}_2\sin(\theta_2 - \theta_c) + \dot{X}_s\cos\theta_2 + \dot{z}_s\sin\theta_2 - L_{78}\dot{\theta}_7\sin\theta_7$$
$$\qquad - \ell_8\dot{\theta}_8\sin\theta_8 - X_s\dot{\theta}_2\sin\theta_2 + z_s\dot{\theta}_2\cos\theta_2$$

$$\dot{z}_8 = \dot{z}_2 + L_{27}\dot{\theta}_2\cos(\theta_2 - \theta_c) - \dot{X}_s\sin\theta_2 + \dot{z}_s\cos\theta_2 - L_{78}\dot{\theta}_7\cos\theta_7$$
$$\qquad - \ell_8\dot{\theta}_8\cos\theta_8 - X_s\dot{\theta}_2\cos\theta_2 - z_s\dot{\theta}_2\sin\theta_2$$

$$\ddot{x}_1 = \ddot{x}_2 + \ell_2\ddot{\theta}_2\sin\theta_2 + L_n\ddot{\theta}_n\sin\theta_n + \ell_1\ddot{\theta}_1\sin\theta_1 - \ddot{L}_n\cos\theta_n - c\ddot{\theta}_1\cos\theta_1$$
$$+ \ell_2\dot{\theta}_2^2\cos\theta_2 + L_n\dot{\theta}_n^2\cos\theta_n + \ell_1\dot{\theta}_1^2\cos\theta_1 + 2\dot{L}_n\dot{\theta}_n\sin\theta_n + c\dot{\theta}_1^2\sin\theta_1$$

$$\ddot{z}_1 = \ddot{z}_2 + \ell_2\ddot{\theta}_2\cos\theta_2 + L_n\ddot{\theta}_n\cos\theta_n + \ell_1\ddot{\theta}_1\cos\theta_1 + \ddot{L}_n\sin\theta_n + c\ddot{\theta}_1\sin\theta_1$$
$$- \ell_2\dot{\theta}_2^2\sin\theta_2 - L_n\dot{\theta}_n^2\sin\theta_n - \ell_1\dot{\theta}_1^2\sin\theta_1 + 2\dot{L}_n\dot{\theta}_n\cos\theta_n + c\dot{\theta}_1^2\cos\theta_1$$

$$\ddot{x}_2 = \ddot{x}_2$$

$$\ddot{z}_2 = \ddot{z}_2$$

$$\ddot{x}_3 = \ddot{x}_2 - (L_{23}-\ell_2)\ddot{\theta}_2\sin\theta_2 - \ell_3\ddot{\theta}_3\sin\theta_3 - (L_{23}-\ell_2)\dot{\theta}_2^2\cos\theta_2 - \ell_3\dot{\theta}_3^2\cos\theta_3$$

$$\ddot{z}_3 = \ddot{z}_2 - (L_{23}-\ell_2)\ddot{\theta}_2\cos\theta_2 - \ell_3\ddot{\theta}_3\cos\theta_3 + (L_{23}-\ell_2)\dot{\theta}_2^2\sin\theta_2 + \ell_3\dot{\theta}_3^2\sin\theta_3$$

$$\ddot{x}_4 = \ddot{x}_2 - (L_{23}-\ell_2)\ddot{\theta}_2\sin\theta_2 - L_{34}\ddot{\theta}_3\sin\theta_3 - \ell_4\ddot{\theta}_4\sin\theta_4$$
$$- (L_{23}-\ell_2)\dot{\theta}_2^2\cos\theta_2 - L_{34}\dot{\theta}_3^2\cos\theta_3 - \ell_4\dot{\theta}_4^2\cos\theta_4$$

$$\ddot{z}_4 = \ddot{z}_2 - (L_{23}-\ell_2)\ddot{\theta}_2\cos\theta_2 - L_{34}\ddot{\theta}_3\cos\theta_3 - \ell_4\ddot{\theta}_4\cos\theta_4 \qquad (5)$$
$$+ (L_{23}-\ell_2)\dot{\theta}_2^2\sin\theta_2 + L_{34}\dot{\theta}_3^2\sin\theta_3 + \ell_4\dot{\theta}_4^2\sin\theta_4$$

$$\ddot{x}_5 = \ddot{x}_2 - (L_{23}-\ell_2)\ddot{\theta}_2\sin\theta_2 - L_{34}\ddot{\theta}_3\sin\theta_3 - L_{45}\ddot{\theta}_4\sin\theta_4 - \ell_5\ddot{\theta}_5\sin\theta_5$$
$$- (L_{23}-\ell_2)\dot{\theta}_2^2\cos\theta_2 - L_{34}\dot{\theta}_3^2\cos\theta_3 - L_{45}\dot{\theta}_4^2\cos\theta_4 - \ell_5\dot{\theta}_5^2\cos\theta_5$$

$$\ddot{z}_5 = \ddot{z}_2 - (L_{23}-\ell_2)\ddot{\theta}_2\cos\theta_2 - L_{34}\ddot{\theta}_3\cos\theta_3 - L_{45}\ddot{\theta}_4\cos\theta_4 - \ell_5\ddot{\theta}_5\cos\theta_5$$
$$+ (L_{23}-\ell_2)\dot{\theta}_2^2\sin\theta_2 + L_{34}\dot{\theta}_3^2\sin\theta_3 + L_{45}\dot{\theta}_4^2\sin\theta_4 + \ell_5\dot{\theta}_5^2\sin\theta_5$$

$$\ddot{x}_6 = \ddot{x}_2 - (L_{23}-\ell_2)\ddot{\theta}_2\sin\theta_2 - L_{34}\ddot{\theta}_3\sin\theta_3 - L_{45}\ddot{\theta}_4\sin\theta_4 - L_{56}\ddot{\theta}_5\sin\theta_5 - \ell_6\ddot{\theta}_6\sin\theta_6$$
$$- (L_{23}-\ell_2)\dot{\theta}_2^2\cos\theta_2 - L_{34}\dot{\theta}_3^2\cos\theta_3 - L_{45}\dot{\theta}_4^2\cos\theta_4 - L_{56}\dot{\theta}_5^2\cos\theta_5 - \ell_6\dot{\theta}_6^2\cos\theta_6$$

$$\ddot{z}_6 = \ddot{z}_2 - (L_{23}-\ell_2)\ddot{\theta}_2\cos\theta_2 - L_{34}\ddot{\theta}_3\cos\theta_3 - L_{45}\ddot{\theta}_4\cos\theta_4 - L_{56}\ddot{\theta}_5\cos\theta_5 - \ell_6\ddot{\theta}_6\cos\theta_6$$
$$+ (L_{23}-\ell_2)\dot{\theta}_2^2\sin\theta_2 + L_{34}\dot{\theta}_3^2\sin\theta_3 + L_{45}\dot{\theta}_4^2\sin\theta_4 + L_{56}\dot{\theta}_5^2\sin\theta_5 + \ell_6\dot{\theta}_6^2\sin\theta_6$$

$$\ddot{x}_7 = \ddot{x}_2 + L_{27}\ddot{\theta}_2\sin(\theta_2-\theta_c) - (x_5\sin\theta_2 - z_5\cos\theta_2)\ddot{\theta}_2 - \ell_7\ddot{\theta}_7\sin\theta_7$$
$$+ \ddot{x}_5\cos\theta_2 + \ddot{z}_5\sin\theta_2 + L_{27}\dot{\theta}_2^2\cos(\theta_2-\theta_c) - \ell_7\dot{\theta}_7^2\cos\theta_7$$
$$- 2\dot{x}_5\dot{\theta}_2\sin\theta_2 + 2\dot{z}_5\dot{\theta}_2\cos\theta_2 - \dot{\theta}_2^2(x_5\cos\theta_2 + z_5\sin\theta_2)$$

$$\ddot{z}_7 = \ddot{z}_2 + L_{27}\ddot{\theta}_2\cos(\theta_2-\theta_c) - (x_5\cos\theta_2 + z_5\sin\theta_2)\ddot{\theta}_2 - \ell_7\ddot{\theta}_7\cos\theta_7$$
$$- \ddot{x}_5\sin\theta_2 + \ddot{z}_5\cos\theta_2 - L_{27}\dot{\theta}_2^2\sin(\theta_2-\theta_c) + \ell_7\dot{\theta}_7^2\sin\theta_7$$
$$- 2\dot{x}_5\dot{\theta}_2\cos\theta_2 - 2\dot{z}_5\dot{\theta}_2\sin\theta_2 + \dot{\theta}_2^2(x_5\sin\theta_2 - z_5\cos\theta_2)$$

$$\ddot{X}_8 = \ddot{X}_2 + L_{27}\ddot{\theta}_2 \sin(\theta_2-\theta_c) - (X_S \sin\theta_2 - Z_S \cos\theta_2)\ddot{\theta}_2 - L_{78}\ddot{\theta}_7 \sin\theta_7$$
$$- \ell_8 \ddot{\theta}_8 \sin\theta_8 + \ddot{X}_S \cos\theta_2 + \ddot{Z}_S \sin\theta_2 + L_{27}\dot{\theta}_2^2 \cos(\theta_2-\theta_c)$$
$$- L_{78}\dot{\theta}_7^2 \cos\theta_7 - \ell_8 \dot{\theta}_8^2 \cos\theta_8 - 2\dot{X}_S \dot{\theta}_2 \sin\theta_2 + 2\dot{Z}_S \dot{\theta}_2 \cos\theta_2$$
$$- \dot{\theta}_2^2 (X_S \cos\theta_2 + Z_S \sin\theta_2)$$

$$\ddot{Z}_8 = \ddot{Z}_2 + L_{27}\ddot{\theta}_2 \cos(\theta_2-\theta_c) - (X_S \cos\theta_2 + Z_S \sin\theta_2)\ddot{\theta}_2 - L_{78}\ddot{\theta}_7 \cos\theta_7$$
$$- \ell_8 \ddot{\theta}_8 \cos\theta_8 - \ddot{X}_S \sin\theta_2 + \ddot{Z}_S \cos\theta_2 - L_{27}\dot{\theta}_2^2 \sin(\theta_2-\theta_c)$$
$$+ L_{78}\dot{\theta}_7^2 \sin\theta_7 + \ell_8 \dot{\theta}_8^2 \sin\theta_8 - 2\dot{X}_S \dot{\theta}_2 \cos\theta_2 - 2\dot{Z}_S \dot{\theta}_2 \sin\theta_2$$
$$+ \dot{\theta}_2^2 (X_S \sin\theta_2 - Z_S \cos\theta_2)$$

2.2 FORMULATION OF THE EQUATIONS OF MOTION

The equations of motion describing the dynamic behavior of the eight-segment articulated occupant were derived using the Lagrangian formulation

$$\frac{d}{dt}\frac{\partial T}{\partial \dot{q}_i} - \frac{\partial T}{\partial q_i} + \frac{\partial V}{\partial q_i} + \frac{\partial D}{\partial q_i} = Q_i \tag{6}$$

where T is the total system kinetic energy; V, the system potential energy; D, the system energy dissipation function; Q_{q_i}, the classical generalized force acting on generalized coordinate q_i.

The body kinetic energy (exclusive of neck mass) expressed in the inertial coordinates of the centers of mass is:

$$T = \frac{1}{2}\sum_{i=1}^{8}\left\{ m_i\left[\dot{x}_i^2 + \dot{z}_i^2\right] + I_i\dot{\theta}_i^2 \right\} \tag{7}$$

Equations 4 are used to express the kinetic energy in terms of the system generalized coordinates and velocities. It is noted here that the kinetic energy terms in Equation 6 can be reduced to the form

$$\frac{d}{dt}\frac{\partial T}{\partial \dot{q}_i} - \frac{\partial T}{\partial q_i} = \sum_{j=1}^{8} m_j\left(\ddot{x}_j\frac{\partial x_j}{\partial q_i} + \ddot{z}_j\frac{\partial z_j}{\partial q_i}\right) + \sum_{j=1}^{8} I_j\ddot{\theta}_j\frac{\partial \theta_j}{\partial q_i} \tag{8}$$

(See Reference 10).

The extensible neck element is considered to have a total mass m_n which is lumped at the extremities of the element, at the head-neck and neck-torso joints. Where α is an input parameter, the masses at the upper and lower neck joints are αm_n and $(1-\alpha)m_n$, respectively. Neck moment of inertia about a neck center of gravity would be redundant since the neck mass is already distributed. The value m_n is allowed to be zero. The kinetic energy of the neck is

$$T_n = 1/2 \ \alpha m_n (\dot{X}_1^J)^2 + 1/2 \ (1-\alpha)m_n(\dot{X}_2^J)^2 \quad . \tag{9}$$

This leads to additional terms for the Lagrange equations (6). They are:

$$\frac{d}{dt}\frac{\partial T_n}{\partial \dot{q}_i} - \frac{\partial T_n}{\partial q_i} = \alpha m_n \left(\ddot{X}_1^J \frac{\partial X_1^J}{\partial q_i} + \ddot{Z}_1^J \frac{\partial Z_1^J}{\partial q_i} \right)$$

$$+ (1-\alpha)m_n \left(\ddot{X}_2^J \frac{\partial X_2^J}{\partial q_i} + \ddot{Z}_2^J \frac{\partial Z_2^J}{\partial q_i} \right) \tag{10}$$

The derivatives of X_1^J and X_2^J are obtained from Equation 1.

The effects of gravity and joint springs can be included in terms of a potential function, V, as follows.

$$V = \sum_{i=1}^{8} m_i \ g \left[Z_i(0) - Z_i \right] + \frac{1}{2}\sum_{i=1}^{8} K_{i,1} \left[\theta_i^R - \theta_{i0}^R \right]^2 + \frac{1}{2} K_{N,1} \left[L_n - L_n(0) \right]^2$$

$$+ \frac{1}{2} K_{S,1} \left[L_S \right]^2 + \sum_{i=1}^{8} \int_{\theta_i'} T_i^m d\theta_i' + \sum_{j=2}^{3} \frac{1}{(j+1)} K_{N,j} \left[L_n - L_n(0) \right]^{j+1}$$

$$+ \sum_{j=2}^{3} \frac{1}{(j+1)} K_{S,j} \left[L_S - R_S \right]^{j+1} \tag{11}$$

Here, relative joint angles are defined by

$$\theta_m^R = \theta_j - \theta_k,$$

where the indices are related as follows:

m	1	2	3	4	5	6	7	8
j	9	2	3	4	5	6	7	8
k	1	9	2	3	4	5	2	7

The second term in equation 11 is for linear (elastic) joint stiffnesses.
The third and fourth terms represent lengthwise elastic deformation of the
neck* and shoulder spring elements which connect joints 1-2 and 7-9,
respectively. θ_i' in the fifth term is angular deformation beyond a
motion limiting stop and T_i^n is the associated nonlinear torque, defined
by Equation 33. The last two terms are for nonlinear resistance to
lengthwise deformation of the neck and shoulder elements. R_s is the radius
of a "stop" circle for shoulder element deformation. (Force is zero unless
$L_s > R_s$.)

$$
\frac{\partial V}{\partial q_j} = -g \sum_{i=1}^{8} m_i \frac{\partial z_i}{\partial q_j} + \sum_{m=1}^{6} K_{m,1} \left[\theta_m^R - \theta_{m0}^R \right] \frac{\partial \theta_m^R}{\partial q_j} + K_{N,1} \left[L_m - L_m(0) \right] \frac{\partial L_m}{\partial q_j}
$$
$$
+ K_{S,1} L_s \frac{\partial L_s}{\partial q_j} + \sum_{m=1}^{8} T_m^m \frac{\partial \theta_m'}{\partial q_j} + \sum_{m=2}^{3} K_{N,m} \left[L_m - L_m(0) \right]^m \frac{\partial L_m}{\partial q_j}
$$
$$
+ \sum_{m=2}^{3} K_{S,m} \left[L_s - R_s \right]^m \frac{\partial L_s}{\partial q_j} + \left[\frac{1}{2} L_s^2 \frac{\partial K_{S,1}}{\partial q_j} + \sum_{m=2}^{3} \frac{1}{(m+1)} \left[L_s - R_s \right]^{m+1} \frac{\partial K_{S,m}}{\partial q_j} \right] \tag{12}
$$

or

$$
\frac{\partial V}{\partial q_j} = -g \sum_{i=1}^{8} m_i \frac{\partial z_i}{\partial q_j} + \sum_{m=1}^{8} T_m^\ell \frac{\partial \theta_m^R}{\partial q_j} + F_N^\ell \frac{\partial L_m}{\partial q_j} + F_s^\ell \frac{\partial L_s}{\partial q_j}
$$
$$
+ \sum_{m=1}^{6} T_m^m \frac{\partial \theta_m'}{\partial q_j} + F_N^m \frac{\partial L_m}{\partial q_j} + F_s^m \frac{\partial L_s}{\partial q_j} + T_{SM,j} \tag{13}
$$

*The neck is allowed to have different characteristics for elongation
and compression. See Cards 213 and 242.

21

The torques T_m^{ℓ} and the forces F_N^{ℓ}, F_S^{ℓ}, F_N^n, F_S^n, and $T_{SH,j}$ are defined implicitly by Equations 12 and 13.

Although the generalized coordinates for the flexible shoulder are X_s and Z_s, the equivalent coordinates (L_s, θ_s) are used instead in some parts of the analysis, as in Equation 11. Figure 6 and Equations 14 define and relate these quantities.

$$L_s = \sqrt{X_s^2 + Z_s^2} \; ; \qquad \dot{L}_s = \frac{X_s \dot{X}_s + Z_s \dot{Z}_s}{L_s}$$

$$\theta_s = \tan^{-1}\frac{-Z_s}{X_s} \; ; \qquad \dot{\theta}_s = \frac{Z_s \dot{X}_s - X_s \dot{Z}_s}{L_s^2}$$

$$\frac{\partial L_s}{\partial X_s} = \frac{X_s}{L_s} \; ; \qquad \frac{\partial L_s}{\partial Z_s} = \frac{Z_s}{L_s} \qquad\qquad (14)$$

$$\frac{\partial \theta_s}{\partial X_s} = \frac{\partial \dot{\theta}_s}{\partial \dot{X}_s} = \frac{Z_s}{L_s^2}$$

$$\frac{\partial \theta_s}{\partial Z_s} = \frac{\partial \dot{\theta}_s}{\partial \dot{Z}_s} = -\frac{X_s}{L_s^2}$$

The last term in Equation 6 results from an assumed dependence of the resistance to lengthening of L_s on the angular direction of the deformation. The stiffnesses $K_{s,i}$ are inputted as tabular, periodic functions of θ_s on Cards 239-241. Then the partial derivatives are found as

so that
$$\frac{\partial K_{s,i}}{\partial q_j} = \frac{d K_{s,i}}{d \theta_s}\frac{\partial \theta_s}{\partial q_j}$$

$$\qquad\qquad (15)$$

$$T_{SH,X_s} = \frac{Z_s}{L_s^2}\left[\frac{1}{2} L_s^2 K_{s,1}'(\theta_s) + \sum_{m=2}^{3} \frac{1}{m+1}[L_s - R_s]^{m+1} K_{s,m}'(\theta_s) \right]$$

and

$$T_{SH,Z_s} = -\frac{X_s}{L_s^2}\left[\frac{1}{2} L_s^2 K_{s,1}'(\theta_s) + \sum_{m=2}^{3} \frac{1}{m+1}[L_s - R_s]^{m+1} K_{s,m}'(\theta_s) \right]$$

22

The individual contributions to the equations of motion   from gravity and springs in Equation 13 are:

$$\frac{\partial V}{\partial X_2} = 0$$

$$\frac{\partial V}{\partial Z_2} = -A_1 g - m_n g$$

$$\frac{\partial V}{\partial \theta_1} = -A_2 g \cos\theta_1 - T_1 - A_{41} g \sin\theta_1$$

$$\frac{\partial V}{\partial \theta_2} = -\left[A_3 \cos\theta_2 - A_{40}\cos(\theta_2 - \theta_c) - A_{18}(X_5 \cos\theta_2 + Z_5 \sin\theta_2)\right] g + T_2 - T_3 - T_7$$
$$- m_n g \, \ell_2 \cos\theta_2$$

$$\frac{\partial V}{\partial \theta_3} = A_4 g \cos\theta_3 + T_3 - T_4$$

$$\frac{\partial V}{\partial \theta_4} = A_5 g \cos\theta_4 + T_4 - T_5 \tag{16}$$

$$\frac{\partial V}{\partial \theta_5} = A_6 g \cos\theta_5 + T_5 - T_6$$

$$\frac{\partial V}{\partial \theta_6} = A_7 g \cos\theta_6 + T_6$$

$$\frac{\partial V}{\partial \theta_7} = A_8 g \cos\theta_7 + T_7 - T_8$$

$$\frac{\partial V}{\partial \theta_8} = A_9 g \cos\theta_8 + T_8$$

$$\frac{\partial V}{\partial \theta_n} = -m_1 L_n g \cos\theta_n + T_1 - T_2 - \alpha m_n g L_n \cos\theta_n$$

$$\frac{\partial V}{\partial L_n} = -m_1 g \sin\theta_n + F_N - \alpha m_n g \sin\theta_n$$

23

$$\frac{\partial V}{\partial X_s} = A_{18}\, g \, \sin \theta_2 + F_s \frac{X_s}{L_s} + T_{SH,X_s}$$

$$\frac{\partial V}{\partial Z_s} = -A_{18}\, g \, \cos \theta_2 + F_s \frac{Z_s}{L_s} + T_{SH,Z_s}$$

The quantities A_i are constants defined in Equation 24. The torques T and

forces F are a sum of linear and nonlinear parts from Equation 13, i.e.,

$$T_m = T_m^\ell + T_m^n$$

$$F_N = F_N^\ell + F_N^n \qquad\qquad (17)$$

$$F_S = F_S^\ell + F_S^n$$

Energy dissipation occurs at the joints through the mechanisms of

friction and viscocity. The energy dissipation function may be obtained

by integrating the torque over the angular velocity, as in the first term of

of Eq. 18. The last two terms of this equation are for viscous damping along

neck and shoulder links.

$$D = \sum_{i=1}^{8} \int_{\dot\theta_i^R} \left(T_i^f + T_i^v \right) \partial \dot\theta_i^R + \tfrac{1}{2} C_N \dot{L}_N^2 + \tfrac{1}{2} C_S \dot{L}_S^2 \qquad (18)$$

With the definition $T_i' = T_i^f + T_i^v$ we obtain the contributions to the

equations of motion of energy dissipating torques and forces as:

$$\frac{\partial D}{\partial \dot X_2} = \frac{\partial D}{\partial \dot Z_2} = 0$$

$$\frac{\partial D}{\partial \dot\theta_1} = -T_1' \qquad\qquad (19)$$

$$\frac{\partial D}{\partial \dot\theta_2} = T_2' - T_3' - T_7'$$

$$\frac{\partial D}{\partial \dot\theta_3} = T_3' - T_4'$$

$$\frac{\partial D}{\partial \dot\theta_4} = T_4' - T_5'$$

24

$$\frac{\partial D}{\partial \dot{\theta}_5} = T_5' - T_6'$$

$$\frac{\partial D}{\partial \dot{\theta}_6} = T_6'$$

$$\frac{\partial D}{\partial \dot{\theta}_7} = T_7' - T_8'$$

$$\frac{\partial D}{\partial \dot{\theta}_8} = T_8'$$ (19)

(continued)

$$\frac{\partial D}{\partial \dot{\theta}_m} = T_1' - T_2'$$

$$\frac{\partial D}{\partial \dot{L}_m} = c_N \dot{L}_N = F_N'$$

$$\frac{\partial D}{\partial \dot{x}_s} = c_s \dot{L}_s \frac{x_s}{L_s} = F_s' \frac{x_s}{L_s}$$

$$\frac{\partial D}{\partial \dot{z}_s} = c_s \dot{L}_s \frac{z_s}{L_s} = F_s' \frac{z_s}{L_s}$$

For solution purposes, the equations of motion for the fourteen degree[*] of freedom occupant model may be arranged in matrix form as

$$[M] [\ddot{q}] = -[B] + [C] + [D] + [E] \qquad (20)$$

where the elements of the matrix [M] and the vectors [$\ddot{q}$], [B], [C], [D],[E] will be given in the text which follows. The vector [$\ddot{q}$] contains all the second order derivatives of the generalized coordinates. Equation 20 is solved for these generalized accelerations before each integration step in the calculation procedure.

---

[*] Additional degrees of freedom are associated with user-defined non-body links, which are discussed in Section 2.10.

$$[\ddot{q}] = \begin{bmatrix} \ddot{x}_2 \\ \ddot{z}_2 \\ \ddot{\theta}_1 \\ \ddot{\theta}_2 \\ \ddot{\theta}_3 \\ \ddot{\theta}_4 \\ \ddot{\theta}_5 \\ \ddot{\theta}_6 \\ \ddot{\theta}_7 \\ \ddot{\theta}_8 \\ \ddot{\theta}_n \\ \ddot{L}_n \\ \ddot{X}_s \\ \ddot{Z}_s \end{bmatrix} \tag{21}$$

The matrix of coefficients, [M], is given by Equation 22 where the constant

multipliers, A, are defined in Equation 24.* The vector [B] includes the

effect of centrifugal forces resulting from body kinetic energy* (Equation 7)

and gravitational forces (part of Equation 12). The components of vector [B]

are given as Equation 25. The effects of joint linear and nonlinear torsional

springs (Equation 12) as well as joint dissipative effects (Equation 19 are

lumped together to form the vector [C] as given in Equation 27. The vector

E is developed in Section 2.3.2. It accounts for the effect of time-dependent

muscle contraction forces.

_____

* The contributions of neck mass and moment of inertia to [M] and [B] are

M^N_{ij} and B^N_i in Equations 22 and 25. Their non-zero values are given in

Equations 23 and 26.

The elements of [M] given in Equation 22 are the non-zero elements in the upper triangle. The elements in the lower triangle are $M_{ji} = M_{ij}$.

$$M_{11} = A_1 + M_{11}^N$$

$$M_{13} = A_2 \sin\theta_1 - A_{41} \cos\theta_1$$

$$M_{14} = A_3 \sin\theta_2 - A_{40} \sin(\theta_2 - \theta_c) + A_{18}(-X_s \sin\theta_2 + Z_s \cos\theta_2)$$

$$M_{15} = -A_4 \sin\theta_3 \qquad\qquad + M_{14}^N$$

$$M_{16} = -A_5 \sin\theta_4$$

$$M_{17} = -A_6 \sin\theta_5$$

$$M_{18} = -A_7 \sin\theta_6$$

$$M_{19} = -A_8 \sin\theta_7$$

$$M_{1,10} = -A_9 \sin\theta_8$$

$$M_{1,11} = m_1 L_m \sin\theta_m + M_{1,11}^N$$

$$M_{1,12} = -m_1 \cos\theta_m + M_{1,12}^N$$

$$M_{1,13} = A_{18} \cos\theta_2$$

$$M_{1,14} = A_{18} \sin\theta_2$$

$$M_{22} = A_1 + M_{22}^N$$

$$M_{23} = A_2 \cos\theta_1 + A_{41} \sin\theta_1$$

$$M_{24} = A_3 \cos\theta_2 - A_{40} \cos(\theta_2 - \theta_c) - A_{18}(X_s \cos\theta_2 + Z_s \sin\theta_2)$$

$$M_{25} = -A_4 \cos\theta_3 \qquad\qquad + M_{24}^N$$

(22)

$$M_{26} = -A_5 \cos \theta_4$$

$$M_{27} = -A_6 \cos \theta_5$$

$$M_{28} = -A_7 \cos \theta_6$$

$$M_{29} = -A_8 \cos \theta_7$$

$$M_{2,10} = -A_9 \cos \theta_8$$

$$M_{2,11} = m_1 L_m \cos \theta_m + M_{2,11}^N$$

$$M_{2,12} = m_1 \sin \theta_m + M_{2,12}^N$$

$$M_{2,13} = -A_{18} \sin \theta_2$$

$$M_{2,14} = A_{18} \cos \theta_2$$

$$M_{33} = A_{10} + A_{41} c$$

$$M_{34} = A_{19} \cos(\theta_2 - \theta_1) - A_{41} \ell_2 \sin(\theta_2 - \theta_1)$$

$$M_{3,11} = A_2 L_m \cos(\theta_m - \theta_1) - A_{41} L_m \sin(\theta_m - \theta_1)$$

$$M_{3,12} = A_2 \sin(\theta_m - \theta_1) + A_{41} \cos(\theta_m - \theta_1)$$

$$M_{44} = A_{11} + A_{18}\left[L_{27}^2 + X_s^2 + z_s^2 - 2 L_{27}(X_s \cos \theta_c + z_s \sin \theta_c) \right] + M_{44}^N$$

$$M_{45} = A_{24} \cos(\theta_3 - \theta_2)$$

$$M_{46} = A_{25} \cos(\theta_4 - \theta_2)$$

$$M_{47} = A_{26} \cos(\theta_5 - \theta_2)$$

$$M_{48} = A_{27} \cos(\theta_6 - \theta_2)$$

$$M_{49} = -A_{28} \cos\left[\theta_7 - (\theta_2 - \theta_c)\right] + A_8\left[X_s \cos(\theta_7 - \theta_2) - z_s \sin(\theta_7 - \theta_2) \right]$$

$$M_{4,10} = -A_{29} \cos\left[\theta_8 - (\theta_2 - \theta_c)\right] + A_9\left[X_s \cos(\theta_8 - \theta_2) - z_s \sin(\theta_8 - \theta_2) \right]$$

$$M_{4,11} = A_{21} L_m \cos(\theta_m - \theta_2) + M_{4,11}^N$$

$$M_{4,12} = A_{21} \sin(\theta_m - \theta_2) + M_{4,12}^N$$

$$M_{4,13} = A_{18}\left(z_s - L_{27} \sin \theta_c \right)$$

$$M_{4,14} = A_{18}\left(-X_s + L_{27} \cos \theta_c \right)$$

$$M_{55} = A_{12}$$

$$M_{56} = A_{30} \cos(\theta_4 - \theta_3)$$

$$M_{57} = A_{31} \cos(\theta_5 - \theta_3)$$

$$M_{58} = A_{32} \cos(\theta_6 - \theta_3)$$

$$M_{66} = A_{13}$$

$$M_{67} = A_{33} \cos(\theta_5 - \theta_4)$$

$$M_{68} = A_{34} \cos(\theta_6 - \theta_4)$$

$$M_{77} = A_{14}$$

$$M_{78} = A_{35} \cos(\theta_6 - \theta_5)$$

$$M_{88} = A_{15}$$

$$M_{99} = A_{16}$$

$$M_{9,10} = A_{23} \cos(\theta_8 - \theta_7)$$

$$M_{9,13} = -A_8 \sin(\theta_7 - \theta_2)$$

$$M_{9,14} = -A_8 \cos(\theta_7 - \theta_2)$$

$$M_{10,10} = A_{17}$$

$$M_{10,13} = -A_9 \sin(\theta_8 - \theta_2)$$

$$M_{10,14} = -A_9 \cos(\theta_8 - \theta_2)$$

$$M_{11,11} = m_1 L_m^2 + M_{11,11}^N \qquad M_{13,13} = A_{18}$$

$$M_{12,12} = m_1 + M_{12,12}^N \qquad M_{14,14} = A_{18}$$

29

$$M^N_{11} = m_n$$

$$M^N_{14} = m_n \, l_2 \, \sin \theta_2$$

$$M^N_{1,11} = \alpha \, m_n \, L_n \, \sin \theta_n$$

$$M^N_{1,12} = -\alpha \, m_n \, \cos \theta_n$$

$$M^N_{22} = m_n$$

$$M^N_{24} = m_n \, l_2 \, \cos \theta_2$$

$$M^N_{2,11} = \alpha \, m_n \, L_n \, \cos \theta_n$$

$$M^N_{2,12} = \alpha \, m_n \, \sin \theta_n$$

$$M^N_{44} = m_n \, l_2^2$$

$$M^N_{4,11} = \alpha \, m_n \, l_2 \, L_n \, \cos (\theta_n - \theta_2)$$

$$M^N_{4,12} = \alpha \, m_n \, l_2 \, \sin (\theta_n - \theta_2)$$

$$\quad (23)$$

$$M^N_{11,11} = \alpha \, m_n \, L_n^2$$

$$M^N_{12,12} = \alpha \, m_n$$

$$A_1 = \sum_{i=1}^{8} m_i$$

$$A_2 = m_1 \ell_1$$

$$A_3 = m_1 \ell_2 - (L_{23} - \ell_2) \sum_{i=3}^{6} m_i$$

$$A_4 = m_3 \ell_3 + L_{34} \sum_{i=4}^{6} m_i$$

$$A_5 = m_4 \ell_4 + L_{45} \sum_{i=5}^{6} m_i$$

$$A_6 = m_5 \ell_5 + m_6 L_{56}$$

$$A_7 = m_6 \ell_6$$

$$A_8 = m_7 \ell_7 + m_8 L_{78}$$

$$A_9 = m_8 \ell_8$$

$$A_{10} = I_1 + m_1 \ell_1^2$$

$$A_{11} = I_2 + m_1 \ell_2^2 + (L_{23} - \ell_2)^2 \sum_{i=3}^{6} m_i$$

$$A_{12} = I_3 + m_3 \ell_3^2 + L_{34}^2 \sum_{i=4}^{6} m_i$$

$$A_{13} = I_4 + m_4 \ell_4^2 + L_{45}^2 \sum_{i=5}^{6} m_i$$

$$A_{14} = I_5 + m_5 \ell_5^2 + m_6 L_{56}^2$$

$$A_{15} = I_6 + m_6 \ell_6^2$$

$$A_{16} = I_7 + m_7 \ell_7^2 + m_8 L_{78}^2$$

$$A_{17} = I_8 + m_8 \ell_8^2$$

$$A_{18} = \sum_{i=7}^{8} m_i$$

$$A_{19} = A_2 \ell_2$$

$$A_{20} = L_{23} - \ell_2$$

$$A_{21} = m_1 \ell_2$$

$$A_{22} = A_{18} L_{27}$$

$$A_{23} = A_9 L_{78}$$

$$A_{24} = A_4 A_{20}$$

$$A_{25} = A_5 A_{20}$$

$$A_{26} = A_6 A_{20}$$

$$A_{27} = A_7 A_{20}$$

$$A_{28} = A_8 L_{27}$$

$$A_{29} = A_9 L_{27}$$

$$A_{30} = A_5 L_{34}$$

$$A_{31} = A_6 L_{34}$$

(24)

$$A_{32} = A_7 L_{34}$$

$$A_{33} = A_6 L_{45}$$

$$A_{34} = A_7 L_{45}$$

$$A_{35} = A_7 L_{56}$$

$$A_{36} = 2 m_1$$

$$A_{37} = 2 A_{18}$$

$$A_{38} = 2 A_{21}$$

$$A_{39} = 2 A_{22}$$

$$A_{40} = - A_{18} L_{27}$$

$$A_{41} = m_1 c$$

$$B_1 = \sum_{i=1}^{9} \dot{\theta}_i^2 M_{2,i+2} + \dot{\theta}_n \dot{L}_n A_{36} \sin\theta_n - A_{37} \dot{\theta}_2 \left(\dot{X}_s \sin\theta_2 - \dot{Z}_s \cos\theta_2 \right)$$
$$+ B_1^N + B_1^C$$

$$B_2 = -\sum_{i=1}^{9} \dot{\theta}_i^2 M_{1,i+2} + \dot{\theta}_n \dot{L}_n A_{36} \cos\theta_n - A_{37} \dot{\theta}_2 \left(\dot{X}_s \cos\theta_2 + \dot{Z}_s \sin\theta_2 \right)$$
$$+ B_2^N + B_2^C$$

$$B_3 = A_2 \left[-\ell_2 \dot{\theta}_2^2 \sin(\theta_2 - \theta_1) - L_n \dot{\theta}_n^2 \sin(\theta_n - \theta_1) + 2 \dot{L}_n \dot{\theta}_n \cos(\theta_n - \theta_1) \right] + B_3^C$$

$$B_4 = A_{19} \dot{\theta}_1^2 \sin(\theta_2 - \theta_1) - A_{24} \dot{\theta}_3^2 \sin(\theta_3 - \theta_2) - A_{25} \dot{\theta}_4^2 \sin(\theta_4 - \theta_2)$$
$$- A_{26} \dot{\theta}_5^2 \sin(\theta_5 - \theta_2) - A_{27} \dot{\theta}_6^2 \sin(\theta_6 - \theta_2)$$
$$- A_{21} L_n \dot{\theta}_n^2 \sin(\theta_n - \theta_2) + A_{38} \dot{L}_n \dot{\theta}_n \cos(\theta_n - \theta_2)$$
$$+ A_8 \dot{\theta}_7^2 \left[L_{27} \sin(\theta_7 - \theta_2 + \theta_c) - X_s \sin(\theta_7 - \theta_2) - Z_s \cos(\theta_7 - \theta_2) \right]$$
$$+ A_9 \dot{\theta}_8^2 \left[L_{27} \sin(\theta_8 - \theta_2 + \theta_c) - X_s \sin(\theta_8 - \theta_2) - Z_s \cos(\theta_8 - \theta_2) \right]$$
$$+ A_{37} \dot{\theta}_2 \left[\left(-\dot{X}_s \sin\theta_2 + \dot{Z}_s \cos\theta_2 \right) \frac{\partial X_7}{\partial \theta_2} - \left(\dot{X}_s \cos\theta_2 + \dot{Z}_s \sin\theta_2 \right) \frac{\partial Z_7}{\partial \theta_2} \right] + B_4^N$$
$$+ B_4^C \qquad (25)$$

$$B_5 = A_{24} \dot{\theta}_2^2 \sin(\theta_3 - \theta_2) - A_{30} \dot{\theta}_4^2 \sin(\theta_4 - \theta_3) - A_{31} \dot{\theta}_5^2 \sin(\theta_5 - \theta_3)$$
$$- A_{32} \dot{\theta}_6^2 \sin(\theta_6 - \theta_3)$$

$$B_6 = A_{25} \dot{\theta}_2^2 \sin(\theta_4 - \theta_2) + A_{30} \dot{\theta}_3^2 \sin(\theta_4 - \theta_3) - A_{33} \dot{\theta}_5^2 \sin(\theta_5 - \theta_4)$$
$$- A_{34} \dot{\theta}_6^2 \sin(\theta_6 - \theta_4)$$

$$B_7 = A_{26} \dot{\theta}_2^2 \sin(\theta_5 - \theta_2) + A_{31} \dot{\theta}_3^2 \sin(\theta_5 - \theta_3) + A_{33} \dot{\theta}_4^2 \sin(\theta_5 - \theta_4)$$
$$- A_{35} \dot{\theta}_6^2 \sin(\theta_6 - \theta_5)$$

$$B_8 = A_{27} \dot{\theta}_2^2 \sin(\theta_6 - \theta_2) + A_{32} \dot{\theta}_3^2 \sin(\theta_6 - \theta_3) + A_{34} \dot{\theta}_4^2 \sin(\theta_6 - \theta_4)$$
$$+ A_{35} \dot{\theta}_5^2 \sin(\theta_6 - \theta_5)$$

$$B_9 = -A_8\left[\dot{\theta}_2^2\left\{L_{27}\sin(\theta_7-\theta_2+\theta_c) - X_s\sin(\theta_7-\theta_2) - z_s\cos(\theta_7-\theta_2)\right\}\right.$$
$$\left. + 2\dot{\theta}_2\left\{-\dot{X}_s\cos(\theta_7-\theta_2) + \dot{z}_s\sin(\theta_7-\theta_2)\right\}\right] - A_{23}\dot{\theta}_8^2\sin(\theta_8-\theta_7)$$

$$B_{10} = A_9\left[-\dot{\theta}_2^2\left\{L_{27}\sin(\theta_8-\theta_2+\theta_c) - X_s\sin(\theta_8-\theta_2) - z_s\cos(\theta_8-\theta_2)\right\}\right.$$
$$\left. - 2\dot{\theta}_2\left\{-\dot{X}_s\cos(\theta_8-\theta_2) + \dot{z}_s\sin(\theta_8-\theta_2)\right\} + L_{78}\dot{\theta}_7^2\sin(\theta_8-\theta_7)\right]$$

$$B_{11} = L_n\left\{A_2\dot{\theta}_1^2\sin(\theta_n-\theta_1) + A_{21}\dot{\theta}_2^2\sin(\theta_n-\theta_2) + A_{36}\dot{L}_n\dot{\theta}_n\right\} + B_{11}^N + B_{11}^C$$

$$B_{12} = -A_2\dot{\theta}_1^2\cos(\theta_n-\theta_1) - A_{21}\dot{\theta}_2^2\cos(\theta_n-\theta_2) - m_1 L_n\dot{\theta}_n^2 + B_{12}^N + B_{12}^C$$

$$B_{13} = A_{18}\dot{\theta}_2\left[2\dot{z}_s + \dot{\theta}_2(L_{27}\cos\theta_c - X_s)\right] - A_8\dot{\theta}_7^2\cos(\theta_7-\theta_2) \tag{25}$$
$$- A_9\dot{\theta}_8^2\cos(\theta_8-\theta_2) \qquad \text{continued}$$

$$B_{14} = -A_{18}\dot{\theta}_2\left[2\dot{X}_s + \dot{\theta}_2(z_s - L_{27}\sin\theta_c)\right] + A_8\dot{\theta}_7^2\sin(\theta_7-\theta_2)$$
$$+ A_9\dot{\theta}_8^2\sin(\theta_8-\theta_2)$$

$$B_1^N = m_n\ell_2\dot{\theta}_2^2\cos\theta_2 + \alpha m_n\dot{\theta}_n\left[L_n\dot{\theta}_n\cos\theta_n + 2\dot{L}_n\sin\theta_n\right]$$

$$B_2^N = -m_n\ell_2\dot{\theta}_2^2\sin\theta_2 + \alpha m_n\dot{\theta}_n\left[-L_n\dot{\theta}_n\sin\theta_n + 2\dot{L}_n\cos\theta_n\right] \tag{26}$$

$$B_4^N = \alpha m_n\ell_2\dot{\theta}_n\left[2\dot{L}_n\cos(\theta_n-\theta_2) - L_n\dot{\theta}_n\sin(\theta_n-\theta_2)\right]$$

$$B_{11}^N = \alpha m_n L_n\left[2\dot{L}_n\dot{\theta}_n + \ell_2\dot{\theta}_2^2\sin(\theta_n-\theta_2)\right]$$

$$B_{12}^N = \alpha m_n\left[-L_n\dot{\theta}_n^2 - \ell_2\dot{\theta}_2^2\cos(\theta_n-\theta_2)\right]$$

33

$$B_1^c = A_{41} \dot{\theta}_1^2 \sin \theta_1$$

$$B_2^c = A_{41} \dot{\theta}_1^2 \cos \theta_1$$

$$B_3^c = -A_{41} \left[\ell_2 \dot{\theta}_2^2 \cos(\theta_2 - \theta_1) + L_m \dot{\theta}_m^2 \cos(\theta_m - \theta_1) \right.$$
$$\left. + 2 \dot{L}_m \dot{\theta}_m \sin(\theta_m - \theta_1) \right]$$

$$B_4^c = A_{41} \ell_2 \dot{\theta}_1^2 \cos(\theta_2 - \theta_1)$$

$$B_{11}^c = A_{41} L_m \dot{\theta}_1^2 \cos(\theta_m - \theta_1)$$

$$B_{12}^c = A_{41} \dot{\theta}_1^2 \sin(\theta_m - \theta_1)$$

(26.1)

34

Where $\overline{T}_i = T_i + T_i'$, $\overline{F}_N = F_N + F_N'$, and $\overline{F}_s = F_s + F_s'$,

$$[C] = \begin{bmatrix} 0 \\ 0 \\ \overline{T}_1 \\ \overline{T}_3 - \overline{T}_2 + \overline{T}_7 \\ \overline{T}_4 - \overline{T}_3 \\ \overline{T}_5 - \overline{T}_4 \\ \overline{T}_6 - \overline{T}_5 \\ -\overline{T}_6 \\ \overline{T}_8 - \overline{T}_7 \\ -\overline{T}_8 \\ \overline{T}_2 - \overline{T}_1 \\ -\overline{F}_N \\ -\overline{F}_s \dfrac{X_s}{L_s} \\ -\overline{F}_s \dfrac{Z_s}{L_s} \end{bmatrix} \qquad (27)$$

Classical generalized forces result from the action of restraint belts and contact between vehicle contact surfaces and the crash victim. These are combined in the Q_{q_i} of Equation 28. The specific analytical content

$$[D] = \begin{bmatrix} Q_{X_2} \\ Q_{Z_2} \\ Q_{\theta_1} \\ Q_{\theta_2} \\ Q_{\theta_3} \\ Q_{\theta_4} \\ Q_{\theta_5} \\ Q_{\theta_6} \\ Q_{\theta_7} \\ Q_{\theta_8} \\ Q_{\theta_n} \\ Q_{L_n} \\ Q_{X_s} \\ Q_{Z_s} \end{bmatrix} \quad (28)$$

of Equations 27 and 28 due to joint, belt and contact forces will be defined in detail in the sections which follow.

2.3 ADDITION OF JOINT TORQUES TO THE EQUATIONS OF MOTION

Moments acting at each of the eight simulated joints are assumed to be derived from five sources: biodynamic muscle tension, elasticity, viscous damping, coulomb friction, and nonlinear energy-dissipating, motion-restricting stops. The joints are numbered as shown in Figure 1. Muscle tension is dealt with in Section 2.3.2 and the others in Section 2.3.1.

2.3.1 Passive Joint Torques

A constant frictional torque is simulated when the magnitude of the relative angular velocity θ_i^V, is greater than a small velocity threshold, V_i^J. For velocities smaller than the threshold, the friction torque is assumed to be a linear ramp function of velocity to reduce occurrence of friction-induced oscillations in the solution. A schematic of joint friction is included as Figure 7. Relative angles are given by:

$$\theta_i^R = \theta_i - \theta_{i-1} \quad , \quad i = 3, 4, 5, 6, 8$$
$$\theta_1^R = \theta_9 - \theta_1$$
$$\theta_2^R = \theta_2 - \theta_9$$
$$\theta_7^R = \theta_7 - \theta_2$$

(29)

The relative velocities are $\theta_i^V = \dot{\theta}_i^R$.

If $|\theta_i^V| \geq v_i^J$, the frictional torque is given by

$$T_i^f = F_i^J \ \text{sgn} \ \theta_i^V \qquad i = 1, \dots, 8$$

(30)

where the value of the friction torque constant, F_i^J, is specified as program input data. When $|\theta_i^V| < v_i^J$,

$$T_i^f = F_i^J \left(\frac{\theta_i^V}{v_i^J} \right)$$

(31)
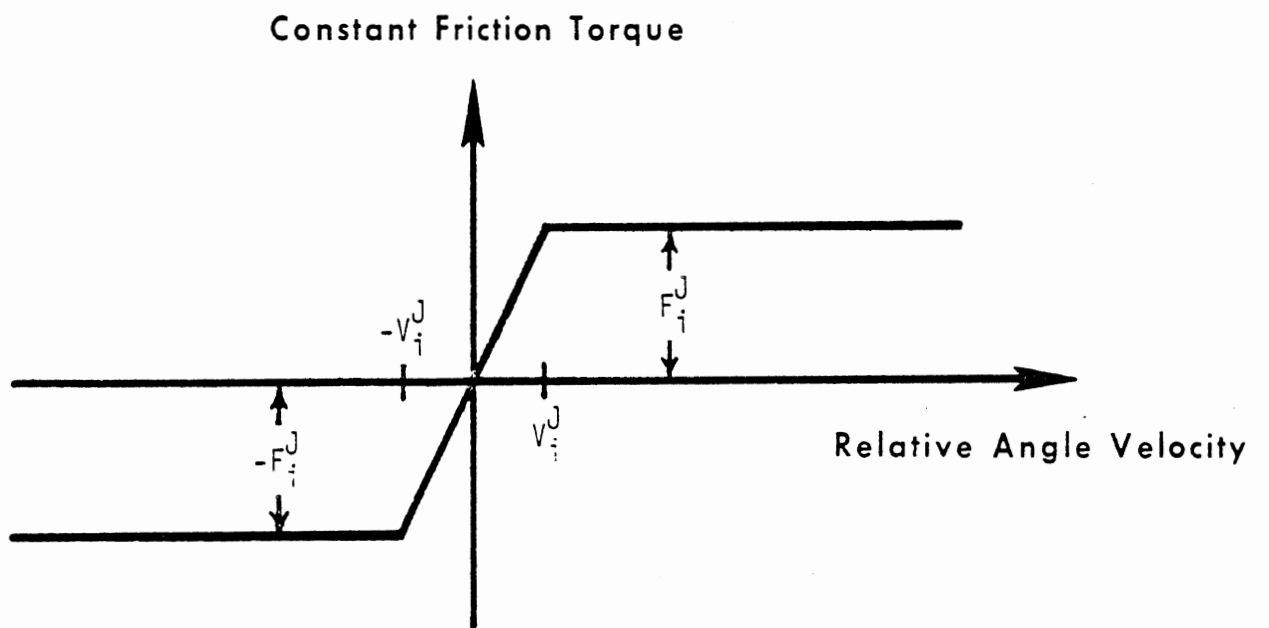
FIGURE 7. Joint friction at joint "i"

The effect of a linear elastic torsional spring is included as

$$T_i^\ell = K_{i,1} (\theta_i^R - \theta_i^R(0))$$ (32)

where the elastic constant, $K_{i,1}$, is given as program input and $\theta_i^R(0)$ is the rest angle relative orientation of adjacent body sections. The non-linear terms which model energy-absorbing, motion-restricting stops are given by equation (33) or alternatively by torque versus deflection tables.*

$$T_i^n = K_{i,1} (\theta_i^R - \theta_{i,j}^S) + (-1)^{j+1} K_{i,2} (\theta_i^R - \theta_{i,j}^S)^2$$

where
$$+ K_{i,3} (\theta_i^R - \theta_{i,j}^S)^3 \qquad i = 1, 2, \ldots, 8$$ (33)

$$j = \begin{cases} 1, & \theta_i^R > \theta_{i,1}^S \\ 2, & \theta_i^R \le \theta_{i,2}^S \end{cases}$$

$K_{i,1}$, $K_{i,2}$ and $K_{i,3}$ are bending stiffness coefficients for the joint-stop torques.

$\theta_{i,j}^S$ are the locations where the joint stops become active (Figure 8)

If $\theta_i^R \ge \theta_{i,2}^S$ and $\theta_i^R \le \theta_{i,1}^S$, then $T_i^n = 0$. Hysteresis dependent on the ratio of conserved to total energy absorbed by the stop is represented. A schematic illustrating these spring properties is included as Figure 8.

---

*The term "nonlinear joint torque" is used throughout to mean "joint-stop torque," and it can include a linear term (eq. 33) whenever the elastic torque (eq. 32) is not included in a simulation. When joint "materials" are defined more generally by use of input data cards 243 through 247, the elastic linear term may always be used and joint-stop stiffnesses and hysteretic unloading characteristics may be tabularly specified if desired as functions of deflection against the stop. Also, joint stop viscous damping coefficients may be specified for both positive and negative deflection rates.

1/6/82

The figure shows the case where the linear elastic coefficient is non-zero. The torque-deflection curve is zero in the range $[\theta^S_{i,2}, \theta^S_{i,1}]$ when this coefficient is zero. The sign conventions for defining relative angles and angular limits for joint-stop torque initiation are shown in Figures 9 and 10.

Viscous damping is included as a linear function of the relative angular velocity between body segments;

$$T^V_i = C^J_i \theta^V_i \tag{34}$$

where C^J_i is the damping coefficient which must be included as input data to the program.*

Combining equations (30), (31), (32), (33), and (34) yields

$$\bar{T}_i = T^f_i + T^\ell_i + T^n_i + T^V_i \tag{35}$$

This provides the necessary formulae for inclusion in vector [C] in the equations of motion (See Eqns. 20, 27).

---

*If cards 243-247 are used to defined joint - stop "materials," C_i^j can be specified to have separate constant values for cases of positive and negative deflection rates when the deflection is into a joint stop. The joint stop damping coefficient replaces, rather than adds to, the elastic range damping coefficient for deflections into a stop.
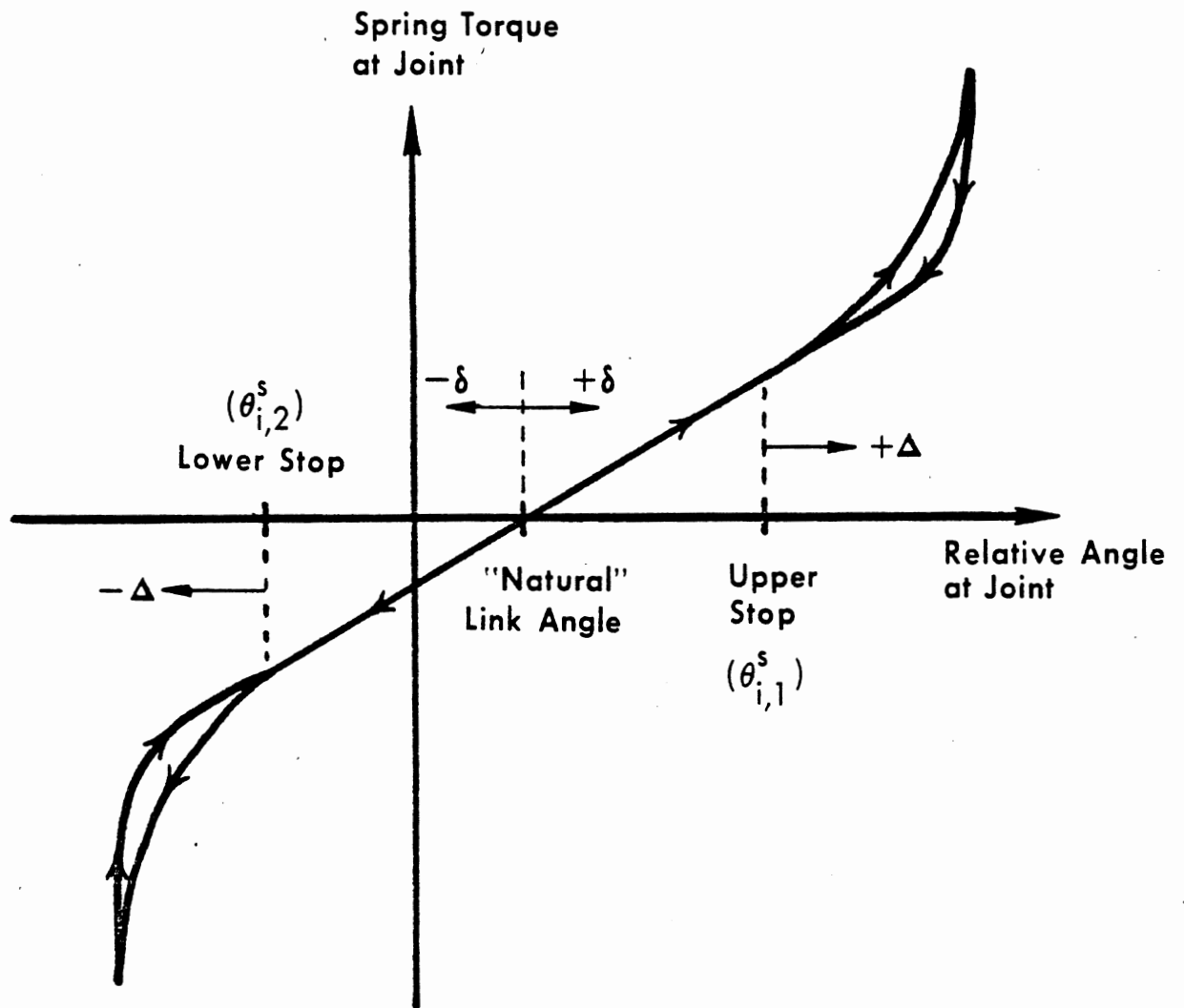
$$\underset{\text{TORQUE}}{\text{SPRING}} = -k_{\text{ELASTIC}} \; \delta \; - \left\{ K_{1,\text{STOP}} |\Delta| + K_{2,\text{STOP}} \Delta^2 + K_{3,\text{STOP}} |\Delta^3| \right\} \, \text{sgn} \, \Delta$$

Linear, elastic   Nonlinear, joint-stop component
component

FIGURE 8.   Elastic and Joint-Stop Torques
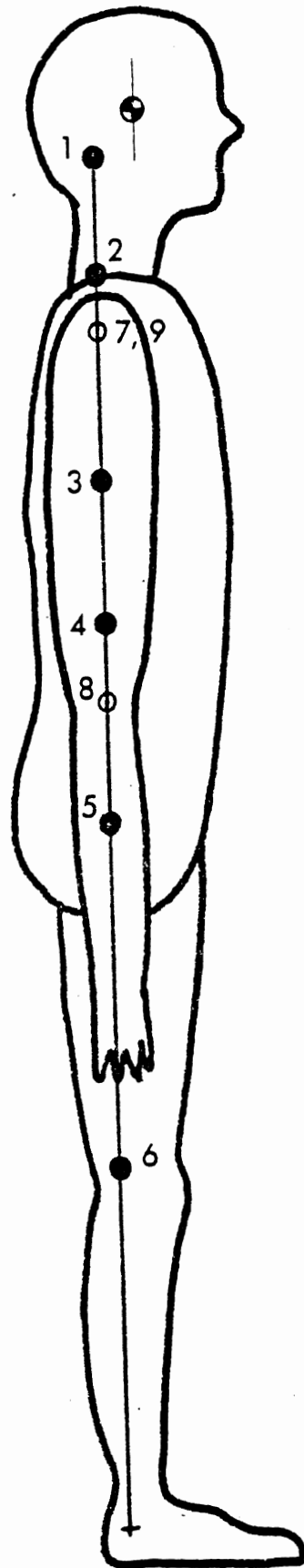
Positive Relative Angle

In-Line Orientation

L_α

L_β
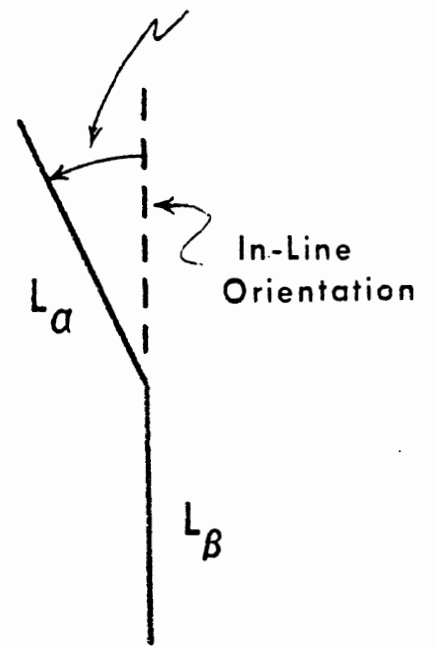
L_α = body link nearer to head

L_β = body link nearer to feet

FIGURE 9 In-line Orientation

42

Lower
Joint Stop

"Natural"
Link Position

Upper
Joint Stop

In-Line Orientation

L_α

L_β

(α,β) - joint

L_α = body link nearer
to head

L_β = body link nearer
to feet

+ rotation
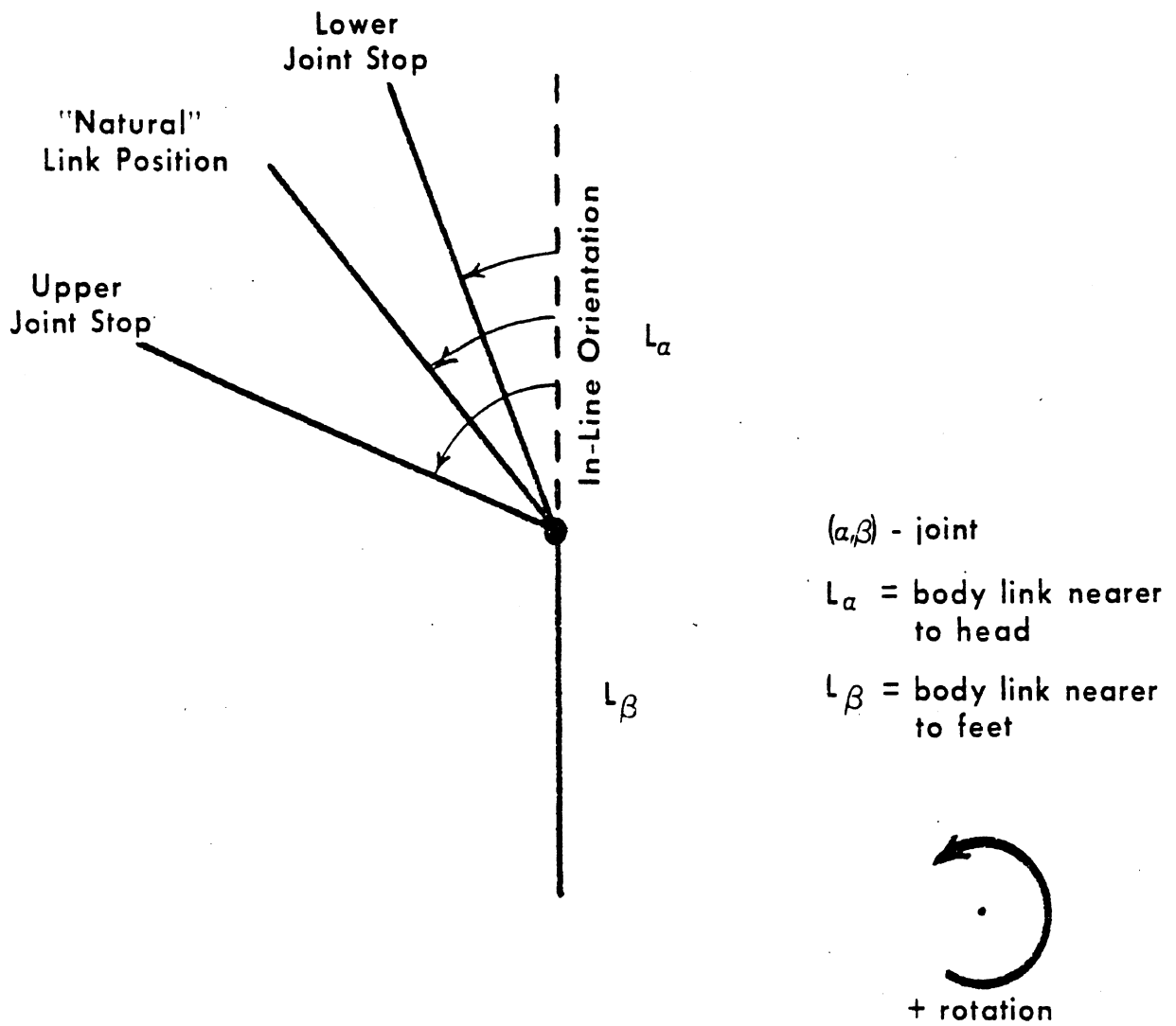
FIGURE 10   Definition of joint stop angles and
natural link position

2.3.2 Muscle Tension Forces

In most crash situations a vehicle occupant is aware that a collision is impending. In such a case it is natural for him to involuntarily tighten his muscles in anticipation of the impact. Even when he is not aware that a collision is impending, it can be expected that reflex action of body musculature will occur as a result of the impact. Contraction of the muscles can have a significant effect on the crash dynamics of the system. Analytical representation of the effect would seem to be of obvious value.
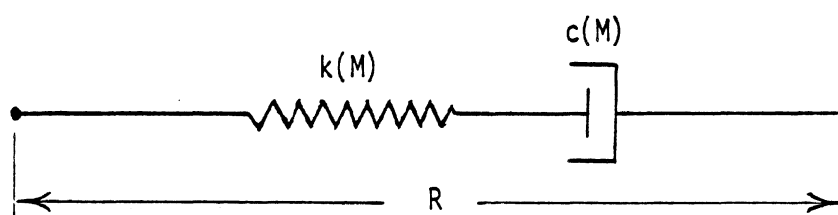
Figure 11. Generalized Muscle Element Model
The associated relative coordinate R may be either an angle or a length.

Experimental work done by Moffatt, Harris, and Haslam (11) involving the knee joint indicates that this property is properly represented by a Maxwell element, i.e., a spring and damper in series, with spring and damping coefficients that are simple functions of the voluntary static knee moment, M. (See Figure 11.) Equations 37 and 38 give these coefficients as linear functions of the absolute value of M, i.e., of the "tightness" of the muscles.

$$k = a_1 + a_2 \, |M| \tag{37}$$
$$c = a_3 \, |M| \tag{38}$$

The values of the constants a_1, a_2, and a_3 are joint properties and depend on the person involved. It is clear that when the muscles are completely relaxed (M = 0) the Maxwell element has no effect on motion at the joint since c is then zero.

The tests of Moffatt, Harris, and Haslam, involved forced sinusoidal motion, with amplitude up to 12°, about an initial value of the joint angle.

44

They state that in the tests performed there was no discernable dependence of the model coefficients upon joint angle and, also, no systematic dependence upon test amplitude.

In order to include muscle tension as a bio-dynamic property of the occupant model, the muscle contraction parameters M_i are considered functions of time, $M_i = M_i(t)$ (i = 1, ..., 11), which are inputted in tabular form on 238-cards. The results (37) and (38) will be assumed to hold, in form, at all joints -- not only at the knee. Generalized forces are found for muscle tension torques at the eight joints. A similar torque is calculated to resist θ_s-motion for the shoulder link. Muscle tension resistance to elongatfon of the neck and shoulder links is also modeled.

Bowman (10) shows that, where R is the relative coordinate associated with a Maxwell element internal to the linkage of a dynamic system and F is the force (or moment) that the Maxwell element exerts on the system through the coordinate R, the generalized forces on the system are

$$Q_k = F \frac{\partial R}{\partial q_k} \tag{39}$$

where F is determined from

$$\dot{F} + \frac{k}{c}F = -k\dot{R} \quad . \tag{40}$$

Thus, since the eleven relative coordinates R_i constrained by muscle elements $(\theta_1^R, \theta_2^R, ..., \theta_8^R, \theta_s, L_n, L_s)$ are functions of the generalized coordinates, there are eleven first-order equations with the form of (40) which are coupled to the system of 14 second-order Lagrange equations. They are integrated together as a system of simultaneous first-order equations. (Note that the inversion required to solve for the generalized accelerations is unaffected; it is still for a 14 x 14 algebraic system.)

The elements of the vector [E] in Equation 20 are thus determined from (39) and (40).

$$[E] = \begin{bmatrix} 0 \\ 0 \\ -F_{\theta_1^R} \\ F_{\theta_2^R} - F_{\theta_3^R} - F_{\theta_7^R} - F_{\theta_S} \\ F_{\theta_3^R} - F_{\theta_4^R} \\ F_{\theta_4^R} - F_{\theta_5^R} \\ F_{\theta_5^R} - F_{\theta_6^R} \\ F_{\theta_6^R} \\ F_{\theta_7^R} - F_{\theta_8^R} \\ F_{\theta_8^R} \\ F_{\theta_1^R} - F_{\theta_2^R} \\ F_{L_m} \\ F_{\theta_S} \dfrac{z_S}{L_S^2} + F_{L_S} \dfrac{x_S}{L_S} \\ -F_{\theta_S} \dfrac{x_S}{L_S^2} + F_{L_S} \dfrac{z_S}{L_S} \end{bmatrix} \qquad (41)$$

46

2.4 ADDITION OF FORCES TO THE EQUATION OF MOTION

Several features of the model represent force producers which contribute to the generalized force vector, [D], of the equations of motion (see equations 20 and 28). Two examples are the restraint belt forces and the forces generated due to contact between the occupant and the vehicle. The properties of the force-deformation or force-strain relations allowed in this model as well as the means used to compute the generalized forces for the various cases are discussed in this section.

2.4.1 Force-Deformation Relations

Consider a typical force-producer. It may be a belt pulling on the occupant, an ellipse impinging against a contact line, a collapsible steering column pressing against a chest, etc. The force produced by such a feature has been generally treated in the past as a function of deflection and deflection rate, where deflection is defined appropriately for each feature. The usual analytical form for the force is a sum of polynomials, one in deflection plus another in deflection rate.

Extensive experience with this type of model has lead to the conclusion that the deflection rate polynomial is useful only in very special cases and is often destructive to the accuracy of the model. A more useful model has been suggested by Danforth and Randall (Reference 12) which consists of two functions of deflection over different ranges which are added to obtain the total force. One function models the static deformation of the material and another function models the deformation due to dynamic effects. It has been noted that the dynamic effects usually take the form of a high spike which dies out rapidly as a function of deflection and which does not reappear with repeated loadings. We shall call these two functions the Static Curve and the Inertial Spike Curve. A general description of these functions is given in Figure 12.

47
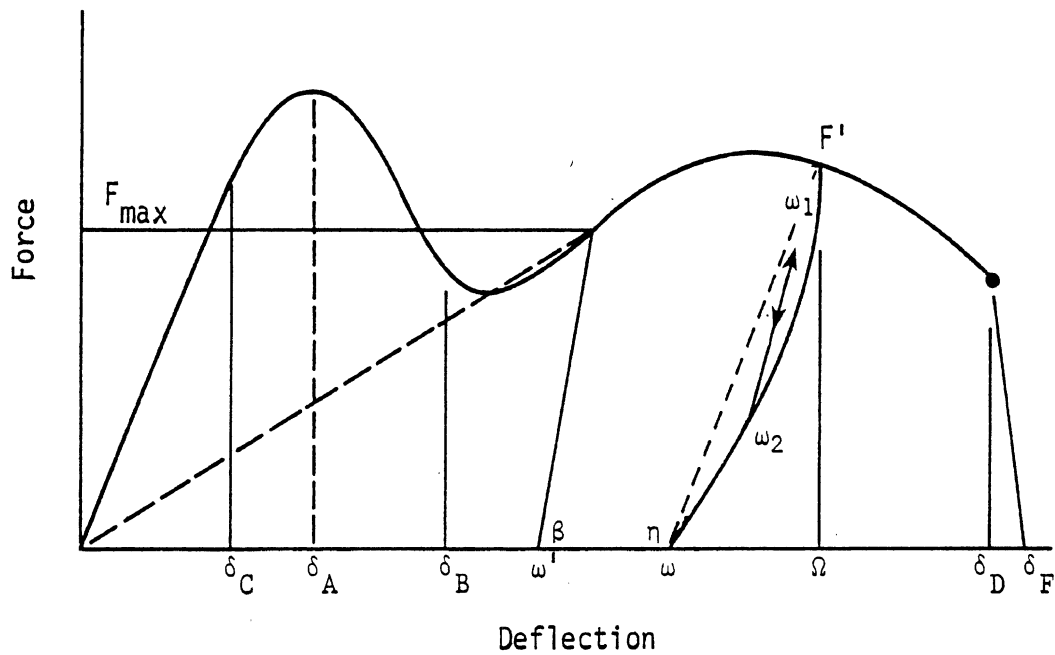
where

δ_A = deflection at peak inertial force

δ_C = deflection at elastic limit (yield point)

δ_B = termination of use of auxiliary polynomial

F_{max} = saturation force limit

Ω = deflection at which unloading begins, that is, the maximum deflection for the particular load-unload cycle

ω = calculated permanent deflection for cycle (unsaturated)

ω' = calculated permanent deflection for cycle (saturated)

ω_1 = maximum partial reload point after partial unload

ω_2 = point of return on unload curve after partial unload-partial reload

β = slope of saturation unloading curve

δ_D = breaking point

δ_F = endpoint of break down curve

η = total permanent deformation

F' = force at maximum deflection

Figure 12. HSRI Representation of Force-Deflection Curves

48

For purposes of explanation, let us assume that a completely rigid sphere is being gradually impressed upon a planar panel of some flexible material such as sheet metal. The description to the model of the load-deflection properties of the panel centers around seven input constants: δ_A, δ_B, δ_C, δ_D, δ_F, F_{max}, and β. The first three quantities are defined as shown in Figure 12 and have been suggested by the work of Danforth and Randall. The other four quantities control extensions of that work. The first six quantities must be non-negative. The first two quantities together with the fourth and fifth must form a monotonically increasing sequence. The fourth and fifth must not be equal. Before undertaking a physical description of these seven quantities, it is necessary to specify the form of the two functions together with two additional input quantities.

The Static Loading Curve consists of a sixth order polynomial in deflection (the constant coefficient is assumed zero) or a table of Force versus Deflection which is linearly interpolated between points. The Inertial Spike Curve may also be a polynomial or a table as described above. An additional restriction that this curve assume a zero value at deflection equal to δ_B must be adhered to in order to avoid possible premature termination of the model run.

The first additional input quantity is the G-factor which is defined as the fraction of permanent deflection over maximum deflection. The G-factor must be in a closed interval from zero to one and can be supplied to the model as either a constant value or a table of G-Factor versus Deflection as above.

The last input quantity is the R-factor which is defined as the fraction of conserved energy over total energy. It too must be in the closed interval from zero and one and can be supplied as a constant value or a table of R-Factor

versus Deflection. It should be understood that G and R-factors include all the accumulated effects for a particular deflection and are used only at the beginning of the unloading part of each cycle.

The quantity δ_A can be described as the deflection at which the inertial effects of the panel begin to break down irreparably. Usually this quantity is set to the deflection at which the maximum of the Inertial Spike Curve occurs although this is not a requirement. If unloading begins before this point is passed and the elastic yield point δ_C is also not passed, loading, unloading, and reloading are all along the Combined Curve. The Combined Curve is defined as the sum of the Inertial Spike Curve and the Static Curve at each point. If the elastic yield point has been passed, regular unloading (explained below) takes place but reloading is again to the Combined Curve.

The quantity δ_B can be described as the deflection at which all inertial effects cease. If δ_A has been exceeded and δ_B has not been exceeded, regular loading is on the Combined Curve. If unloading begins and the elastic yield point has not been passed, unloading is along a linear segment connecting the point of maximum deflection (Ω) with the origin and reloading will be to the Static Curve at Ω. If the yield point has been passed, unloading is regular and reloading will also be to the Static Curve at Ω.

The quantity δ_D can be described as the deflection at which massive breakdown of the whole panel begins. If δ_B has been exceeded and δ_D has not been reached, regular loading is on the Static Curve. If the yield point has not been reached, unloading and reloading are also along the Static Curve. If the yield point has been passed, regular unloading takes place and reloading is to the Static Curve at Ω.

δ_F can be described as the deflection at which complete failure takes place. Once δ_F has been exceeded, the model will always produce zero force. If δ_D has been exceeded and δ_F has not been reached, loading is along a linear segment connecting the point on the Static Curve at δ_D with a zero at δ_F.

$$B(\delta) = \ell_3 + a_3 \delta \tag{42}$$

where
$$a_3 = \frac{-F_B}{\delta_F - \delta_D}$$

$$\tag{43}$$

$$\ell_3 = \frac{\delta_F F_B}{\delta_F - \delta_D}$$

where F_B is value of force at δ_D. If unloading takes place before failure is complete and if the yield point has not been reached, unloading and reloading are along the minimum of the Static Curve and the value of the linear segment at Ω. If the yield point has been passed, normal unloading takes place and reloading is to the linear segment at Ω.

F_{max} is called the Saturation Force Limit and is intended to model special materials which exhibit the property of breaking down in such a way as to maintain a specific maximum force until reaching the breaking point. This feature is applied only to the Static Curve. Whenever the Saturation Force Limit is exceeded by the Static Curve, the regular loading sequence is superseded. Note that the Inertial Spike Curve is unaffected, and if the Combined Curve is being used, the Inertial Spike Curve will continue to be added until δ_B is reached. Once static curve saturation comes into play, the force for loading on the Static Curve is set to F_{max} until δ_D is reached. If unloading takes place on the saturated Static Curve, normal unloading is replaced by the use of the seventh input constant, β which is called the Saturation Unloading Slope. If β is negative, the G factor is used to determine the permanent deformation. If β is positive, it is taken as a linear slope to determine the permanent deformation. In either case, if the new permanent deformation fails to exceed the old permanent deformation or β is zero, the old permanent deformation is used. Unloading and reloading are along

a linear segment connecting a zero at the point of permanent deformation to F_{max} at Ω.

$$F_{us}(\delta) = \mathcal{b}_4 + a_4 \delta \tag{44}$$

where

$$\mathcal{b}_4 = \frac{-\omega F'}{\Omega - \omega}$$

$$a_4 = \frac{F'}{\Omega - \omega} \tag{45}$$

and where

$$\omega = G\Omega \qquad if \quad \beta < 0 . \tag{46}$$

Otherwise

$$\omega = max\left(\omega_t , \Omega - \frac{F'}{\beta}\right) \tag{47}$$

where ω_t is the last established ω. If this unloading takes place in the range where the combined curve is used, the same rules apply as were explained above except the F_{max} replaces the Static Curve. Note that the elastic yield point has effect before saturation and during break down after saturation but not during saturation.

Normal unloading is modeled by determination of permanent deformation and conserved energy using the G and R factors evaluated at the maximum deflection (Ω). Let ω be the permanent deformation, F' be the force at Ω, and E' be the conserved energy. Then, as was done in the HSRI two dimensional model (Reference 13), a quadratic is fitted which unloads to the permanent deformation with the proper conserved energy.

The regular unloading curve is

$$F(\delta) = \mu_1 + \mu_2\delta + \mu_3\delta^2 \tag{48}$$

where

$$\mu_1 = \frac{\omega\left[F'(\Omega-\omega)(\omega+2\Omega)-6E'\Omega\right]}{(\Omega-\omega)^3}$$

$$\mu_2 = \frac{2\left[3(\Omega+\omega)E'-(\Omega+2\omega)(\Omega-\omega)F'\right]}{(\Omega-\omega)^3} \tag{49}$$

$$\mu_3 = \frac{3\left[F'(\Omega-\omega)-2E'\right]}{(\Omega-\omega)^3} \cdot$$

It will occasionally happen that the curvature of a quadratic is not adequate to achieve both the proper zero and the proper area without the physically unrealistic effect of a negative force loop. If this contingency arises, then the second zero of the unloading curve lies between ω and Ω.

The location of the second zero is

$$\hat{\delta} = \Omega + \frac{(\Omega-\omega)^2 F'}{6E'-3(\Omega-\omega)F'} \tag{50}$$

The quantity $\hat{\delta}$ is tested for $\hat{\delta} \in [\omega, \Omega]$. If $\hat{\delta}$ is in this range, then the unloading and reloading are computed from two linear segments which maintain the proper permanent deformations and conserved energy.

For $\omega \le \delta \le \Delta$,

$$F_\mu(\delta) = \beta_1 + a_1\delta \tag{51}$$

and for $\Delta \le \delta \le \Omega$,

$$F_\mu(\delta) = \beta_2 + a_2\delta \tag{52}$$

where $\quad F_u \quad$ = force during an unloading cycle

$$a_1 \quad = \frac{M}{\Delta - \omega} \tag{53}$$

53

$$b_1 = -\frac{\omega M}{\Delta - \omega}$$

$$a_2 = \frac{F' - M}{\Omega - \Delta}$$

$$b_2 = \frac{\Omega M - F'\Delta}{\Omega - \Delta}$$

(53) (cont'd.)

Δ = $\omega + \varepsilon(\Omega - \omega)$ (δ at intersection of line segments)

M = $(2\lambda + \varepsilon - 1)F'$ (force at intersection of line segments; note that $1 - 2\lambda \leq \varepsilon \leq 1$ is range of no negative loop)

λ = $\dfrac{E'}{F'(\Omega - \omega)}$ (energy ratio)

E' = conserved energy.

If $0 < \lambda < 1$, then $\varepsilon = 1 - \lambda$; otherwise ε is chosen to yield a straight line unloading to ω, i.e., λ is set to .5, yielding $\varepsilon = .5$.

An unloading curve may be determined by interpolating between user-specified unloading curves instead of from G and R ratios, as just described. If both types of unloading specifications are included in the data deck for a material, then G and R ratios are ignored. Unloading from the static loading curve is described by a family of bilinear unloading curves, as illustrated in Figure 12-1. Any number of bilinear unloading curves may be prescribed. One of the curves should have a δ_3 coordinate greater than the greatest deflection expected for simulation. The user describes each bilinear curve by five input parameters: deflections δ_1, δ_2, and δ_3 at the line segment endpoints
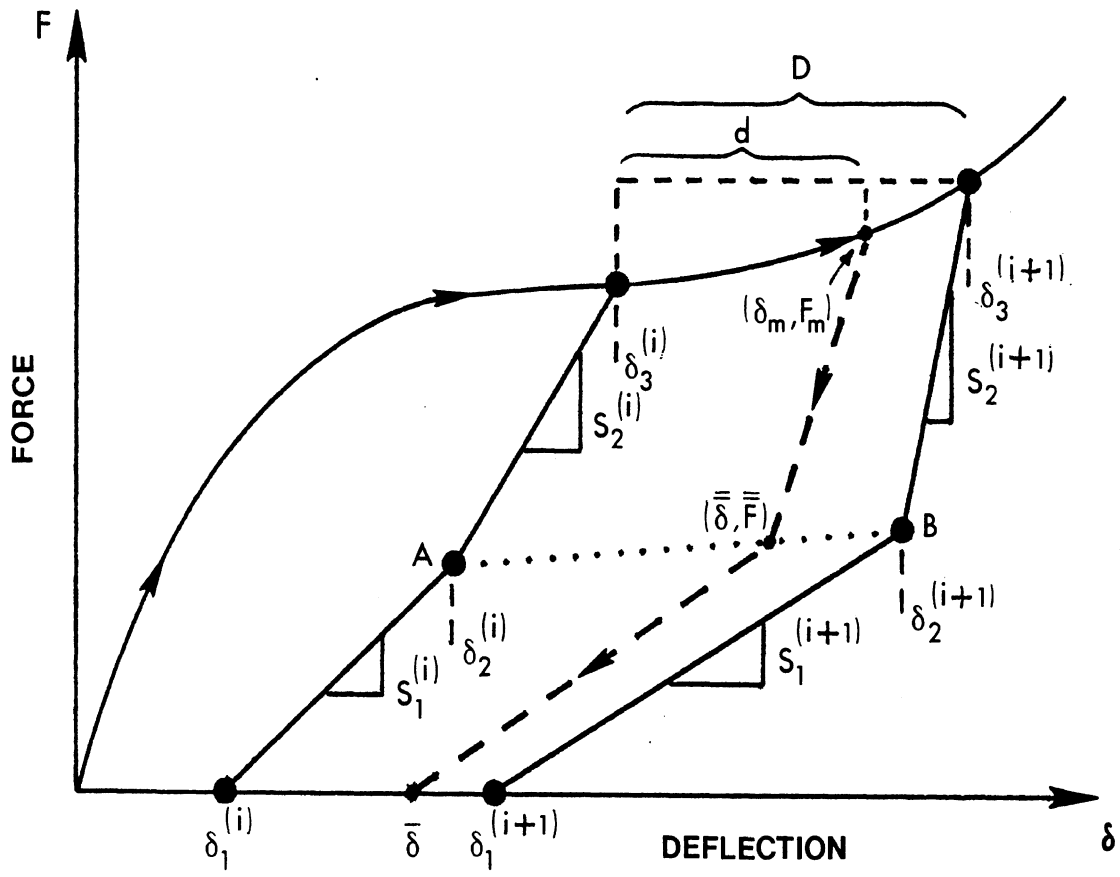
Figure 12-1. Bilinear Unloading Curves

and slopes S_1 and S_2.

A bilinear unloading curve for unloading from a deflection δ_m between $\delta_3^{(i)}$ and $\delta_3^{(i+1)}$ for two adjacent user-prescribed unloading curves is determined by interpolation in the following manner. Define quantities D and d as

$$D = \delta_3^{(i+1)} - \delta_3^{(i)}$$
$$d = \delta_m - \delta_3^{(i)} \quad . \tag{53-1}$$

Consider the dotted line between points A and B. The "breakpoint" for the computed bilinear curve is required to lie on this line at a point between A and B. It will be at endpoint A for d/D equal to 0 and at endpoint B for d/D equal to 1. Intermediate positions are in proportion to d/D, i.e., the coordinates of the point $(\bar{\bar{\delta}}, \bar{\bar{F}})$ are

$$\bar{\bar{\delta}} = \delta_2^{(i)} + \frac{d}{D}\left(\delta_2^{(i+1)} - \delta_2^{(i)}\right) \tag{53-2}$$

$$\bar{\bar{F}} = S_1^{(i)}\left(\delta_2^{(i)} - \delta_1^{(i)}\right) + \frac{d}{D}\left[S_1^{(i+1)}\left(\delta_2^{(i+1)} - \delta_1^{(i+1)}\right) - S_1^{(i)}\left(\delta_2^{(i)} - \delta_1^{(i)}\right)\right] \quad .$$

Similarly, the point on the F = 0 axis which divides the segment between $\delta_1^{(i)}$ and $\delta_1^{(i+1)}$ in the ratio d/D is $(\bar{\delta}, \bar{F})$, where

$$\bar{\delta} = \delta_1^{(i)} + \frac{d}{D}\left(\delta_1^{(i+1)} - \delta_1^{(i)}\right)$$
$$\bar{F} = 0 \quad . \tag{53-3}$$

Let each segment of the bilinear unloading from δ_m be expressed by

$$F = S\delta + K, \tag{53-4}$$

where S is the slope and K is the F-intercept. The parameters of the bilinear unloading curve may be determined from the foregoing results as

lower segment
$$\begin{cases} \bar{S}_1 = \dfrac{\bar{\bar{F}}}{\bar{\bar{\delta}} - \bar{\delta}} \\[4mm] \bar{K}_1 = -\bar{S}_1 \bar{\delta} \end{cases}$$

$$\hspace{4cm} (53\text{-}5)$$

upper segment
$$\begin{cases} \bar{\bar{S}}_2 = (F_m - \bar{\bar{F}})/(\delta_m - \bar{\bar{\delta}}) \\[4mm] \bar{\bar{K}}_2 = \bar{\bar{F}} - \bar{\bar{S}}_2 \bar{\bar{\delta}} \end{cases} .$$

Reloading is always along a straight line toward the point on the Static Curve from which the previous unloading began. This reloading model is reasonable for normal materials. Whether the permanent deformation associated with unloading is large or small, reloading hysteresis exhibited by normal materials is approximated by this model. The equation of the reloading curve is

$$F_R(\delta) = \eta_1 + \eta_2 \delta \hspace{3cm} (54)$$

where
$$\eta_1 = f - \omega_2 (F' - f)/(\Omega - \omega_2) \hspace{2cm} (55)$$

and
$$\eta_2 = (F' - f)/(\Omega - \omega_2) \hspace{2.5cm} (56)$$

One special case which should be mentioned is described by the line
$\overline{\omega \; \omega_2 \; \omega_1}$ in Figure 9. The material unloads partially from point F' to
ω_2 and then reloads partially from ω_2 to ω_1. In this case, unloading from ω_1
proceeds back down the same curve to ω_2 where the normal unloading to ω is
resumed.

In the case of belts, force-strain is allowed as an optional replacement
for force-deflection. If this option is elected, then δ_A, δ_B, δ_C, δ_D, δ_F, β,
and the specifications of both the Static Curve and the Inertial Spike Curve
are treated as strain instead of deflection. The Static and Inertial Spike
Curves are evaluated after the current deflection has been converted to strain.
Unloading and reloading are carried out as described above except that the
input quantities are first converted to deflections before being used.

2.4.2   Mutual Deformation Between Two Force Producers

In the real world, when two bodies are pushed into each other, both will deform although by different amounts depending on material properties. If we imagine an ellipse being pushed into a line, (see Figure 13) the combined deflection (δ) is defined as the distance from the undisturbed line to the tangent line of the ellipse parallel to the line. The combined deflection is distributed between the two surfaces, each deflection being the distance from the undeformed shape to the deformed shape.

At any point in time, we know everything about the past, we are able to compute the combined deformation, and we know the force-deformation properties for each surface. The two components of the total deformation are assumed at each time to be such that the two force producers yield balancing (equal) forces. Expressed mathematically, we assume that we have found the actual deformation when we satisfy the following system of equations.

$$\delta_1 + \delta_2 = \delta$$
$$F(\delta_1) = G(\delta_2) \tag{57}$$

Here,

δ = the combined deflection

δ_1 = the deflection felt by the first force producer

δ_2 = the deflection felt by the second force producer

$F(\delta_1)$ = force-deformation function of the first force producer

$G(\delta_2)$ = force-deformation function of the second force producer.

This system can be simplified by solving the first equation for one of the unknowns and substituting into the second equation.

$$\Delta(\delta_1) = F(\delta_1) - G(\delta-\delta_1) = 0 \tag{58}$$
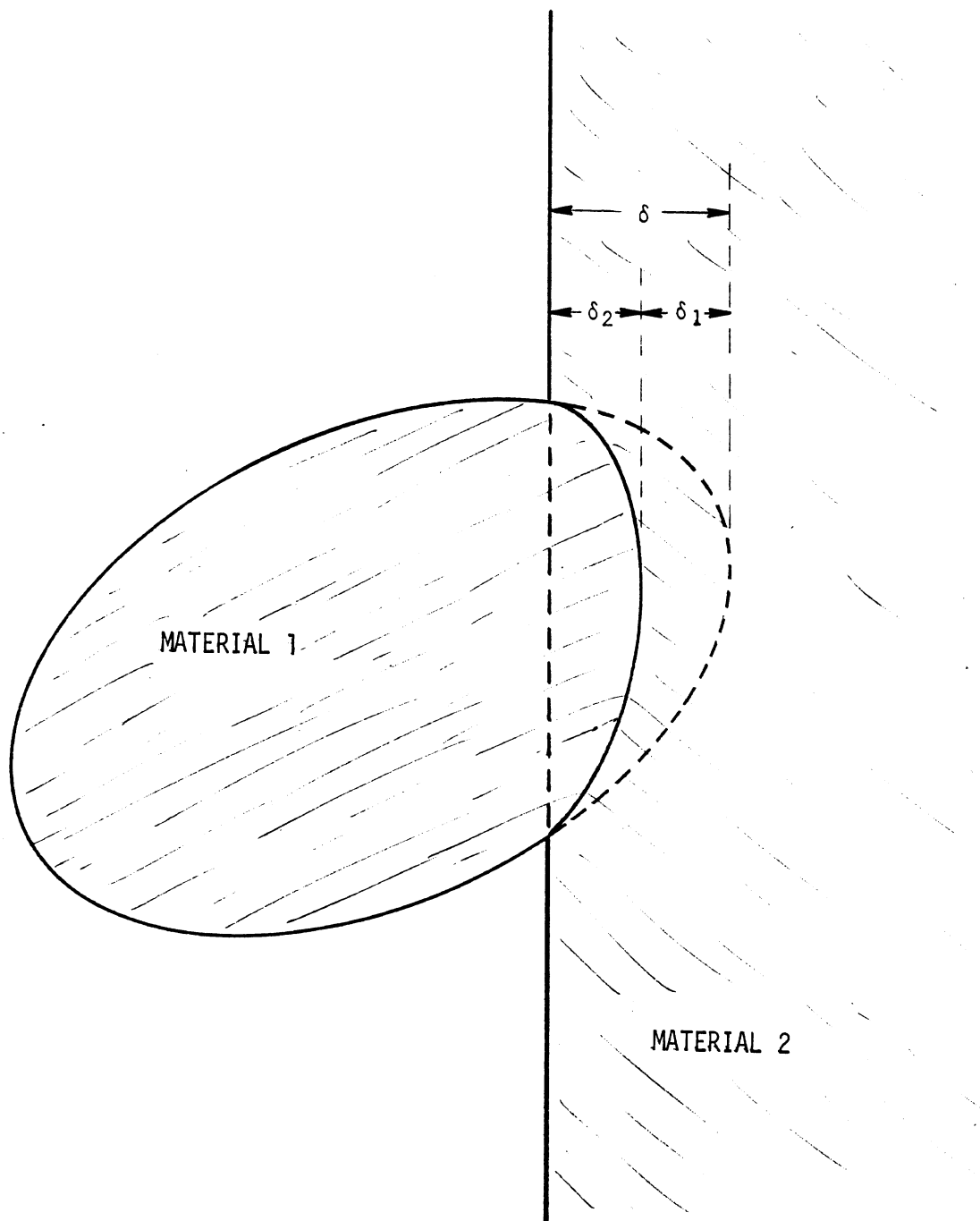
Figure 13. Mutual Deformation of an Ellipse on a Line

Satisfying (57) amounts to finding the zero of a single variable function in (58) and then recovering δ_2 from the first equation of (57). The system (57) is solved using an iteration based on three basic methods. Since all the deflections can be considered functions of time and since the integration of the equations of motion require frequent evaluations in time, the first step of the iteration is based on a linear extrapolation of the two load-deformation curves.

$$\delta_1(t) = \delta_1(t-\Delta t) + \frac{G'(\delta-\delta_1)\big|_{t=t-\Delta t}\left[\delta(t)-\delta(t-\Delta t)\right]}{\left[F'(\delta_1) + G'(\delta-\delta_1)\right]\big|_{t=t-\Delta t}} \tag{59}$$

where

$$G'(\delta-\delta_1) = \frac{dG}{d(\delta-\delta_1)}$$

$$F'(\delta_1) = \frac{dF}{d\delta_1}$$

and Δt = the time since the last evaluation.

The second step is a direct application of Newton's method.

$$\delta_{12} = \delta_{11} - \frac{\Delta(\delta_{11})}{\Delta'(\delta_{11})} \tag{60}$$

where

the second subscript on the δ's signifies the iteration step number

and

$$\Delta' = \frac{\partial\Delta}{\partial\delta} = F' + G'$$

The third step employed depends upon the outcome of the second step. If the second step or any later step is on the opposite side of the zero of $\Delta(\delta_1)$ from the previous step, the method of halving the interval is employed to complete the iteration.

58   1/6/82

$$\delta_{1n} = 1/2(\delta_{1+} + \delta_{1-}) \tag{61}$$

where δ_{1+} and δ_{1-} are chosen from all previous values of δ_1 such that $\Delta(\delta_{1+}) > 0$, $\Delta(\delta_{1-}) < 0$, and $|\delta_{1+} - \delta_{1-}|$ is minimized.

If at the third step or later steps it has not yet happened that two evaluations of $\Delta(\delta_1)$ have straddled the zero point, the classical secant method is employed.

$$\delta_{1m} = \delta_{1,m-1} - \frac{\Delta(\delta_{1,m-1})\left[\delta_{1,m-1} - \delta_{1,m-2}\right]}{\Delta(\delta_{1,m-2}) - \Delta(\delta_{1,m-1})} \tag{62}$$

This type of step is continued until a point is obtained for which the value of $\Delta(\delta_1)$ has the opposite sign of previous evaluations. The total number of steps due to all methods is limited to an inputted number.

2.4.3 Addition of Generalized Forces from Contacts

Suppose the occupant to be in contact with a force producer of the type of Sections 2.4.1 and 2.4.2, i.e., one for which the contact force is definable in terms of deformation. The potential energy associated with such an interaction is

$$V = \int_0^\delta f(x)dx, \tag{63}$$

where $f(x)$ is the force-deflection relationship. Contributions to Equation 6 will be of the form

$$Q_i = -\frac{\partial V}{\partial q_i} = -\frac{\partial V}{\partial \delta}\frac{\partial \delta}{\partial q_i} = -f(\delta)\frac{\partial \delta}{\partial q_i} \tag{64}$$

$$\text{for } i = 1, \ldots, 14$$

The quantity $\partial \delta/\partial q_i$ will be referred to as the "lever arm." If the generalized coordinate is rotational and the force for the force producer such that it tends to push or pull the body segment in a direction perpendicular to the line joining the center of rotation to the point of application of the force, then this quantity will be the actual length of that line and hence, the lever arm. In other cases, it contains factors which yield the perpendicular component of the force as well as is an "effective lever arm." Equation 64 strongly resembles the relation Torque = Force X Lever arm; thus the reason for adopting this nomenclature. In general, the generalized forces Q_i are

$$Q_i = -\sum_{j=1}^{N} f_j \frac{\partial \delta_j}{\partial q_i} \tag{65}$$

for N such force producers.

A convenient usage of the lever arms is noted here. The chain rule gives

$$\frac{d}{dt}\left[\delta(\varphi_1, \cdots, \varphi_N)\right] = \sum_{k=1}^{N} \frac{\partial \delta}{\partial \varphi_k} \frac{d\varphi_k}{dt} \tag{66}$$

60

where the ϕ's are the variables, including the 14 generalized coordinates, upon which deflection depends. Hence, $\dot{\delta}$, whenever needed, can be computed by summing up each lever arm times the corresponding generalized velocity. In most cases, this is the actual technique employed.

Contact forces, deflection and lever arms will be explicitly defined in Section 2.6.

2.4.4 <u>Addition of Generalized Forces from Belts, Airbag, and Steering Assembly</u>

In the derivation of the generalized force corresponding to each generalized coordinate, it is assumed that the applied forces are resolved to two components of force along the inertial axis directions at the segment center of mass, and a moment of force about the center of mass as shown in Figure 14.

The virtual work done during a virtual displacement and rotation of the center of mass is:

$$\sum_i P_i^x \, \delta x_i + P_i^z \, \delta z_i + M_i^f \, \delta \theta_i = \delta W \qquad (67)$$

or:

$$\sum_j \sum_i P_i^x \frac{\partial x_i}{\partial q_j} \delta q_j + P_i^z \frac{\partial z_i}{\partial q_j} \delta q_j + M_i^f \frac{\partial \theta_i}{\partial q_j} \delta q_j = \delta W \qquad (68)$$

or

$$\sum_j Q_{q_j} \, \delta q_j = \delta W \qquad (69)$$

Consequently, since the virtual displacements of the generalized coordinates are independent and arbitrary,
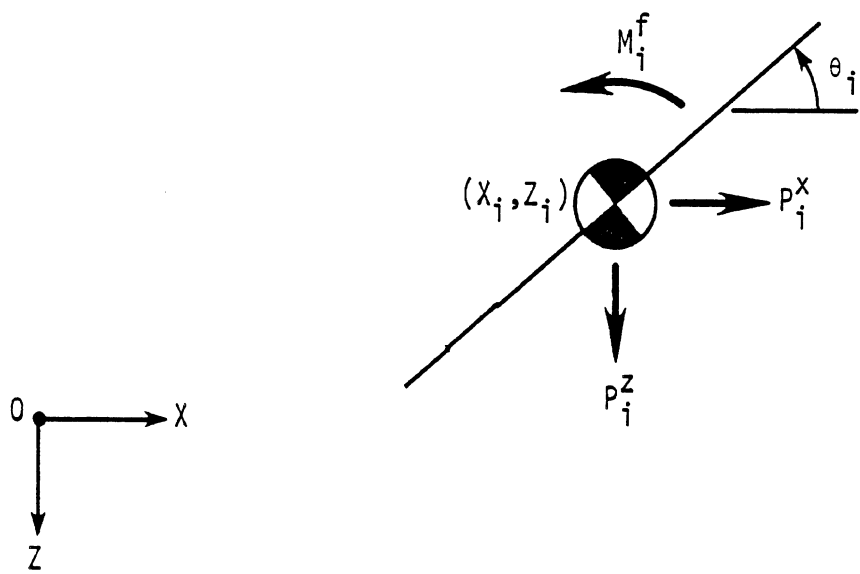
Figure 14. Resultant Forces and Moment on Body Segment i

$$Q_{q_j} = \sum_i \left(P_i^x \frac{\partial x_i}{\partial q_j} + P_i^z \frac{\partial z_i}{\partial q_j} + M_i^f \frac{\partial \theta_i}{\partial q_j} \right) \qquad (70)$$

Carrying out the indicated operations for the generalized coordinates for forces and moments that exist at any time, t, we obtain Equations (71):(see next page.)

The components of force and moment acting on each segment are obtained from the summation of the individual external forces derived in following sections for belts*, airbag, and steering assembly.

---

* Generalized forces for the advanced belt system (BELT2) are found as forces multiplied by lever arms in the manner of Section 2.4.3 rather than as explained in this section for the MODROS belt model (BELT).

$$Q_{x_2} = \sum_{i=1}^{8} P_i^x$$

$$Q_{z_2} = \sum_{i=1}^{8} P_i^z$$

$$Q_{\theta_1} = P_1^x \ell_1 \sin\theta_1 + P_1^z \ell_1 \cos\theta_1 + M_1^f$$

$$Q_{\theta_2} = P_1^x \ell_2 \sin\theta_2 - (L_{23} - \ell_2)\left[P_3^x + P_4^x + P_5^x + P_6^x\right]\sin\theta_2 + P_1^z \ell_2 \cos\theta_2$$
$$- (L_{23} - \ell_2)\left[P_3^z + P_4^z + P_5^z + P_6^z\right]\cos\theta_2 + (P_7^x + P_8^x)(-L_{27}\sin\theta_{27}$$
$$- X_S \sin\theta_2 + z_S \cos\theta_2) + (P_7^z + P_8^z)(-L_{27}\cos\theta_{27} - X_S \cos\theta_2 - z_S \sin\theta_2) + M_2^f$$

$$Q_{\theta_3} = -\left\{\left[P_3^x \ell_3 + L_{34}(P_4^x + P_5^x + P_6^x)\right]\sin\theta_3 + \left[P_3^z \ell_3 + L_{34}(P_4^z + P_5^z + P_6^z)\right]\cos\theta_3\right\} + M_3^f$$

$$Q_{\theta_4} = -\left\{\left[P_4^x \ell_4 + L_{45}(P_5^x + P_6^x)\right]\sin\theta_4 + \left[P_4^z \ell_4 + L_{45}(P_5^z + P_6^z)\cos\theta_4\right]\right\} + M_4^f$$

$$Q_{\theta_5} = -\left\{(P_5^x \ell_5 + L_{56} P_6^x)\sin\theta_5 + (P_5^z \ell_5 + L_{56} P_6^z)\cos\theta_5\right\} + M_5^f$$

$$Q_{\theta_6} = -\left[P_6^x \ell_6 \sin\theta_6 + P_6^z \ell_6 \cos\theta_6\right] + M_6^f \tag{71}$$

$$Q_{\theta_7} = -\left[(P_7^x \ell_7 + L_{78} P_8^x)\sin\theta_7 + (P_7^z \ell_7 + L_{78} P_8^z)\cos\theta_7\right] + M_7^f$$

$$Q_{\theta_8} = -\left[P_8^x \ell_8 \sin\theta_8 + P_8^z \ell_8 \cos\theta_8\right] + M_8^f$$

$$Q_{\theta_n} = P_1^x L_n \sin\theta_n + P_1^z L_n \cos\theta_n$$

$$Q_{L_n} = -P_1^x \cos\theta_n + P_1^z \sin\theta_n$$

$$Q_{X_S} = (P_7^x + P_8^x)\cos\theta_2 - (P_7^z + P_8^z)\sin\theta_2$$

$$Q_{z_S} = (P_7^x + P_8^x)\sin\theta_2 + (P_7^z + P_8^z)\cos\theta_2$$

2.4.5 Addition of Head Applied Forces

Provision is made for direct application of a time-dependent force to any specified point on the head. Force components F_X and F_Z may be specified either in head coordinates or inertial coordinates. Tabular force-time curves are inputted on 606-cards.

The generalized forces for a force $\vec{F}$ applied at a point with inertial position vector $\vec{r}$ are

$$Q_k = \vec{F} \cdot \frac{\partial \vec{r}}{\partial q_k} \quad . \tag{71.1}$$

Let F_X and F_Z be applied force components in the head frame. Let a and c be the coordinates in the head system of the point of force application (see Fig. 15).

Then, where I and K are the inertial unit vectors, equation 71.1 becomes

$$Q_k = \left(F_X \hat{\imath}_1 + F_Z \hat{k}_1 \right) \cdot \frac{\partial \left(x_1 I + z_1 K + a \hat{\imath}_1 + c \hat{k}_1 \right)}{\partial q_k} . \tag{71.2}$$

It is easily shown that equation 71.2 becomes

$$Q_k = \left(F_X \cos\theta_1 + F_Z \sin\theta_1 \right) \frac{\partial x_1}{\partial q_k}$$
$$+ \left(-F_X \sin\theta_1 + F_Z \cos\theta_1 \right) \frac{\partial z_1}{\partial q_k} + \begin{cases} \left(c F_X - a F_Z \right) & \text{if } q_k = \theta_1 \\ 0 & \text{if } q_k \neq \theta_1 \end{cases} \tag{71.3}$$

where the head coordinates (x_1, z_1) are given by equation 3. Clearly, contributions to the equations of motion result only for $q_k = (x_2, z_2, \theta_1, \theta_2, \theta_n, L_n)$.

If inertial force components $\overline{F}_X$ and $\overline{F}_Z$ are inputted, then equation 71.3 still applies, but the force components F_X and F_Z are calculated as:

$$F_X = \overline{F}_X \cos\theta_1 - \overline{F}_Z \sin\theta_1$$
$$F_Z = \overline{F}_X \sin\theta_1 + \overline{F}_Z \cos\theta_1 \quad . \tag{71.4}$$

65
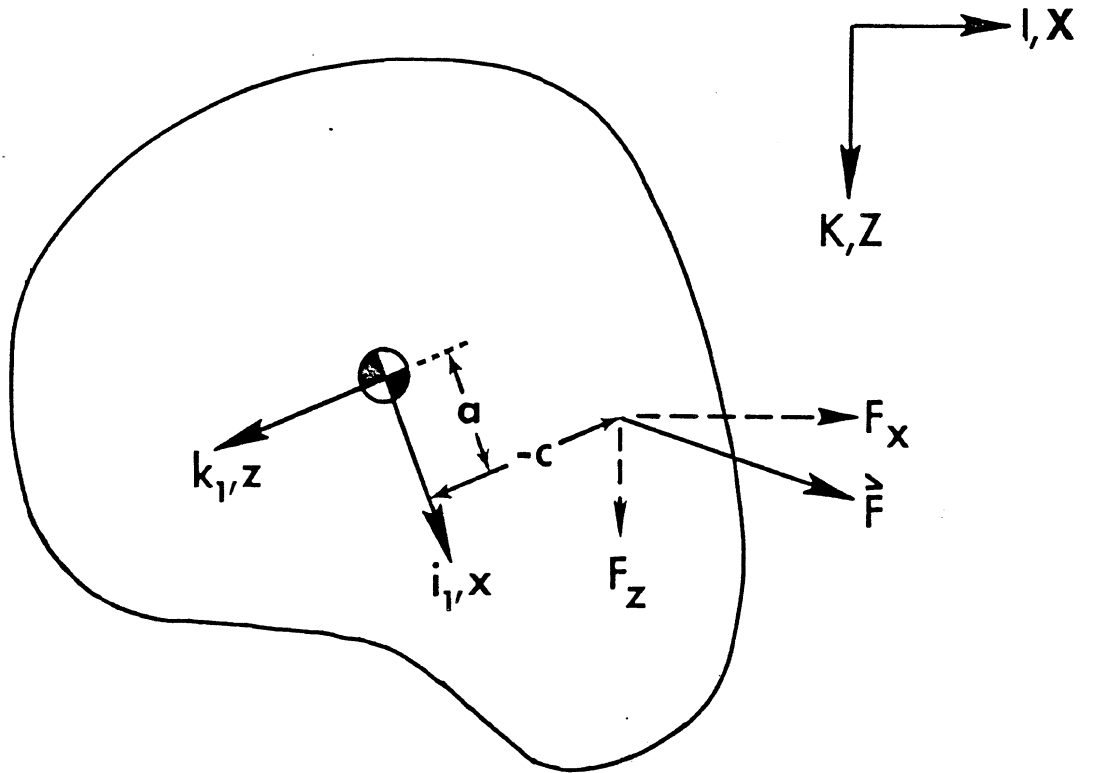
FIGURE 15. Schematic of Force Applied to Head

2.5 COMPUTATION OF BELT FORCES

The MVMA Two-Dimensional Crash Victim Simulator includes two independent belt system models for optional usage. The first, hereafter designated as BELT (Figure 16), consists of: a) a one-piece lap belt attached to the lower torso element and anchored at each end to the vehicle; b) an upper torso harness strap attached to the upper torso element and anchored to the vehicle; c) a lower torso harness strap attached optionally to any torso element and anchored to the vehicle. The second, hereafter designated as BELT2, includes the following features: a) seven belt segments (see Figure 17) which may be independent or, at option, may be paired in certain combinations to act as a lesser number of separate lengths of webbing by use of various free slipping and friction elections at the torso and lap and at slip points; b) a slip point in the three-belt upper harness system; c) a slip point between the lower torso and lap sections; d) optionally, inertia reels (either vehicle sensitive or webbing sensitive) at three of the four anchor locations.

The analysis for the BELT submodel follows in Section 2.5.1. The analysis for the advanced belt system BELT2, is in Section 2.5.2.

2.5.1 A Three-Belt Submodel (BELT)

A lap belt and two individual belt elements attached to the torso provide belt restraint. The lap belt is assumed to pass over the pelvic region at a given point and remain attached to the pelvic segment at that point. The belt anchor points in the vehicle need not be coincident and the right and left sides of the belt can be of unequal length. Equal tension is assumed in the lap belt. The upper torso restraint consists of two individual straps; an upper strap attached to a fixed point either on or off the upper torso link, and a lower strap attached to a fixed point either on or off the upper, mid, or lower torso link. Experience with

67

$+\xi$ downward along body

$+\zeta$ toward back of body

(X_3^{SA}, Z_3^{SA})

ψ_3^B

ξ_2^B

ζ_2^B

1

2

3

ξ_3^B

ζ_3^B

4

$-\zeta_1^B$

(X_4^{SA}, Z_4^{SA})

ψ_4^B

ξ_1^B

ψ_2^b

5

(X_2^{SA}, Z_2^{SA})

ψ_1^b

(X_1^{SA}, Z_1^{SA})

X

X^V

θ_V

Z

Z^V

(X,Z) = inertial coordinates

(X^V, Z^V) = vehicle space
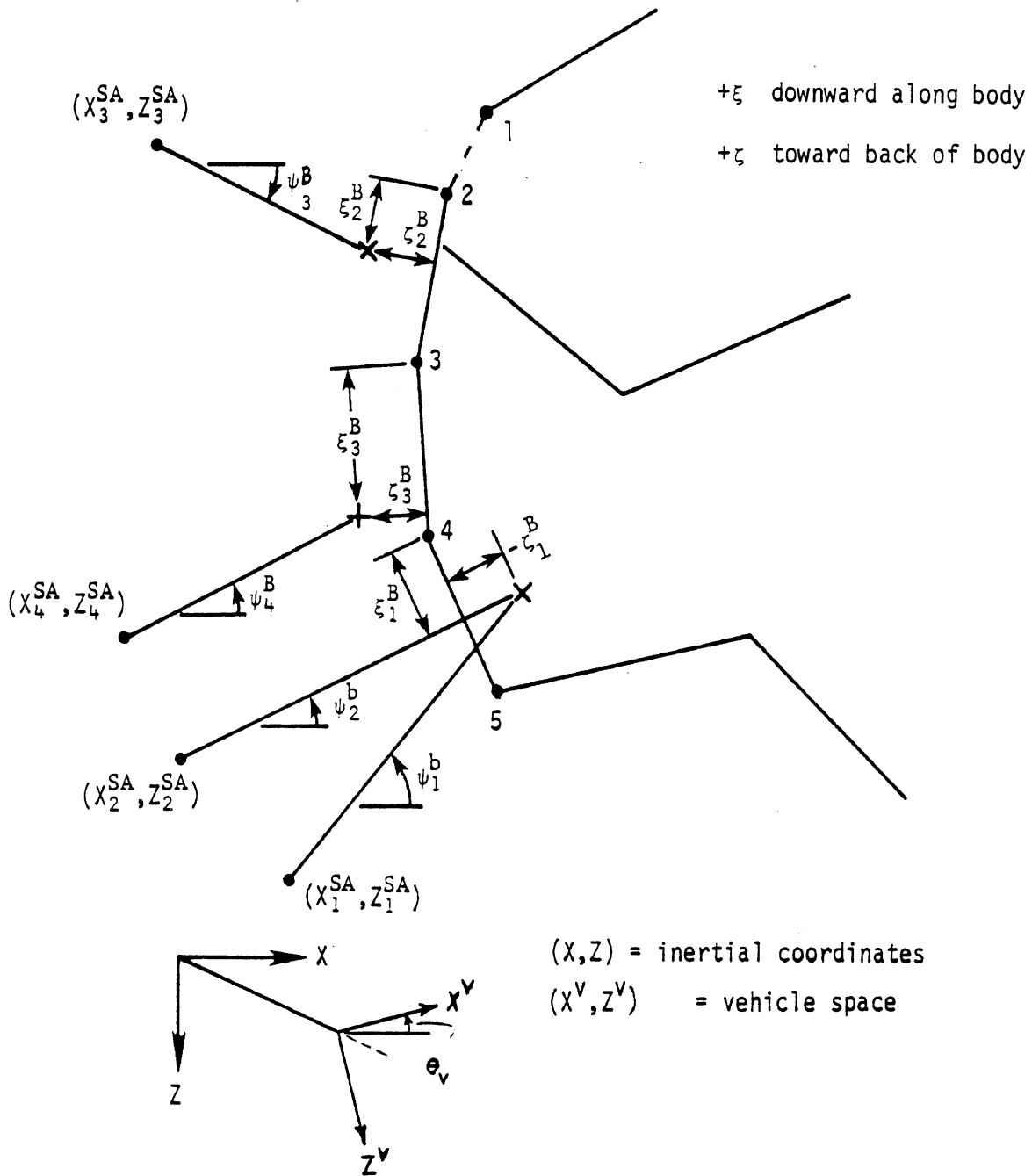
FIGURE 16. Simple Belt System Geometry

68

occupant simulations has shown that independently acting belts can be used to simulate actual belt performance more closely than belts having artificially equal tension. Few changes have been made to the lap belt system incorporated in MODROS (Reference 2). A schematic of belt geometry is included as Figure 12.

TABLE 1
BELT INDEX SPECIFICATIONS (Submodel BELT)

Belt Index	Belt Segment Identification
1	Lap Belt Segment 1 (inboard or outboard)
2	Lap Belt Segment 2 (outboard or inboard)
3	Upper Torso Belt
4	Lower Torso Belt

2.5.1.1 Lap Belt

The position and velocity of the lap belt/pelvic attachment point in space is:

$$
\begin{bmatrix} x_1^B \\ z_1^B \end{bmatrix} = \begin{bmatrix} x_4^J \\ z_4^J \end{bmatrix} + \begin{bmatrix} \cos\theta_4 & \sin\theta_4 \\ -\sin\theta_4 & \cos\theta_4 \end{bmatrix} \begin{bmatrix} \zeta_1^B \\ \zeta_1^B \end{bmatrix} \tag{72}
$$

$$
\begin{bmatrix} \dot{x}_1^B \\ \dot{z}_1^B \end{bmatrix} = \begin{bmatrix} \dot{x}_4^J \\ \dot{z}_4^J \end{bmatrix} + \dot{\theta}_4 \begin{bmatrix} -\sin\theta_4 & \cos\theta_4 \\ -\cos\theta_4 & -\sin\theta_4 \end{bmatrix} \begin{bmatrix} \zeta_1^B \\ \zeta_1^B \end{bmatrix}
$$

where the various geometric quantities are defined in Figure 16, Figure 1 and Equation 1. The positions and velocities in inertial coordinates of the restraint belt anchor positions are given by:

$$\begin{bmatrix} x_i^{SA} \\ z_i^{SA} \end{bmatrix} = \begin{bmatrix} x_v \\ z_v \end{bmatrix} + \begin{bmatrix} \cos\theta_v & \sin\theta_v \\ -\sin\theta_v & \cos\theta_v \end{bmatrix} \begin{bmatrix} x_i^{VA} \\ z_i^{VA} \end{bmatrix}, \quad i = 1, 2, 3, 4$$

(73)

$$\begin{bmatrix} \dot{x}_i^{SA} \\ \dot{z}_i^{SA} \end{bmatrix} = \begin{bmatrix} \dot{x}_v \\ \dot{z}_v \end{bmatrix} + \dot{\theta}_v \begin{bmatrix} -\sin\theta_v & \cos\theta_v \\ -\cos\theta_v & -\sin\theta_v \end{bmatrix} \begin{bmatrix} x_i^{VA} \\ z_i^{VA} \end{bmatrix}, \quad i = 1, 2, 3, 4$$

where

x_v, z_v, θ_v are vehicle coordinates in space.

x_i^{VA}, z_i^{VA} are belt anchor point in vehicle coordinates

The lap belt length is then calculated from

$$\ell^{BL} = \left[(x_1^B - x_1^{SA})^2 + (z_1^B - z_1^{SA})^2 \right]^{1/2}$$
$$+ \left[(x_1^B - x_2^{SA})^2 + (z_1^B - z_2^{SA})^2 \right]^{1/2} + C^{BL}$$

(74)

where C^{BL} is the out of plane webbing length determined from the initial conditions.

$$C^{B} = \ell^{BLO} - \Delta^{BL} - \left[(x_1^B - x_1^{SA})^2 + (z_1^B - z_1^{SA})^2 \right]^{1/2}$$
$$- \left[(x_1^B - x_2^{SA})^2 + (z_1^B - z_2^{SA})^2 \right]^{1/2}$$

(75)

where ℓ^{BLO} is the total measured webbing length and Δ^{BL} is total linear slack.

The lap belt angles are:

$$\psi_i^B = \tan^{-1} \left[\frac{z_i^{SA} - z_1^B}{x_1^B - x_i^{SA}} \right], \quad i = 1, 2$$

(76)

The velocity of belt elongation is:

$$\dot{\ell}^{BL} = \left(\dot{x}_1^B - \dot{x}_1^{SA} \right) \cos \psi_1^B - \left(\dot{z}_1^B - \dot{z}_1^{SA} \right) \sin \psi_1^B$$
$$+ \left(\dot{x}_1^B - \dot{x}_2^{SA} \right) \cos \psi_2^B - \left(\dot{z}_1^B - \dot{z}_2^{SA} \right) \sin \psi_2^B \qquad (77)$$

Finally, the lap belt strain is:

$$\epsilon^{BL} = \frac{\ell^{BL} - \ell^{BLO}}{\ell^{BLO}} \qquad (78)$$

Based on lap belt strain, ϵ^{BL}, and the rate of belt elongation, $\dot{\ell}^{BL}$, a belt force is computed

$$F^{BL} = F^{BL} \left(\dot{\ell}^{BL}, \ \epsilon^{BL} \right) \qquad (79)$$

using the force-deformation rules discussed in Section 2.4.1 and a call to the appropriate HSRI-developed subroutine.* Combining the effects due to both lap belt segments, the components in the x and z inertial directions are

$$F_x^{BL} = - F^{BL} \left(\cos \psi_1^B + \cos \psi_2^B \right)$$
$$F_z^{BL} = F^{BL} \left(\sin \psi_1^B + \sin \psi_2^B \right) \qquad (80)$$

and the moment about the center of gravity of the lower torso element is

$$M_+^B = - F_x^{BL} \left[\left(\xi_1^B - \lambda_4 \right) \sin \theta_4 - \zeta_1^B \cos \theta_4 \right] \qquad (81)$$
$$+ F_z^{BL} \left[\left(\xi_1^B - \lambda_4 \right) \cos \theta_4 + \zeta_1^B \sin \theta_4 \right]$$

*As an option belt force can be determined as a function of elongation instead of strain.

2.5.1.2. "Shoulder" Belt

The shoulder belt is attached at a general point (ξ_2^B, ξ_2^B) on the upper torso element as shown in Figure 16. The length of this belt is

$$\ell^{B3} = \left[(x_2^B - x_3^{SA})^2 + (z_2^B - z_3^{SA})^2 \right]^{1/2} \tag{82}$$

where x_2^B and z_2^B are the locations in space of the belt attachment points on the occupant. They are obtained in a manner similar to the lap belt attachments given in Equation 72. The vehicle anchor points, x_3^{SA} and z_3^{SA}, are given by Equation 73. The shoulder belt angle is given by

$$\psi_3^B = \tan^{-1} \frac{z_3^{SA} - z_2^B}{x_2^B - x_3^{SA}} \tag{83}$$

The shoulder belt strain and rate of elongation are given by ϵ^{BL} and $\dot{\ell}^{B3}$ respectively.

$$\epsilon^{BU} = \left(\ell^{B3} - \ell^{BU} \right) / \ell^{BU}$$

$$\dot{\ell}^{B3} = \left(\dot{x}_2^B - \dot{x}_3^{SA} \right) \cos \psi_3^B - \left(\dot{z}_2^B - \dot{z}_3^{SA} \right) \sin \psi_3^B \tag{84}$$

where ℓ^{BU} is the total unstretched length of the shoulder belt. Belt force is computed as a function of elongation (or strain) and its rate using the general force-deformation relations.

$$F^{BT} = F^{BT} \left(\epsilon^{BU}, \dot{\ell}^{B3} \right) \tag{85}$$

The x and z components of this force are

$$F_x^{BT} = -F^{BT} \cos \psi_3^B \tag{86}$$

$$F_z^{BT} = F^{BT} \sin \psi_3^B$$

and the moment about the center of mass of the upper torso element is:

72

$$M_2^B = F^{BT}\left\{\left[\left(\xi_2^B - \ell_2\right)\sin\Theta_2 - \zeta_2^B\cos\Theta_2\right]\cos\psi_3^B\right.$$
$$\left. - \left[\left(\xi_2^B - \ell_2\right)\cos\Theta_2 + \zeta_2^B\sin\Theta_2\right]\sin\psi_3^B\right\} \qquad (87)$$

2.5.1.3 Lower Torso Belt

A third belt, usually the lower section of the shoulder belt, can be attached at a general point (ξ_3^B, ζ_3^B) located on the lower, middle, or upper torso. The length of this belt is

$$\ell^{B4} = \left[\left(x_3^B - x_4^{SA}\right)^2 + \left(z_3^B - z_4^{SA}\right)^2\right]^{1/2} \qquad (88)$$

where (x_3^B, z_3^B) are the inertial coordinates of the attachment point on the crash victim and (x_4^{SA}, z_4^{SA}) are the inertial coordinates of the belt anchor. The belt angle is

$$\psi_4^B = \tan^{-1}\frac{z_4^{SA} - z_3^B}{x_3^B - x_4^{SA}} \qquad (89)$$

Belt strain and elongation rate are respectively

$$\epsilon^{Bx} = \left(\ell^{B4} - \ell^{BL}\right)/\ell^{BL}$$
$$\dot\ell^{B4} = \left(\dot x_3^B - \dot x_4^{SA}\right)\cos\psi_4^B - \left(\dot z_3^B - \dot z_4^{SA}\right)\sin\psi_4^B \qquad (90)$$

where ℓ^{BL} is the unstretched belt length. The belt force is determined from these quantities in general as

$$F^{BF} = F^{BF}\left(\epsilon^{Bx}, \dot\ell^{B4}\right) \qquad (91)$$

The x and z components of this force are

$$F_x^{BF} = -F^{BF}\cos\psi_4^B$$
$$F_z^{BF} = F^{BF}\sin\psi_4^B \qquad (92)$$

73

and the moment about the center of mass of the particular body segment to
which the belt is attached is given by

$$M_3^B = F^{BF} \left\{ \left[\left(\xi_3^B - \ell_i \right) \sin \theta_i - \xi_3^B \cos \theta_i \right] \cos \psi_4^B \right.$$
$$\left. - \left[\left(\xi_3^B - \ell_i \right) \cos \theta_i + \xi_3^B \sin \theta_i \right] \sin \psi_4^B \right\} \qquad (93)$$

where i = 2, 3, 4 refers to the upper, middle, or lower torso body segment.

2.5.1.4 <u>Addition of Belt Forces to the Equations of Motion</u>

For the three belt elements included in this simulation, the generalized

forces given in Equation 71 reduce to

$$Q_{x_2}^B = P_2^x + P_3^x + P_4^x \quad , \quad Q_{z_2}^B = P_2^z + P_3^z + P_4^z$$

$$Q_{\theta_2}^B = -(L_{23} - \ell_2) \left[(P_3^x + P_4^x) \sin \theta_2 \right.$$
$$\left. + (P_3^z + P_4^z) \cos \theta_2 \right] + M_2^F \qquad (94)$$

$$Q_{\theta_3}^B = - \left[(\ell_3 P_3^x + L_{34} P_4^x) \sin \theta_3 + (\ell_3 P_3^z + L_{34} P_4^z) \cos \theta_3 \right] + M_3^F$$

$$Q_{\theta_4}^B = -\ell_4 \left(P_4^x \sin \theta_4 + P_4^z \cos \theta_4 \right) + M_4^F$$

$$Q_{\theta_1}^B = Q_{\theta_5}^B = Q_{\theta_6}^B = Q_{\theta_7}^B = Q_{\theta_8}^B = Q_{\theta_n}^B = Q_{L_n}^B = Q_{x_s}^B = Q_{z_s}^B = 0$$

For the case of a lap belt only, the various quantities in Equation 94 are

$$P_2^x = P_3^x = P_2^z = P_3^z = M_2^F = M_3^F = 0$$

$$P_4^x = F_x^{BL}, \quad P_4^z = F_z^{BL}, \quad M_4^F = M_4^B \qquad (95)$$

For the case of a lap belt and both torso harnesses on the upper torso

element (2), the various quantities in Equation 94 are

$$P_2^x = F_x^{BT} + F_x^{BF}, \quad P_2^z = F_z^{BT} + F_z^{BF}, \quad M_2^F = M_2^B + M_3^B$$

$$P_3^x = P_3^z = M_3^F = 0 \qquad (96)$$

$$P_4^x = F_x^{BL}, \quad P_4^z = F_z^{BL}, \quad M_4^F = M_4^B$$

For the case of a lap belt, the shoulder harness on the upper torso, and the lower harness on the middle torso, the various quantities in Equation 94 are

$$P_2^x = F_x^{BT}, \quad P_2^z = F_z^{BT}, \quad M_2^F = M_2^B$$

$$P_3^x = F_x^{BF}, \quad P_3^z = F_z^{BF}, \quad M_3^F = M_3^B$$

$$P_4^x = F_x^{BL}, \quad P_4^z = F_z^{BL}, \quad M_4^F = M_4^B \tag{97}$$

For the case of a lap belt and the lower harness attached to the lower torso as well as the shoulder strap attached to the upper torso, the various quantities in Equation 94 are

$$P_2^x = F_x^{BT}, \quad P_2^z = F_z^{BT}, \quad M_2^F = M_2^B$$

$$P_3^x = P_3^z = M_3^F = 0 \tag{98}$$

$$P_4^x = F_x^{BL} + F_x^{BF}, \quad P_4^z = F_z^{BL} + F_z^{BF}, \quad M_4^F = M_4^B + M_3^B$$

With the specific terms defined in Equations 95-98 the generalized force contributions from belts (Equation 94) are entered into the equations of motion through the D vector, Equation 28.

2.5.2 An Advanced Belt System Submodel (BELT2)

The system has four anchor points, designated as A_1, A_2, A_3, A_4. Anchor "deformation" (for frame and/or spoolout) force-deflection data may be specified for any anchor. Any of the anchors A_1, A_2, A_3 may have vehicle-sensitive or webbing-sensitive lockup characteristics. The outboard lap belt anchor A_4 is always locked, i.e., the outboard lap belt segment, if present, fastens securely to this anchor.

The system includes two slip points where three belt segments come together. One is in the upper harness system and one is between the lower

4/3/87

75
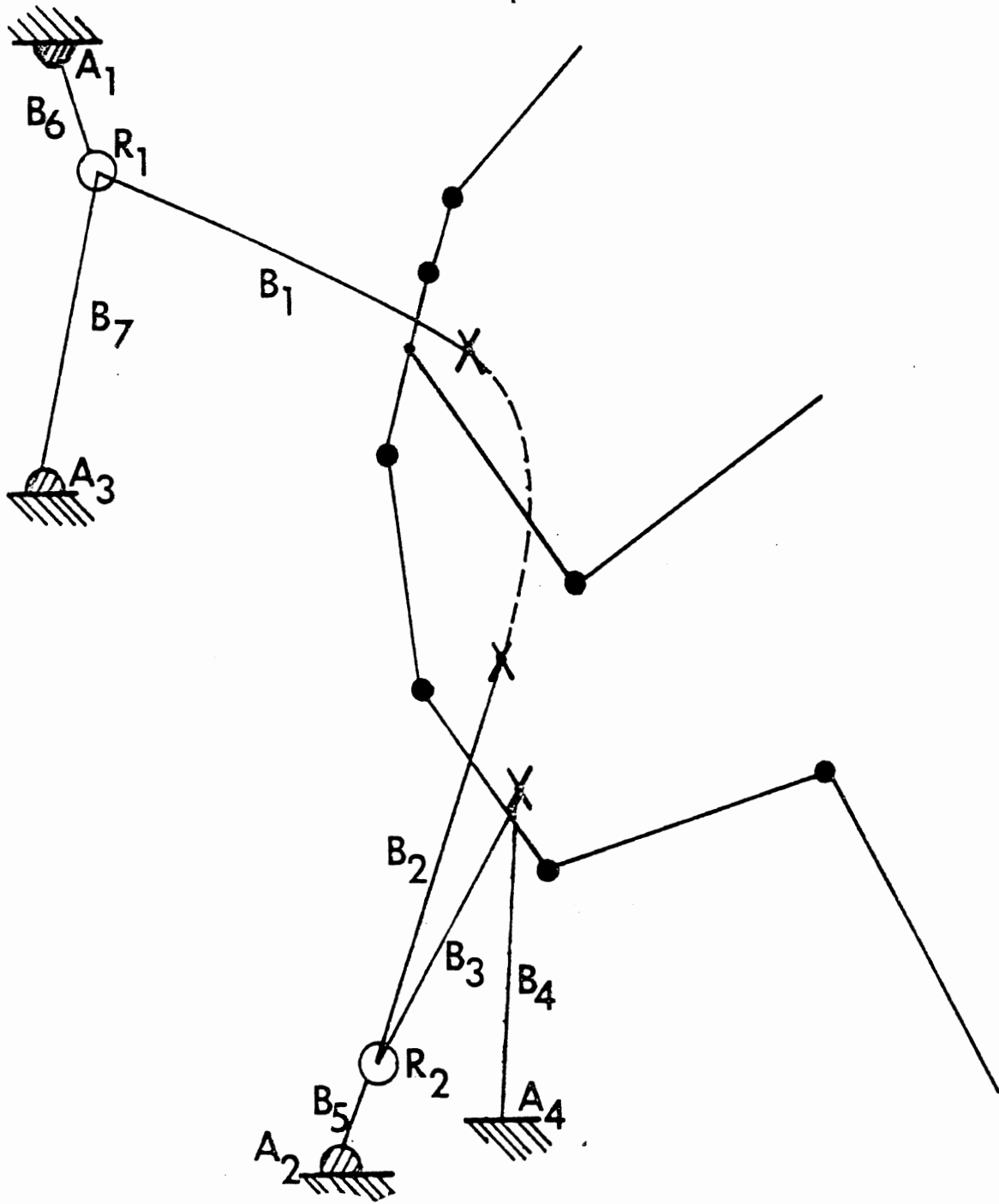
FIGURE 17. Advanced Belt System Geometry

torso and lap sections. The slip points are R_1 and R_2 in Figure 17 and hereafter will be called "ring 1," or the "upper ring," and "ring 2," or the "lower ring." The rings may be fastened to ring straps, which lead to anchors A_1 and A_2, or they may be fixed to the vehicle frame at anchor locations A_1 and A_2, in which case the corresponding ring strap(s) (B_6 and/ or B_5) are absent. Belt segments B_5 and B_6 are always "independent" of other belt segments since they fasten to the slip rings. Through each ring, however, passes a strap of webbing shown in the figure as a pair of belt segments, either B_1 and B_7 or B_2 and B_3. At option the members of these pairs can be made independent by prohibiting slipping of the combined strap through the ring. In this case the ring location is a juncture of three independent straps of webbing. The pairs B_1-B_7 and B_2-B_3, however, may be considered common straps that may slip freely through their respective rings or with an amount of frictional resistance which depends on the resultant normal force at the ring.

TABLE 2.
BELT INDEX SPECIFICATIONS (Submodel BELT2)

Belt Index	Belt Segment Identification
1	Upper torso belt
2	Lower torso belt
3	Inboard lap belt
4	Outboard lap belt
5	Lower ring strap
6	Upper ring strap
7	Upper torso belt extension

The upper and lower torso belts, B_1 and B_2, may be independent or the separate belt forces may be made interdependent by use of inter-belt influence options. These are of three types: a) a force adjustment determined on the basis of normal force friction at the torso surface; b) an adjustment for maintaining a force-difference saturation level; c) a positive or negative percentage influence of one belt force on the other. In addition a force equalization option is available for the torso belt and lap belt combinations. Torso and lap belt segments attach to the occupant at points on the torso elements. The upper torso belt attachment is on the upper torso element and the attachment for lap belt segments is on the lower torso. The user may specify an attachment on any of the three torso elements for the lower torso belt.

Force-deformation relations for belt segments may be inputted in either tabular or polynomial form. They may be either force-strain relations or force-deflection relations, but a mixture for the various belt segments is not allowed. Strain is taken as deflection divided by the unstrained strap length. Further, belts B_1 and B_7 should have the same material unless they are made independent by the conditions at R_1. In general, any belt segments that should be treated as parts of a common strap should be assigned the same material.* Whenever belts should be treated as a common strap but the materials for the separate segments are different, the program arbitrarily uses the material for one of the members.

2.5.2.1 <u>Belt Deflections and Lever Arms</u>

Deflection is defined as elongation beyond the unstrained belt length and is formulated as

$$\delta_n = \ell_n(t) - \ell_n(o) \tag{99}$$

---

*Segments are independent if separated by no-slip specifications at ring or body.

where

$$\ell_n(o) = \left| \vec{P}_T + \vec{\beta}_n - \vec{P}_V - \vec{\alpha}_n \right|_{t=0} + \Delta_n \tag{100}$$

$$\ell_n(t) = \left| \vec{P}_T + \vec{\beta}_n - \vec{P}_V - \vec{\alpha}_n \right| \tag{101}$$

n is belt segment number (1, 2, 3, or 4)

$\vec{\alpha}_n$ is anchor position vector (see Figure 18)

$\vec{\beta}_n$ is attachment position vector

Δ_n is the specified slack in the belt (negative for initial belt tension)

$\vec{P}_T$ is the position vector of the torso element CG

$\vec{P}_V$ is the position vector of the vehicle reference point

The components of $\vec{\alpha}_n$ and $\vec{\beta}_n$ are taken relative to vehicle and torso

element coordinate systems as shown in the following equations:

$$\vec{\alpha}_n = \lambda_n \,\hat{\imath}_V + \nu_n \,\hat{k}_V \tag{102}$$
$$\vec{\beta}_n = r_n \,\hat{\imath}_j + t_n \,\hat{k}_j$$

Here, j can be 2, 3, or 4, corresponding to the three torso elements. The

inertial position of the anchor point is:

$$\hat{X}_n = x^V + \lambda_n \cos\theta^V + \nu_n \sin\theta^V$$

$$\hat{Z}_n = z^V - \lambda_n \sin\theta^V + \nu_n \cos\theta^V \tag{103}$$

and the inertial position of the torso attachment point is:

$$\hat{x}_n = X_j + r_n \cos\theta_j + t_n \sin\theta_j \tag{104}$$

$$\hat{z}_n = z_j - r_n \sin\theta_j + t_n \cos\theta_j$$

Hence,

$$\ell_n = \sqrt{ \left(\hat{X}_n - \hat{x}_n \right)^2 + \left(\hat{Z}_n - \hat{z}_n \right) } \quad . \tag{105}$$

Attachment
to Occupant

Torso Element
CG

$\vec{\beta}_n$

i_j

Torso System j

ℓ_n

k_j

Vehicle
Reference Point

Vehicle
System

i_v

$\vec{\alpha}_n$

k_v

$\vec{P}_T$

Anchor Point

$\vec{P}_V$
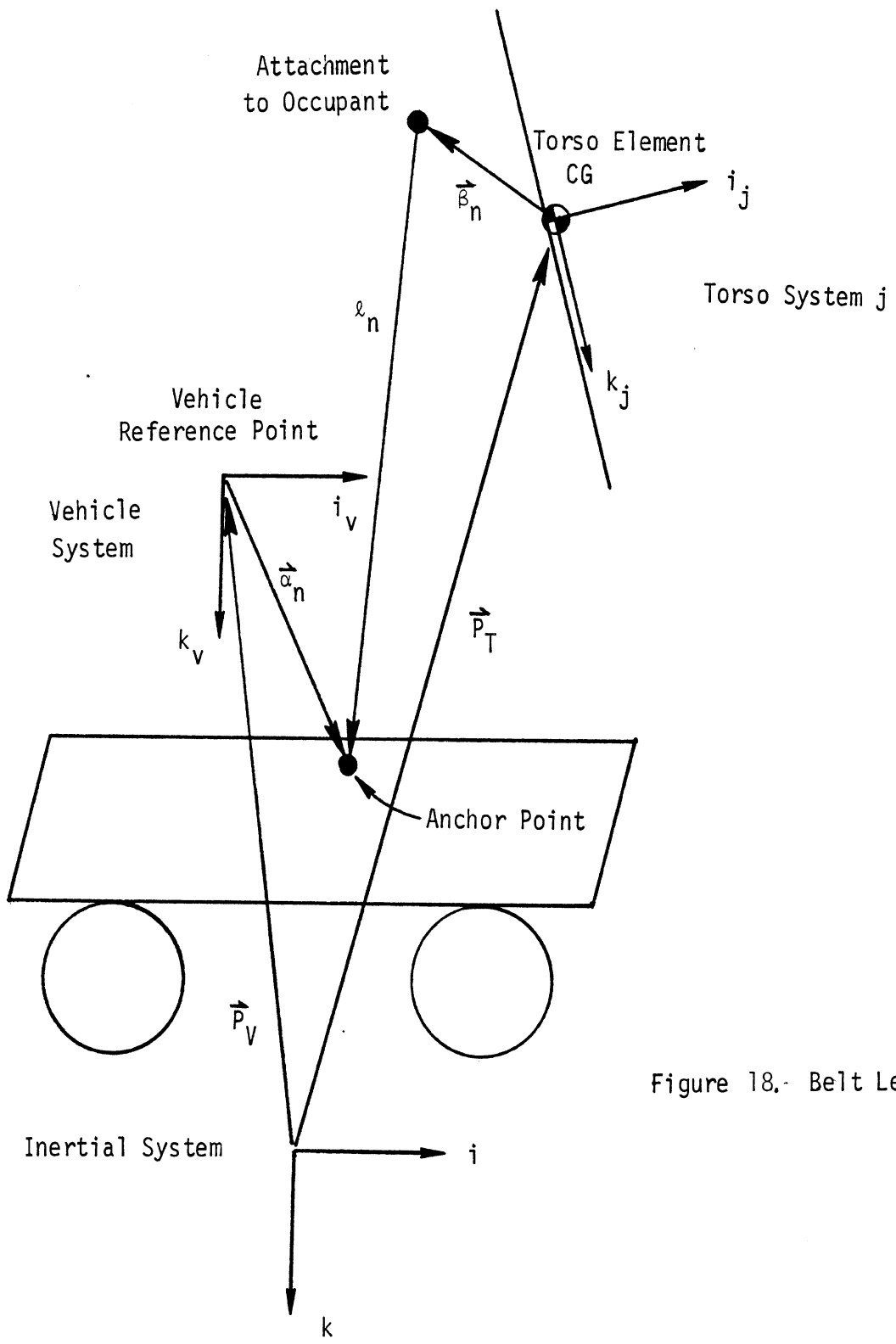
Figure 18.- Belt Length

Inertial System

i

k

80

Lever arms then take the form

$$\frac{\partial \delta_n}{\partial q_i} = \frac{\hat{x}_n - \hat{X}_n}{\ell_n} \frac{\partial \hat{x}_n}{\partial q_i} + \frac{\hat{z}_n - \hat{Z}_n}{\ell_n} \frac{\partial \hat{z}_n}{\partial q_i} \quad . \quad (106)$$

Here, the partials of $\hat{x}_n$ and $\hat{z}_n$ are

$$\frac{\partial \hat{x}_n}{\partial q_i} = \frac{\partial x_j}{\partial q_i} - \left(r_n \sin\theta_j - t_n \cos\theta_j \right) \delta_{i-2,j} \quad (107)$$

$$\frac{\partial \hat{z}_n}{\partial q_i} = \frac{\partial z_j}{\partial q_i} - \left(r_n \cos\theta_j + t_n \sin\theta_j \right) \delta_{i-2,j}$$

where $\delta_{i-2,j}$ is the Kronecker delta, equal to 1 if i-2 = j and 0 otherwise.

Generalized forces are for belts are introduced in the same manner as for

contact forces, i.e., as a summation of forces multiplied by lever arms:

$$Q_i = \sum_{n=1}^{4} F_n \frac{\partial \delta_n}{\partial q_i} \quad , \quad i = 1,2,\cdots,6 \quad (108)$$

Here, F_n is the tension in belt n, determined as explained in later sections.

This method of introducing generalized forces contrasts to that used in the

simpler belt model, explained in Section 2.4.4.

2.5.2.2. Force Equalization (free slipping)

Either the torso belt pair or the lap belt pair (or both) may be "force

equalized." The following simple procedure yields equal tensions in the two

belt segments.

The unstrained strap length for the combined belts is given by

$$L_t = \ell_{i_0} + \Delta_i + \bar{\ell} + \ell_{j_0} + \Delta_j \quad (109)$$
$$(i,j = 1,2 \text{ or } 3,4)$$

where ℓ_{i_0} is the initial length of one belt element, ℓ_{j_0} is the initial

81

length of the other belt element, Δ_i and Δ_j are the slacks in those belts. $\bar{\ell}$ is the length of strap between attachment points on the body and may include an inputted out-of-plane component for either the torso or lap belt combination. At each point in time, belt length is

$$L = \ell_i + \bar{\ell} + \ell_j. \tag{110}$$

The quantity

$$L_t - L = \left(\ell_{io} + \Delta_i - \ell_i\right) + \left(\ell_{jo} + \Delta_j - \ell_j\right) \tag{111}$$

is then determined. If $L_t - L \geq 0$, then $F_i = F_j = 0$. If not, the belt elongation is determined as:

$$\delta = L - L_t \tag{112}$$

This deflection is then used to generate a force based on special material properties which reflect deformation properties of the entire belt loop and the restrained occupant.

2.5.2.3. Torso Belt Interbelt Influence: Adjustment for Belt Slip

In more complex belt and harness arrangements, friction and geometric considerations lead to unequal belt tensions. Three optional methods have been supplied with this model to allow the forces in one torso belt (the influencer) to influence the forces in another belt (the influencee). They are described in the following three sections. The computer program logic allows any of these three influences to be applied to the torso belt pair even if it has previously been force equalized by the method of Section 2.5.2.2 (However, equalized force values will not be further modified by the "force difference saturation" method.)

Normal-force Friction . The first inter-belt influence option is intended to simulate the effect of static and sliding friction between belts and the occupant.

<u>For the Fixed Attachment Method:</u>

Consider a belt pair (i,j) with unadjusted belt tensions $F_i^{(o)} > F_j^{(o)}$. Then belt i is considered to be the influencer and belt j the influencee. The force $F_i^{(o)}$ is adjusted downward and $F_j^{(o)}$ is adjusted upward by an amount estimated to represent the friction effect with the restriction that the influencee tension is never made to exceed the influencer tension. In particular, where μ_k is the sliding coefficient of friction and angles β_i and β_j are as illustrated in Figure 19, we require final (adjusted) forces F_i and F_j such that

$$F_i - F_j = \mu_k(F_i \cos\beta_i + F_j \cos\beta_j)Z. \tag{113}$$

Here, Z is set to zero if the normal force, $F_i\cos\beta_i + F_j\cos\beta_j$, is less than zero. Otherwise, Z is 1.

Specifically, F_i and F_j replace $F_i^{(o)}$ and $F_j^{(o)}$ and

$$F_i = F_i^{(o)} - (1 - \zeta)\Delta \tag{114a}$$

$$F_j = F_j^{(o)} + \zeta\Delta, \tag{114b}$$

where Δ is calculated by the model and where ζ (input) is the fraction of the total friction force adjustment to be apportioned to the influencee (lower tensioned) belt. A value $\zeta = .5$ is most reasonable and is recommended. Equations 113, 114a, and 114b may be solved for F_i, F_j, and Δ to yield:

$$F_i = \frac{(1 + \mu_k\cos\beta_j Z) \, [F_j^{(o)} + \zeta(F_i^{(o)} - F_j^{(o)})]}{(1 - \zeta)(1 - \mu_k\cos\beta_i Z) + \zeta(1 + \mu_k\cos\beta_j Z)} \tag{115a}$$

$$F_j = F_j^{(o)} + \zeta(F_i^{(o)} - F_i)/(1 - \zeta). \tag{115b}$$

$F_i^{(o)}$ and $F_j^{(o)}$ will not be adjusted for slippage if there is no inter-belt influence, i.e., if the input data specifies that the belt attachment points on the occupant are to be considered as fixed end points of separate and independent belt segments. Also, there will be no slipping adjustment if $|F_i^{(o)} - F_j^{(o)}|$ does not exceed a static

6/30/88
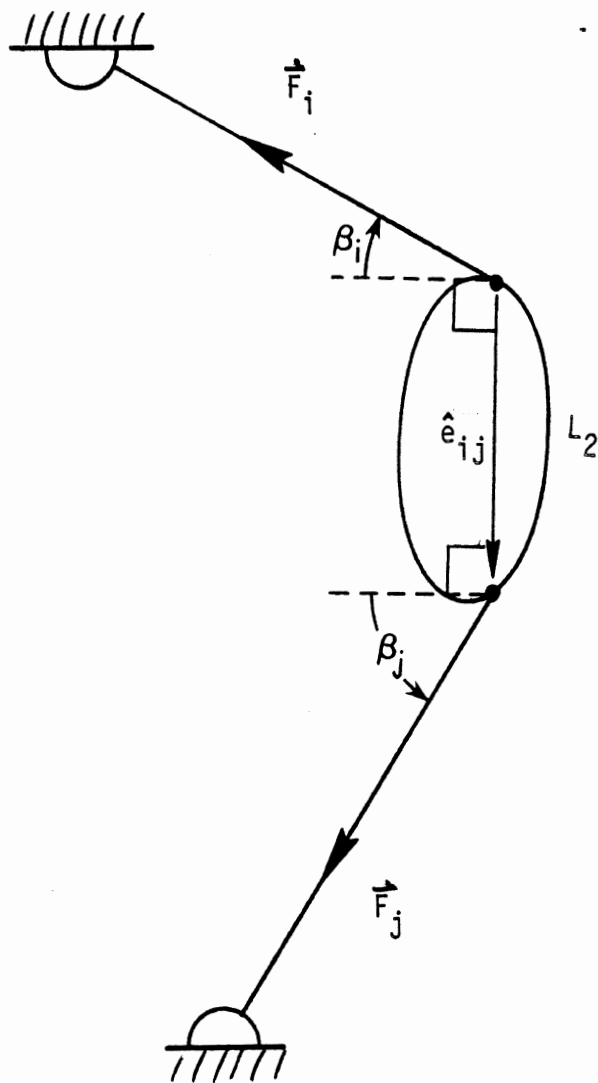
Figure 19. Torso Belt Friction

coefficient of friction μ_s multiplied by the normal force against the
occupant. Note that free-slipping can be guaranteed by inputting μ_k and
μ_s as 0; a non-slip condition is guaranteed by inputting μ_s as a very
large number.

For the Force Equalization Method:

The normal force friction option just described clearly requires
there to be a difference between the initial estimates of the belt tensions,
$F_i^{(o)}$ and $F_j^{(o)}$, if there is to be a nonzero friction adjustment. $F_i^{(o)}$
and $F_j^{(o)}$ will be unequal in general if the force-equalization (free-slipping)
option has not been selected for the torso belts, so in this case it is the
aforedescribed normal force friction model which is used. If the force-
equalization option has been selected, however, the friction adjustment is
calculated as below, where the normal force N is the factor in parentheses
in equation 113:

$$F_i = F_i^{(0)} + (1 - \zeta)\mu N$$
$$F_j = F_j^{(0)} - \zeta\mu N$$
$$\text{where} \quad F_i^{(0)} = F_j^{(0)}$$

and ζ is usually selected as 0.5. The user specifies on Card 719 whether
the belt with the larger tension (F_i) should be the upper torso belt or
the lower.

Force Difference Saturation. An inter-belt influence option can be
selected which will simulate the effect of belt friction in an entirely
different manner. Here, a "force difference saturation" is imputted by
the user for the torso belt pair. Whenever the difference in tension
between the two belts exceeds this force saturation value, the greater
of the forces is reduced by an amount such that the difference in ten-
sions is equal to the saturation value. The tension in the outer belt
is unchanged. This adjustment of the force difference is intended to
represent partial slipping against static friction.

6/30/88

Thus, where F_j is the lesser of the original belt tensions, F_i is the adjusted force for the belt of greater tension, $F_i^{(o)}$ is the unadjusted (original) greater belt tension, and F_s is the inputted force saturation level, the following analysis applies.

If $F_i^{(o)} - F_j \leq F_s$, then no modification of $F_i^{(o)}$ is required; i.e., $F_i = F_i^{(o)}$. However, if $F_i^{(o)} - F_j > F_s$, then we seek the adjustment Δ_{ij} to $F_i^{(o)}$ such that

$$F_i - F_j = F_s$$

where

$$F_i = F_i^{(o)} - \Delta_{ij}.$$

(116)

Clearly, from these conditions,

$$\Delta_{ij} = (F_i^{(o)} - F_j) - F_s.$$

(117)

Percentage Influence. The third interbelt influence option allows the user to specify the positive or negative percentage of the influencer tension which will be applied as an additive adjustment to the influencee. Note that only for this influence option does the user specify which belt is the influencer and which the influencee. (Card 719.) The influencer is determined automatically at each value of time for the other two options. In conjunction with this option, the user supplies a "maximum influence force bound." If the force adjustment, in absolute value, is greater than this bound, then the bound itself is applied as the adjustment to the influencee (with proper sign).

Thus, where $F_b > 0$ is the influence bound, P_{ij} is the fractional, percentage influence factor, F_i is the influencer, and $F_j^{(o)}$ is the unadjusted influencee force, the modified forces are determined as follows. If

$$\left| P_{ij} F_i \right| \leq F_B,$$

then the adjustment to belt j due to belt i is

$$\Delta_{ij} = P_{ij} F_i. \tag{118}$$

Otherwise,

$$\Delta_{ij} = F_B \text{ sgn } P_{ij}. \tag{119}$$

The adjustment to $F_j^{(o)}$ then yields

$$F_j = F_j^{(o)} + \Delta_{ij} \tag{120}$$

If the resulting influence tension F_j is less than zero, then it is set to zero.

2.5.2.4 Inertia Reels: Spoolout, Frame Deformation, Lockup

Spoolout and/or frame deformation can be specified in the form of "anchor deformation" data. Fields 8-9 of Cards 710-716 can be used to designate the name of a force-deflection type material for the anchor.

A maximum of three anchors, A_1, A_2, and A_3, (see Figure 17) may have either vehicle-sensitive or webbing-sensitive lockup characteristics. A vehicle-sensitive reel can be made to lock at some inputted time or, alternatively, when either of two conditions occurs: a) the resultant inertial acceleration at the anchor location exceeds, in absolute value, an inputted limit; b) vehicle pitch exceeds, in absolute value, an inputted limit. A webbing-sensitive reel will lock either when the rate of belt feed-out or the acceleration of belt feed-out exceeds an inputted limit. Since belt feed-out rate and acceleration are obtained from rough numerical differentiations the modeled webbing-sensitive reels may not be as well behaved as vehicle-sensitive reels. Once a reel of either type locks it will remain locked for the duration of the crash history. Since lockup normally occurs at or near time zero, Cards 721-723 are usually not used.

2.5.2.5 Slip Points, or Rings

The upper and lower rings (Figure 17) are either fixed to the vehicle frame or fastened to the end of ring straps, B_5 and B_6. If a ring is not anchored to the vehicle, then its location at any value of time is determined by the condition that x-, y-, and z-forces at the ring location sum to zero.

This involves solving simultaneous nonlinear equations in X_{ring}, Y_{ring}, and Z_{ring} and is done by the method discussed briefly in Section 2.5.2.6. Ring positions, once determined, are considered to be quasi-static anchor points for belt segments 1 to 3.

The primary characteristic of the rings is that the webbing straps passing through them are allowed to slip either freely, or with a desired amount of frictional resistance, or not at all. Free slipping is handled by determining a deflection for the combined belt segment (either B_1-B_7 or B_2-B_3) and then setting both belt segment tensions equal to the resulting belt force. The "no slip" case is handled by treating the individual segments as independent straps.

The case of non-zero frictional resistance to slipping is treated as follows. First, the free slipping tension is determined, as previously explained. Next, the torso belt force is adjusted upward by an amount representing frictional resistance at the ring. The friction force is determined as an inputted coefficient of friction multiplied by a "normal force" at the ring. The normal force is defined as the absolute value of the vector sum of the two force vectors determined from free slipping.
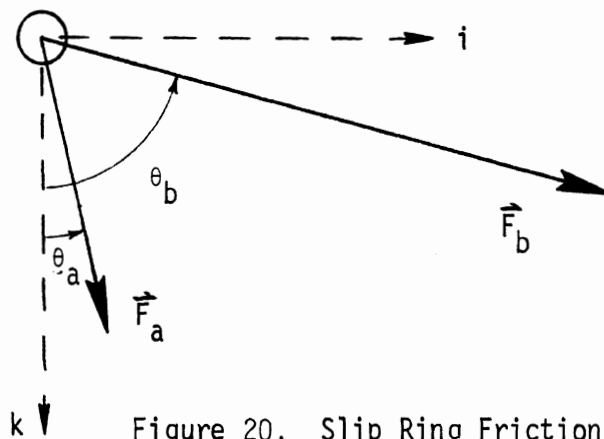
Figure 20. Slip Ring Friction

Where F is the common value of tension for the free slipping pair, we see (with reference to Figure 20) that

3/10/87

88

$$\vec{F}_a = F \sin \theta_a \, \hat{\imath} + F \cos \theta_a \, \hat{k}$$

$$\vec{F}_b = F \sin \theta_b \, \hat{\imath} + F \cos \theta_b \, \hat{k} \; . \tag{121}$$

Hence, the normal force is

$$N = |\vec{F}_a + \vec{F}_b| = F\left[2\left(1 + \cos(\theta_b - \theta_a)\right)\right]^{\frac{1}{2}}. \tag{122}$$

The cosine term is most easily calculated by using the Law of Cosines since the endpoints of both belt segments are known.

Supposing $\vec{F}_b$ to be the unadjusted torso belt force vector, we finally obtain the modified belt tension as

$$T = F + \mu N \; . \tag{123}$$

2.5.2.6 Determination of Ring Position

Ring position at each instant of time is determined by solving the three nonlinear equations of force equilibrium at the ring for ring x, y, and z. The minimization method of Davidon as implemented by Fletcher and Powell (Ref. 2 0) is used. For a set of n equations as shown in eq. 124, an objective function $V^2 = \Sigma R_i^2$ may be defined. Here, {R} is a vector of "residuals" of the n functional relationships. Minimizing the function V^2 yields $R_i = 0$ and thus establishes a solution vector {X}. An initial guess vector {X$_o$} must be provided. For the ring force equilibrium problem, n is equal to 3.

$$R_1 = f_1(x_1, x_2, \ldots, x_n) = 0$$

$$R_2 = f_2(x_1, x_2, \ldots, x_n) = 0$$

$$\vdots \qquad\qquad\qquad \vdots \tag{124}$$

$$R_n = f_n(x_1, x_2, \ldots, x_n) = 0 \; .$$

The method requires values for $\partial f_k/\partial x_j$, the so-called "influence coefficients."
These are determined below for the specific problem at hand (see Figure 21),
i.e., determination of the point (x_c, y_c, z_c) given anchor points (x_1, y_1, z_1),
(x_2, y_2, z_2) and (x_3, y_3, z_3) and the means of determining belt forces acting at
(x_c, y_c, z_c).
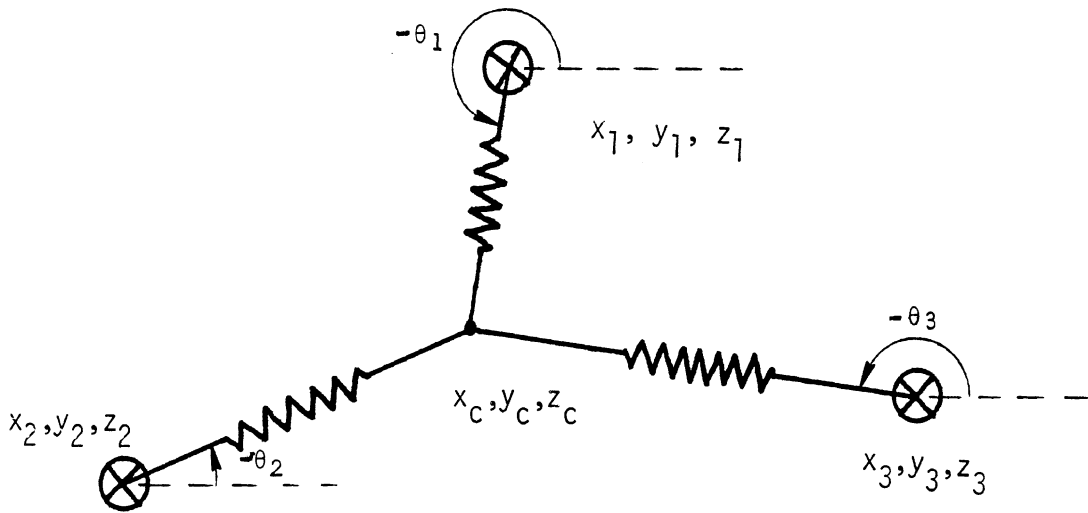
Figure 21. Belt Geometry at a Slip Point

The conditions of force balance at (x_c, y_c, z_c)

$$f_1 = \gamma_1 T_1 \cos\theta_1 + \gamma_2 T_2 \cos\theta_2 + \gamma_3 T_3 \cos\theta_3 = 0 \tag{125}$$

$$f_2 = \gamma_1 T_1 \sin\theta_1 + \gamma_2 T_2 \sin\theta_2 + \gamma_3 T_3 \sin\theta_3 = 0$$

where T_1, T_2, T_3 are the belt tensions in three dimensions and the $\gamma_i T_i$
are the components in the x-z plane. The tensions are known for any deflection
δ, i.e.,

$$T_i = F_i(\delta_i), \quad i = 1, 2, 3. \tag{126}$$

Where Δy_i is a user-specified endpoint-to-endpoint out-of-plane dimension for
belt i, the belt segment lengths are

$$\ell_i = \sqrt{(x_c - x_i)^2 + (\Delta y_i)^2 + (z_c - z_i)^2}, \quad i = 1, 2, 3, \tag{127}$$

and the coefficients γ_i are

$$\gamma_i = \sqrt{\ell_i^2 - \Delta y_i^2}/\ell_i, \quad i = 1, 2, 3. \tag{128}$$

90   3/10/87

Since $\partial \delta_i / \partial(x_c, z_c) = \partial \ell_i / \partial(x_c, z_c)$, we have that

$$\frac{\partial T_i}{\partial x_c} = F_i'(\delta_i) \frac{\partial \ell_i}{\partial x_c} = F_i'(\delta_i) \frac{x_c - x_i}{\ell_i} \qquad (128)$$

$$\frac{\partial T_i}{\partial z_c} = F_i'(\delta_i) \frac{\partial \ell_i}{\partial z_c} = F_i'(\delta_i) \frac{z_c - z_i}{\ell_i} \quad .$$

The sines and cosines of equations 125 are

$$\cos \theta_i = \frac{x_c - x_i}{\sqrt{\ell_i^2 - \Delta y_i^2}} \quad , \quad \sin \theta_i = \frac{z_c - z_i}{\sqrt{\ell_i^2 - \Delta y_i^2}} \quad . \qquad (129)$$

Consequently, the influence coefficients can now be found as:

$$\frac{\partial f_k}{\partial q_i} = \sum_{j=1}^{3} \frac{M\, T_j}{\overline{\ell}_j^2 \ell_j} \left(q_K - Q_{Kj} \right)\left(q_I - Q_{Ij} \right)$$

$$+ \left[\frac{F_j'(\delta_j)}{\ell_j^2} + \frac{T_j \,\Delta y_j^2}{\overline{\ell}_j^2 \ell_j^3} \right] \left(q_i - Q_{ij} \right)\left(q_k - Q_{kj} \right) \qquad (130)$$

where, for k = 1 and 2, $q_1 = x_c$, $q_2 = z_c$, $Q_{1j} = x_j$, $Q_{2j} = z_j$, K=3-k, M=1-2|k-i|, I = 3-i, and $\overline{\ell}_j = \sqrt{\ell_j^2 - \Delta y_j^2}$.

The residuals are

$$R_1 = \gamma_1 T_1 \frac{x_c - x_1}{\overline{\ell}_1} + \gamma_2 T_2 \frac{x_c - x_2}{\overline{\ell}_2} + \gamma_3 T_3 \frac{x_c - x_3}{\overline{\ell}_3}$$

$$R_2 = \gamma_1 T_1 \frac{z_c - z_1}{\overline{\ell}_1} + \gamma_2 T_2 \frac{z_c - z_2}{\overline{\ell}_2} + \gamma_3 T_3 \frac{z_c - z_3}{\overline{\ell}_3} \quad . \qquad (131)$$

The foregoing relationships are modified as necessary for the cases of: a) force-strain relationships instead of force-deflection; b) slipping or friction through the ring, for which case a single deflection is used for the common strap.
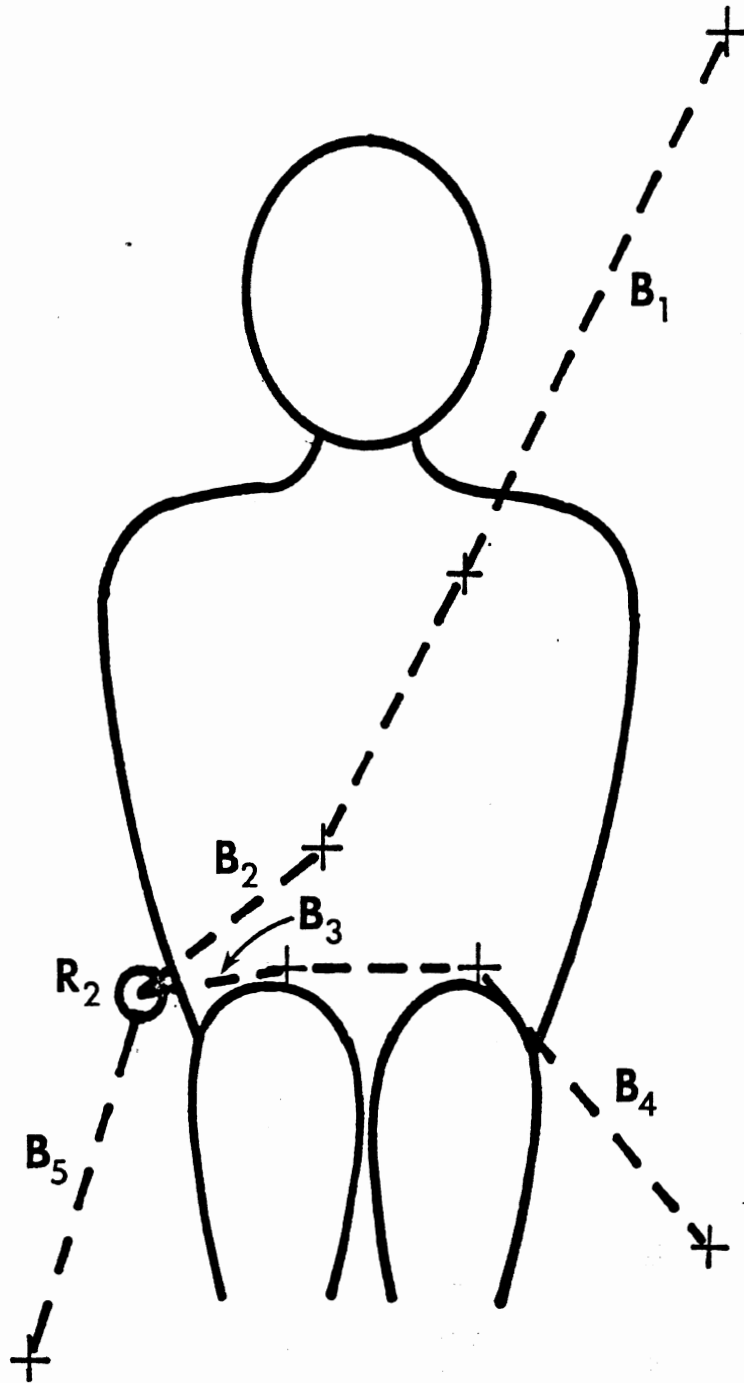
MVMA 2-D BELT SYSTEM: FRONT VIEW

Figure 21-A. Schematic for Out-of-Plane Belt System Dimensions (Δy_i)

2/6/84

2.5.2.7   Adjustment of Lap Belt Attachment Point

The lap belt attachment point on the lower torso link is allowed to vary. Adjustment of the x- and z-coordinate values is most important for cases in which there is significant forward motion of the torso, which occurs when only the lap belt is used or when the torso belt provides only loose restraint for the torso. In these cases the lower torso link can rotate forward (clockwise) to a degree that a fixed lap belt attachment point, moving with the link, would be rotated downward through the upper leg. This is clearly unrealistic and results in lap belt forces being applied at an incorrect angle.

User specifications on Card 712 for the lap belt attachment coordinates on the lower torso link are used at time zero to define constraint conditions from which an adjustment is calculated for the lap belt attachment at each integration time step. The constraint conditions are based on the line between the hip joint and the lap belt attachment point. Specifically, the constraints satisfied at each value of time are: 1) the line length from the hip joint is constant; 2) the link 4 (lower torso) to line to link 5 (upper leg) angles are in constant proportion.

10/14/86

92.2

2.6 COMPUTATION OF CONTACT FORCES

A model based on the interaction of circles with planar contact surfaces, although useful, does not provide sufficient detail to allow accurate prediction of occupant loadings in some cases. A specific problem is the direction of forces applied to the occupant by the contact surfaces. Even though the surface may deform, the force generated is applied in a direction perpendicular to the original position of the contact surface. In some cases this can cause errors in body G-loadings and rebound kinematics.

The proposed solution to this problem is a real line model where a side view section of an automobile is used to accurately describe the vehicle interior. Each contact region (e.g. instrument panel, windshield, seat) will be represented by a network of points with their density determined by the radius of curvature of the particular surface. The objective is improvement of vehicle geometry without extensive expansion of input data requirements. Therefore the new contact model is designed to require a section view of the vehicle plus tabular force-deformation data from standard SAE test procedures where they are available (e.g., an instrument panel pendulum test or an EA column test using a body block).

Contact forces are generated when ellipses attached to the crash victim intersect the vehicle-interior profile.* These ellipses are similar to the body ellipsoids of the HSRI three-dimensional, six-mass model (Reference 14) and are specified by the user. Figure 22 illustrates typical occupant and vehicle-interior profiles for an MVMA 2-D data set.

Consideration was given to using a similar real line concept for the contact-sensing vehicle-occupant outline. It is felt, however, that complexities associated with the interaction between two real line surfaces outweigh whatever advantages this approach may have over the one selected. The representation selected will approximate the arc-line segment representation if properly used.

---

*See Section 2.10.4 regarding allowed/disallowed interactions.
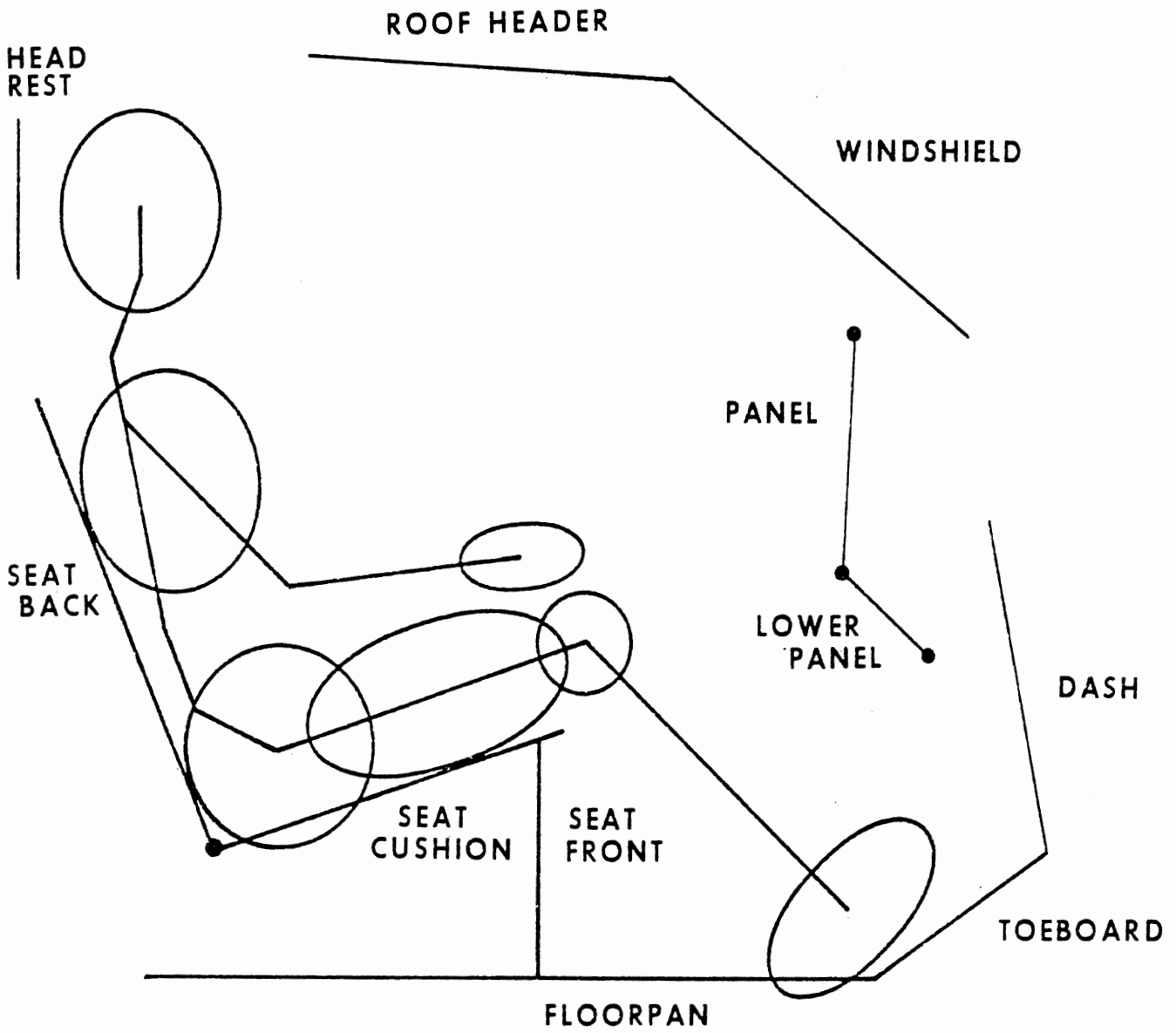
FIGURE 22   Seven Occupant Ellipses and Eleven Line Segments for Potential Contact

94

The real line interior can include various regions, e.g.: roof header, windshield, apex, upper, middle, and lower interior panels, dash, toeboard, floor, seat cushion front, seat cushion and seat back regions, head rest, bulkhead, steering column. This list, however, need not be considered as all inclusive nor are any of these regions required. The vehicle interior can in fact be made up of any connected or disconnected combination of line segments.

Each region is further broken down into a series of straight line segments. The number of these can be chosen to approximate the vehicle interior defined by the side view section drawing as closely as desired.*

End points of each individual element are inputted, in vehicle coordinates, as tabular functions of time so that region deformation and passenger compartment collapse can be represented. In addition elliptically shaped vehicle-interior panels can be specified.

Many of the features included in the contact model have been discussed in previous reports and will be specialized for the two-dimensional model at hand in the text which follows. These include: 1. determination of the penetration, δ, and the penetration rate, $\dot{\delta}$, of a contact sensing ellipse into a real line contact region (generates a force using the input force-deformation tables or polynomials); 2. determination of force multiplication "effectiveness factors" for contacts at edges of line segments; 3. tangential contact forces resulting from friction or plowing of an ellipse laterally into a surface; and, 4. time-dependent tabular input of contact region location and shape to allow user specification of passenger compartment collapse.

---

*However, for optimal model performance, no straight line segment should be much smaller than the largest contact ellipse that is likely to strike it.

Several new features have been added to make the MVMA two-dimensional model even more realistic. These are: 1. the ends of each region may be optionally anchored to the vehicle frame of reference at specified points; 2. the segments of regions describing the vehicle interior can move and deform in response to contact by body ellipses maintaining geometric continuity at corner positions where elements within a region are connected (the migration rule, Section 2.6.9); 3. magnitude and direction of a force will be continuous at corners within regions (See Section 2.6.10); and, 4. when two body ellipses interact simultaneously with same contact surface element, the resulting deflections are computed based on both loads (See Section 2.6.11).

One example of the need for surface geometric continuity is illustrated by Figure 23. The method of representing permanent deformation in previous models has been to offset the deformed surface parallel to its original position by an amount equal to the permanent deformation. It is clearly seen that a surface discontinuity results.

An example of the purpose of combining the influences of two ellipses interacting with one line segment is illustrated by Figure 24. As normally modeled, contact ellipses act independently against a contact surface, as shown at the top of the figure. However, suppose for the sake of illustration that ellipse number 1 depresses the surface before ellipse number 2 approaches. Then ellipse number 2 should interact with a surface displaced from its original position. The overall deformity of the surface caused by ellipse number 1 would be similar to the dotted line shown in the figure at the bottom. It is this surface that ellipse number 2 should see.

2.6.1 General Geometry of a Contact Surface Element

The force interactions between the crash victim and his environment are modeled by impingement of ellipses attached to body segments into line

96
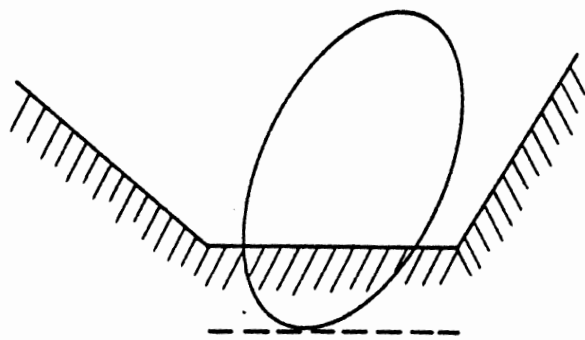
Permanent deformation
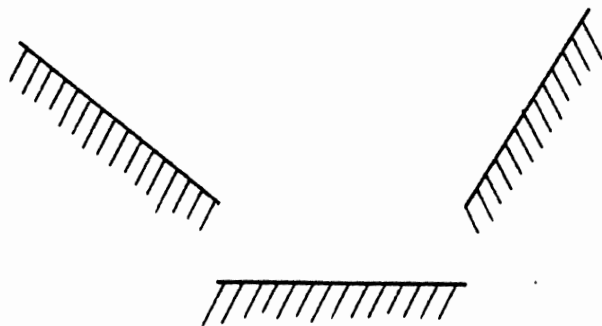
Resulting surface discontinuity

Figure 23. Results of Surface Geometric Discontinuity

No. 1

No. 2

δ_1

δ_2
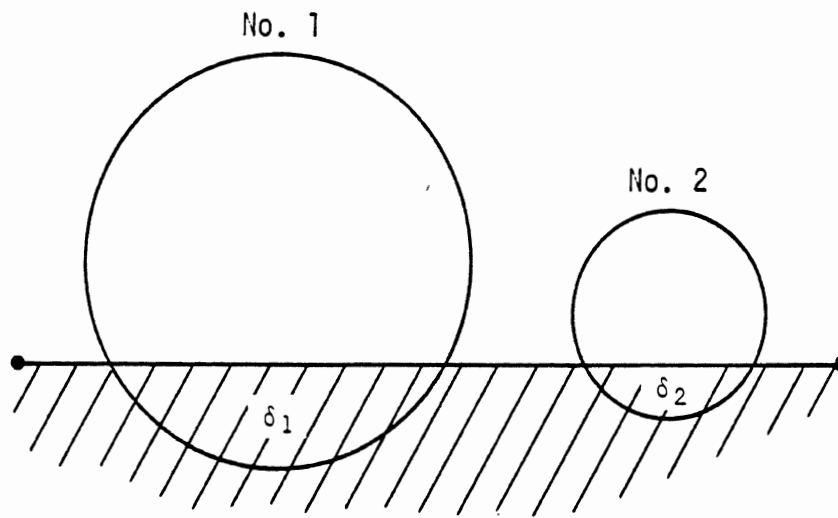
Two Independent interactions with one line segment

No. 1
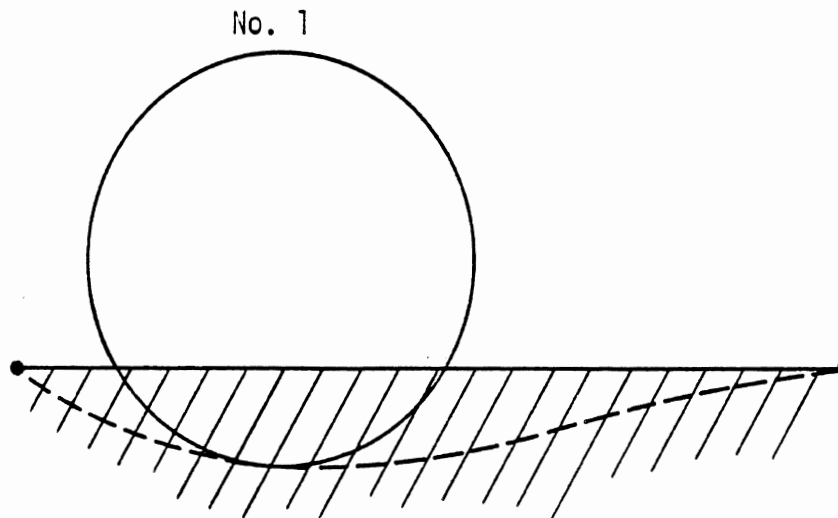
Realistic deformation from single interaction

Figure 24. Multiple Ellipses Interacting With A Single Line Element

elements attached to a moving vehicle reference frame or attached to the inertial reference frame.* This general model is illustrated in Figure 25. Both the ellipse and the line surface can deform as each may have its own unique set of force-deformation characteristics. In addition to this, forces may be generated when an ellipse attached to one body segment interacts with an ellipse attached to another body element (e.g., head on knee).

The normal force generated during such an encounter is dependent on deflection (and not deflection rate) where deflection is defined as the maximum perpendicular distance, δ, the ellipse extends into the contact surface or other ellipse. This force acts to push the ellipse outward perpendicular to the contact surface at the location of maximum deflection. A tangential force also may be generated during contact, which is considered to be a frictional or plowing force. Hence, its value is related to the value of the normal force. The direction of this force depends on the tangential velocity vector which exists between the ellipse and the other surface.

The model user may specify any number of body ellipses, contact regions, individual line elements for constructing the regions, and materials for describing vehicle, crash victim, and belt deformations.

Each of the ellipses can be attached to any of the eight body segments,** centered at an arbitrary displacement from the body segment center of gravity and with principal axes at any desired angle with respect to the body segment coordinate system,as shown in Figure 26, The contact surfaces can be attached to the vehicle (or to the inertial coordinate frame) and moved relative to the reference coordinate system as a function of time to represent such

---

* Body ellipses may also interact with curved elements attached to the vehicle reference frame or the inertial reference frame. See Section 2.10.

** Also, see Section 2.6.6.1 regarding link sharing for ellipse attachment.
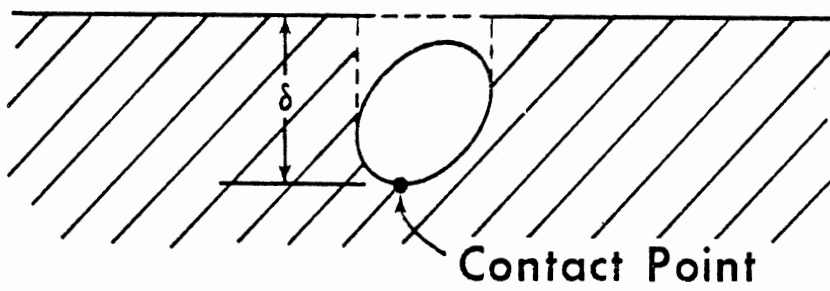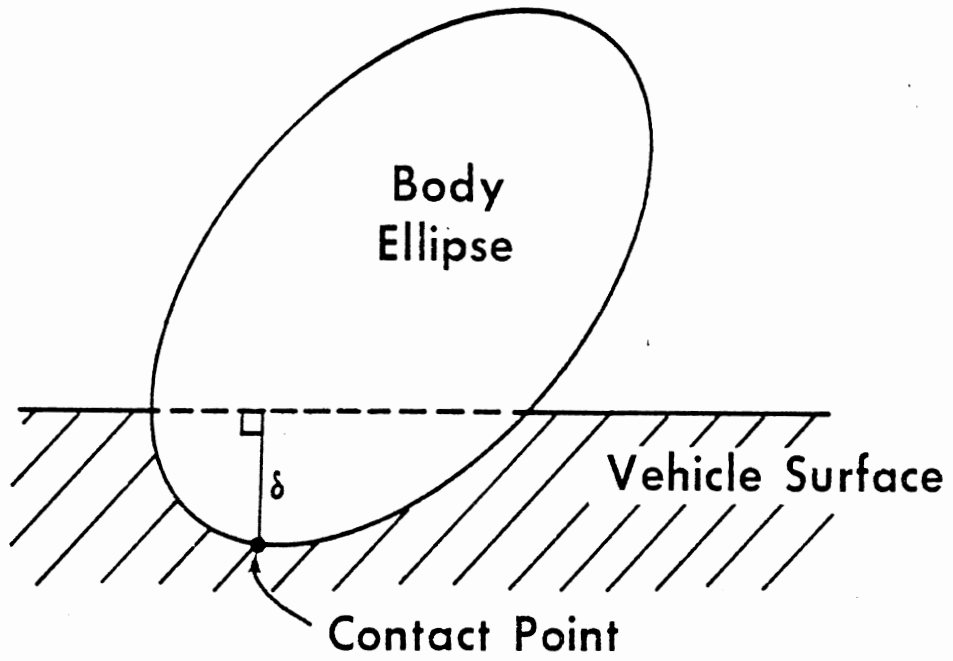
FIGURE 25   Deflection Between a Straight-Line Segment and an Ellipse
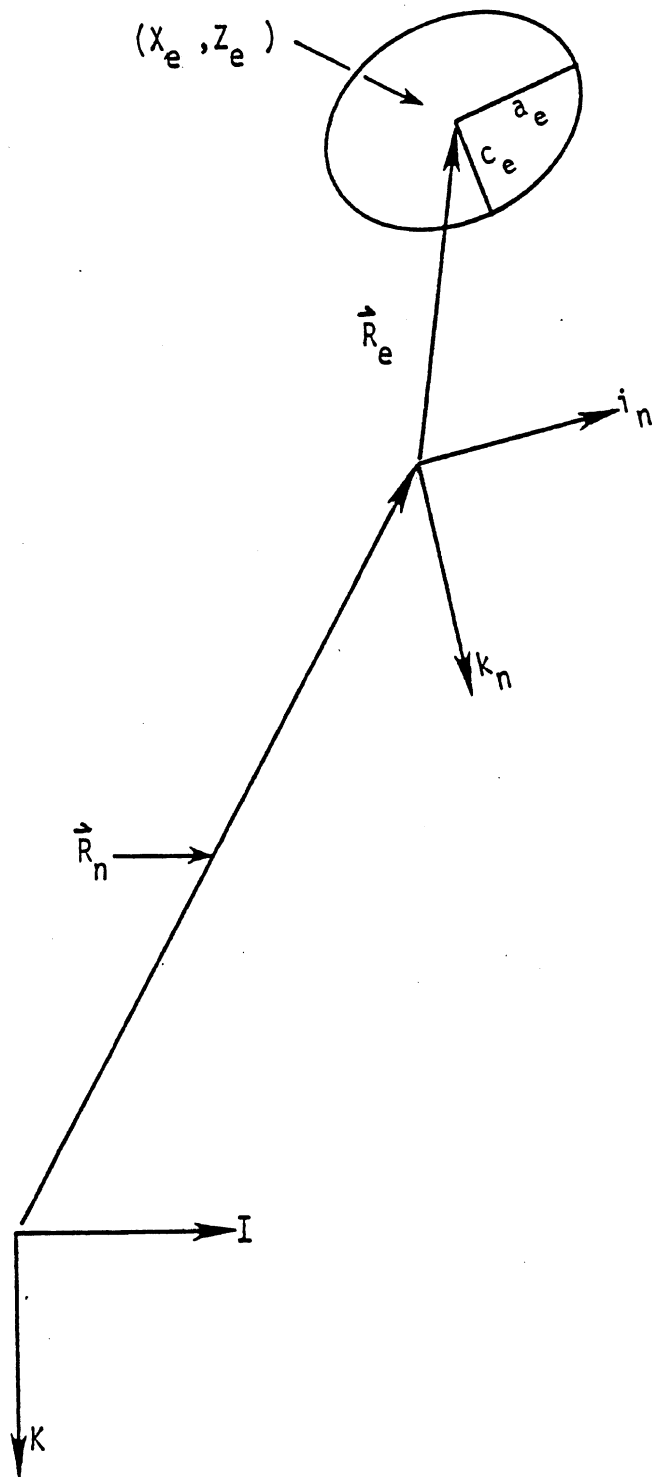
Figure 26. Ellipse 'e' Attached to Reference System 'n'

6/28/85

physical events as occupant compartment deformation or intrusion. Each
contact surface is specified by two corner points given as a function of time
in tabular form relative to the reference coordinate system as shown for a
vehicle in Figure 27. Only the initial location need be specified if the
surface is stationary with respect to the reference coordinate system.

2.6.2 Effects at the Edge of a Contact Surface Element *

The effects at the edge of a contact surface element will be described
in terms of a single linear element within one of the regions. How the
elements are coupled together is discussed later in this part of the report.
Edge properties of a contact surface are illustrated in Figures 28 and 29.

The extent of the contact surface is indicated by Points A and B, which
define the end points of the line in vehicle space. Their coordinates are
provided as input data to the program.

Since the total interaction of the ellipse with the line is represented
by what happens at the point of maximum impingement, a quantity (λ) called the
"edge constant" has been introduced to handle cases where an ellipse inter-
acts with the edge of a contact surface or at a corner where contact surfaces
meet. In this case, maximum impingement lies outside the region defined by
the line but yet the ellipse makes firm contact with the surface. It is
assumed in developing an analytical tool to handle this problem that the
contact force decreases as the point of maximum impingement moves away from the
edge of the contact surface. The computer simulation approximately resolves
these edge problems by employing the following device. The force is
computed using the deflection and deflection rate in the normal manner.
The resulting force is multiplied by an "effectiveness factor" (E) which ranges
from unity in a region in the middle of the contact surface down to zero in the
regions outside the contact surface. The effectiveness factor is illustrated
in Figure 28 by plotting its value corresponding to the various points on

---

* Edge effects can be eliminated in some applications by using curved vehicle
  interior contact surfaces. See Section 2.10.
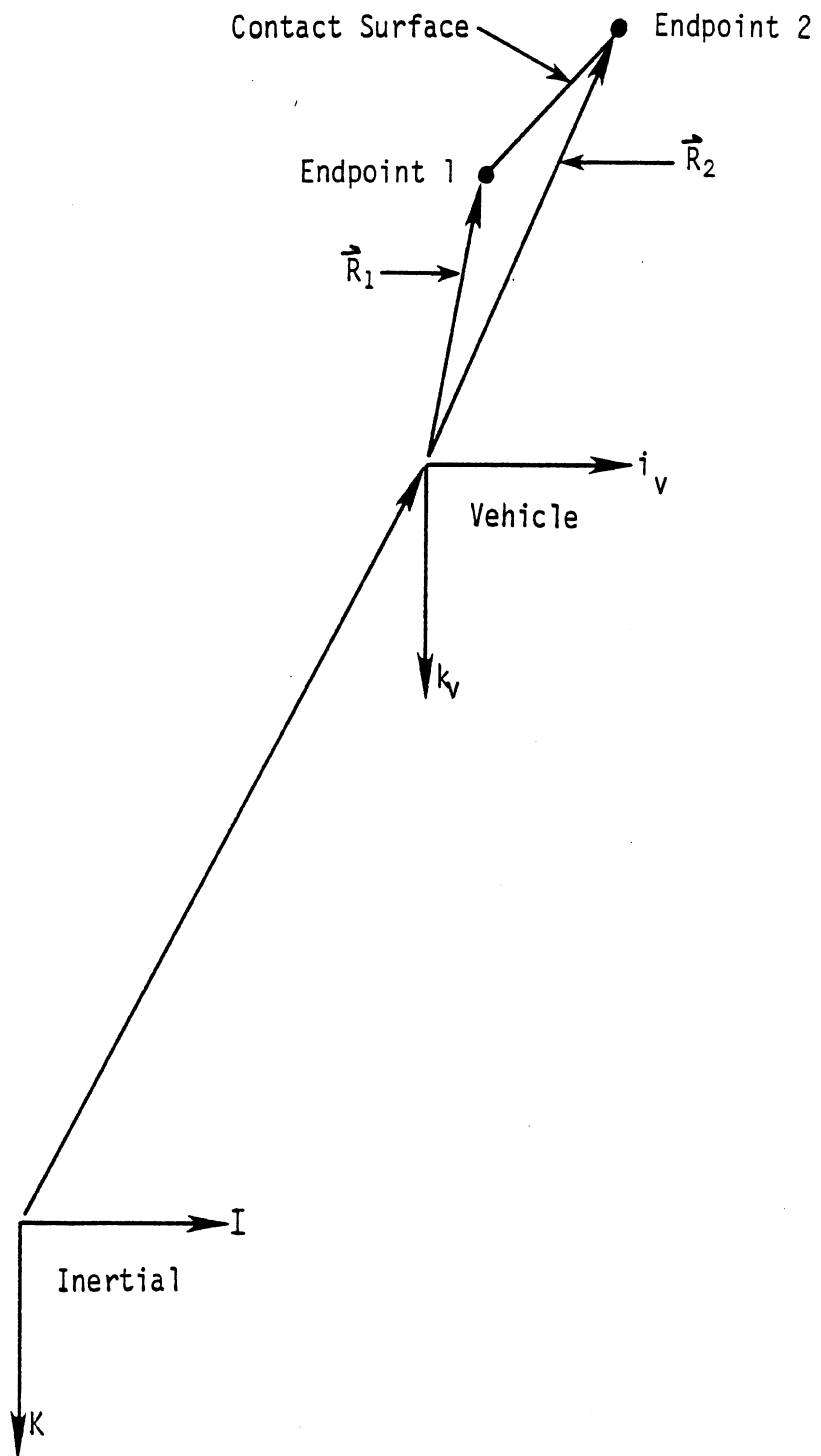
Figure 27. Contact Surface Line Element Attached to the Vehicle
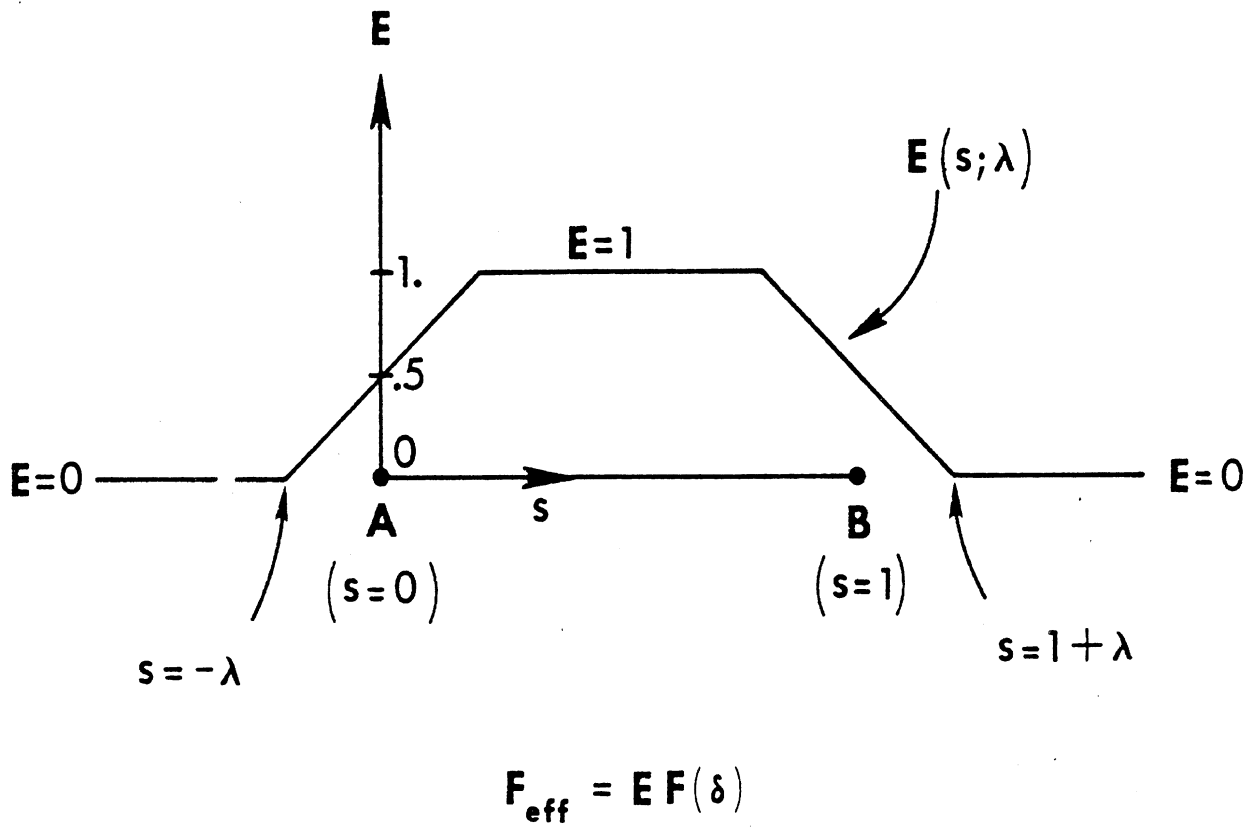
FIGURE 28   Effectiveness Factor E as a Function of s, the Position of
Contact Point with Respect to Line Segment, With Edge
Constant λ as a Parameter
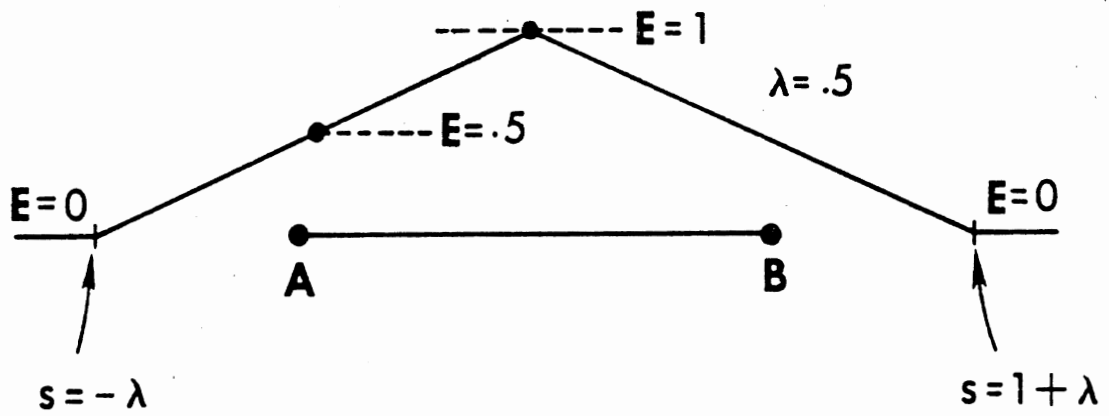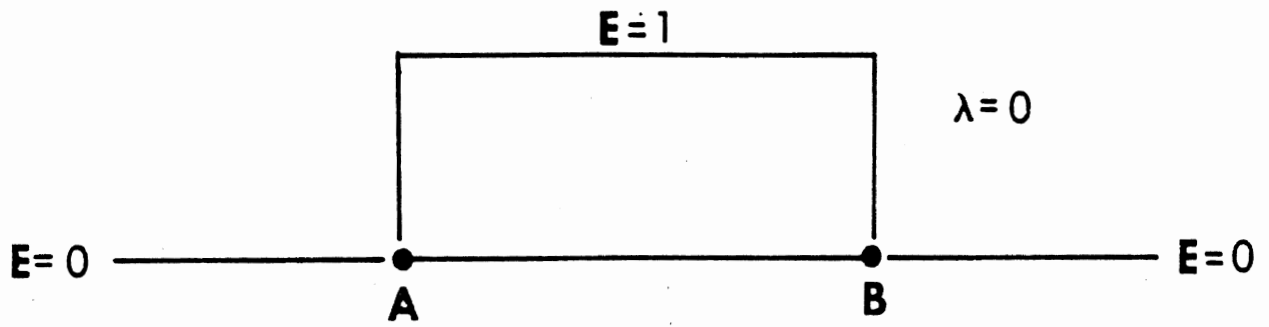
FIGURE 29   Effectiveness Factors for Edge Constant Values of 0. and .5

and near the contact surface above the level of the line. For example:

(1) Effectiveness factor for contact in a range about the midpoint of the contact segment AB has the value of unity;

(2) Effectiveness factor at endpoint A is 0.5;

(3) Effectiveness factor at endpoint B is 0.5;

(4) Away from the contact surface, the effectiveness factor is reduced to zero indicating that no contact will be predicted between the ellipse and the contact surface.

Each ramp is a trace of the values of the factor as the point of maximum impingement of an ellipse into the surface moves toward and beyond the edge of the contact surface along the surface. The result is that for a given deflection, force will be reduced to zero as the ellipse moves off the edge of the surface.

The analysis for edge effects is similar to that used in the HSRI three-dimensional, six-mass model (Reference 14). However, since a straight line segment has one dimension while the contact planes of the three-dimensional model have two dimensions, the effectiveness coefficient E for multiplication with a force has only one factor instead of two. Thus, where λ is an inputted parameter such that

$$0 \leq \lambda \leq .5,$$

the effectiveness coefficient is

$$E = \begin{cases} 0 & \text{for } S \leq -\lambda \\ .5 + \dfrac{.5S}{\lambda} & \text{for } -\lambda < S < \lambda \\ 1. & \text{for } \lambda \leq S \leq 1-\lambda \\ .5 + .5\left(\dfrac{1-S}{\lambda}\right) & \text{for } 1-\lambda < S < 1+\lambda \\ 0 & \text{for } S \geq 1+\lambda \end{cases} \qquad (132)$$

Where a normalized position parameter s indicates the position of arbitrary points on the line, S is the value of s for the projection onto the line of the point of maximum penetration. Now,

$$S = \frac{x - \xi_{11}}{\xi_{21} - \xi_{11}} \qquad (133)$$

where x is the x-coordinate in the vehicle system of a point on the line and the ξ_{ij} are end points of the contact surfaces, $(\hat{x}_1, \hat{z}_1)$ and $(\hat{x}_2, \hat{z}_2)$, defined in vehicle coordinates:

$$\hat{x}_1 = \xi_{11} \quad , \quad \hat{z}_1 = \xi_{12}$$
$$\hat{x}_2 = \xi_{21} \quad , \quad \hat{z}_2 = \xi_{22} \quad . \qquad (134)$$

In cart coordinates the inertial point (x_0, z_0) is

$$\bar{x}_0 = (x_0 - x_v)\cos\theta_v - (z_0 - z_v)\sin\theta_v$$
$$\bar{z}_0 = (x_0 - x_v)\sin\theta_v + (z_0 - z_v)\cos\theta_v \qquad (135)$$

107

It can be shown that the x-coordinate of the projection of $(\bar{x}_0, \bar{z}_0)$ onto the line is

$$x_p = \frac{\bar{x}_0 (f_{21} - f_{11})^2 + f_{11}(f_{22} - f_{12})^2 - (f_{12} - \bar{z}_0)(f_{21} - f_{11})(f_{22} - f_{12})}{(f_{21} - f_{11})^2 + (f_{22} - f_{12})^2} \tag{136}$$

S is equal to $s(x_p)$, so substitution of equation 136 into equation 133 leads to

$$S = \frac{(\bar{x}_0 - f_{11})(f_{21} - f_{11}) + (\bar{z}_0 - f_{12})(f_{22} - f_{12})}{(f_{21} - f_{11})^2 + (f_{22} - f_{12})^2} \tag{137}$$

The edge constant is the mechanism by which a user of the MVMA 2-D model specifies the interaction of a body ellipse with the edge of a contact surface and must be provided as input data for each contact surface in order to exercise the model. It should be selected on the basis of a comparison of the geometries of a particular contact surface and the body ellipse which is most likely to interact with the surface. For instance, assume that the surface shown in Figure 28 is 55 inches long. If it is assumed that a body ellipse with a semi-major axis length of 18.15 inches is the most likely or important interaction, then the edge constant should be selected as

$$\lambda = 18.15 / 55 = 0.33$$

If this value is used, a contact force equal to zero will be predicted if the contact ellipse just misses the surface, but when any part of the ellipse touches an edge of the contact surface, a small force will be computed. This force will be at a maximum when the contact ellipse interacts with the center region of the contact surface.

2.6.3 The Thickness of a Contact Surface Element

Occasionally a body ellipse can approach a contact surface from either side. Consider the case of a contact region representing the top of a dash panel and a body ellipse attached to the knee of an unrestrained occupant. In some vehicles the top of the dash panel is directly above the knees. Consider a hypothetical case where the vehicle is impacted in the rear and is pushed into the path of an oncoming truck. During the rear-end part of the collision, the occupant is often propelled upward along the slope of the seat back. During the frontal collision, the occupant then moves forward. In this series of events it is possible that the knees of the occupant could impact very high on the instrument panel due to the unusual initial positioning for the frontal crash event. It is desired in this case that the knee feel a force from contact with the top of the dash panel and not a large force due to the initial seating position where the knee is below the panel. Another example of this kind of problem is the rear seat passenger which vaults the front seat, striking the front seat back.

This simulation resolves this kind of difficulty by requiring the user to assign a positive or front side to each contact surface. No force will be generated unless the ellipse approaches from the front side. In order to determine simply whether an ellipse has approached from the front or back, the user is required to specify the "penetration limit," a parameter which represents the maximum penetration into the surface which can occur in one integration time step. Then, if an ellipse's first deflection into the surface is greater than this value, the ellipse is assumed to be coming up from behind and no force is computed until the ellipse gets totally in front of the contact surface and then comes back and hits the surface.
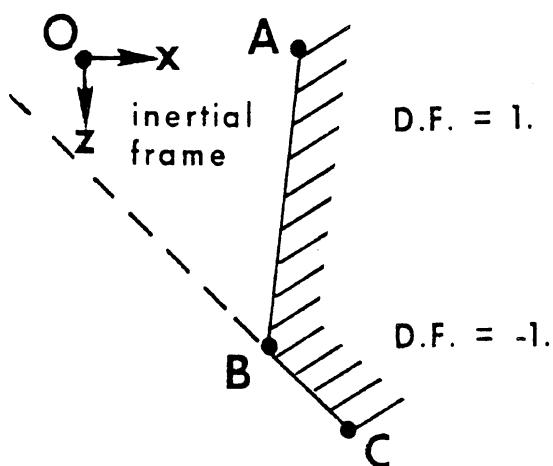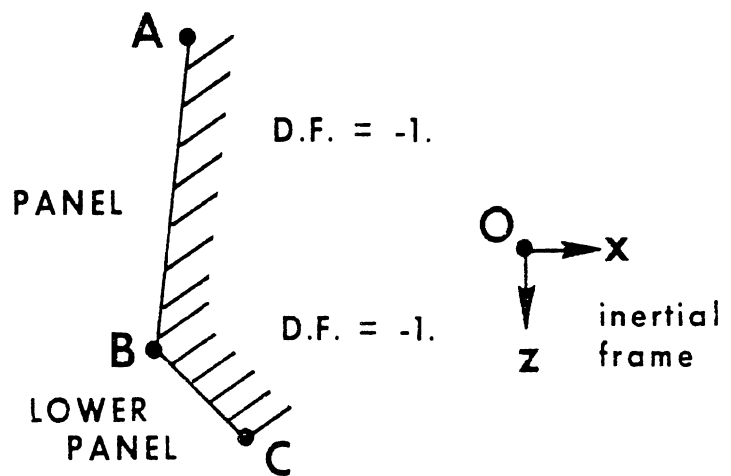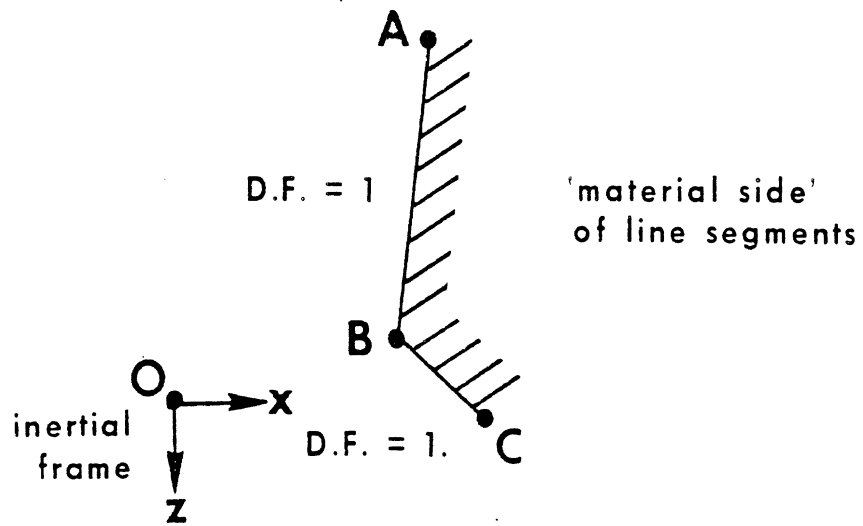
FIGURE 30 Line-Segment Direction Factors, Defined at t = 0

6/28/85

The positive side specification is made by a user input indicating whether the inertial origin lies behind or in front of the contact surface. The inertial origin should not lie exactly on the infinite extension of any of the contact surfaces although it is permissible for any line to pass arbitrarily close to the origin. Figure 30 illustrates definition of direction factors (D.F.) for various line segments.

2.6.4 The Generation of Force between a Contact Ellipse and a Contact Line

2.6.4.1 Definition of Terms

The equations relating contact ellipse and contact line position and geometry to interaction deflections and lever arms are developed in this section.

The following definitions apply to the analysis.

Term	Description
m	reference system for line segment attachment; subscript indicating coordinate system associated with general segment "m" (e.g., 1-8 for body links, 9=vehicle, 10=inertial, >10=user-defined links)
X_m , Z_m	position of origin of the "m" system with respect to the inertial frame
θ_m	orientation angle of the "m" system with respect to the inertial frame (positive counterclockwise)
$(\hat{x}_1,\hat{z}_1) - (\hat{x}_2,\hat{z}_2)$	line segment endpoint coordinates with respect to system "m"
n	reference system for ellipse attachment; subscript indicating coordinate system associated with general segment "n"
X_n , Z_n	position of origin of the "n" system with respect to the inertial frame
θ_n	orientation angle of the "n" system with respect to the inertial frame (positive counterclockwise)
a_e , c_e	semi-axis lengths for ellipse axes 1 and 2
x_e , z_e	position of ellipse center with respect to system "n"

$$\theta_e \qquad \text{orientation angle of ellipse axis 1 with respect to} $$

orientation angle of ellipse axis 1 with respect to x-axis of system "n" (positive counterclockwise)

2.6.4.2 Equation of Line

It is easily shown that the normal form of a line in system "m" is

$$F' = r x' + p z' + s = 0 \tag{138}$$

where

$$r = \frac{\hat{z}_1 - \hat{z}_2}{\pm k}$$

$$p = \frac{\hat{x}_2 - \hat{x}_1}{\pm k} \tag{139}$$

$$s = \frac{\hat{x}_1 \hat{z}_2 - \hat{z}_1 \hat{x}_2}{\pm k}$$

and

$$k = \sqrt{(\hat{x}_2 - \hat{x}_1)^2 + (\hat{z}_2 - \hat{z}_1)^2} \quad .$$

Here, $k \neq 0$ and $p^2 + r^2 = 1$. The sign for $\pm k$ can be taken as $+$ or $-$, but it will be convenient to choose it in a particular way. This will be done later.

The coordinates x' and z' of equation 138 may be eliminated in favor of inertial coordinates X and Z by use of the following coordinate transformations:

$$X = X_m + x' \cos \theta_m + z' \sin \theta_m$$
$$Z = Z_m - x' \sin \theta_m + z' \cos \theta_m \tag{140}$$

This gives

$$F = A X + C Z + D = 0 \tag{141}$$

as the equation of the line in the inertial system. Here,

$$A = r \cos \theta_m + p \sin \theta_m$$
$$C = -r \sin \theta_m + p \cos \theta_m \tag{142}$$

and

$$D = -X_m A - Z_m C + s \quad .$$

The sign for k in equations 139 is selected so that the inertial origin is "behind" the line $A X + C Z + D = 0$. This condition is indicated in

the MVMA 2-D code by $F(0,0) = D > 0$ in equation 141. Here, "behind" means "on the material side of" the line. The material side of the line is specified by the user (on the 409-Card) by indicating for time zero whether or not the inertial origin is on the material side.

Equation 141 is the equation of the line that might be involved in an ellipse interaction. The equation for a potentially interacting ellipse will now be determined.

2.6.4.3 Equation of Ellipse

Consider an ellipse fixed in a local coordinate frame with its center at the origin and with its axes a and c along the x- and z-coordinate axes. The parametric equations for the ellipse in this coordinate system are

$$x = a \cos\alpha$$
$$z = c \sin\alpha \quad , \quad \alpha \text{ a parameter} .$$

A coordinate transformation can be made to show that the parametric equations in inertial coordinates are

$$X = X_\ell + a_\ell \cos(\theta_n + \theta_\ell)\cos\alpha + c_\ell \sin(\theta_n + \theta_\ell)\sin\alpha$$
$$Z = Z_\ell - a_\ell \sin(\theta_n + \theta_\ell)\cos\alpha + c_\ell \cos(\theta_n + \theta_\ell)\sin\alpha \tag{143}$$

Here, X_ℓ and Z_ℓ are the inertial coordinates of the ellipse center:

$$X_\ell = X_n + x_\ell \cos\theta_n + z_\ell \sin\theta_n$$
$$Z_\ell = Z_n - x_\ell \sin\theta_n + z_\ell \cos\theta_n \tag{144}$$

2.6.4.4 Ellipse-Line Deflection

The relative deflection between a contact line and an ellipse will be considered to be the maximum distance from the line to ellipse points that lie behind the line. This is, of course, the distance from the contact line to a line which is tangent to the ellipse and parallel to the contact line. The geometry of contact between an ellipse and a line is illustrated in Figure 30-1.

Let (X_o, Z_o) be the point of tangency. It may be determined by considering
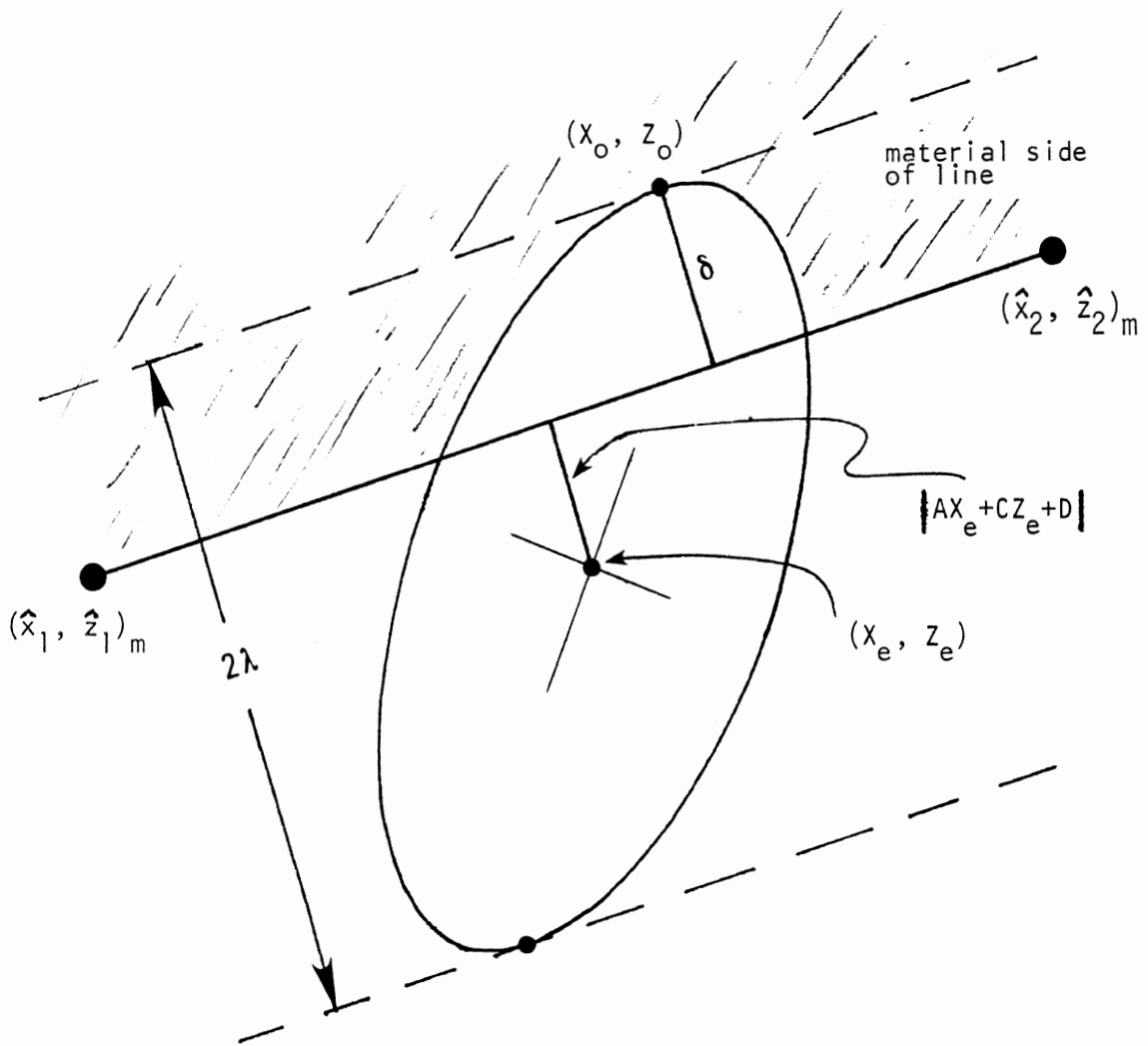
Figure 30-1.   Contact Between an Ellipse and a Line

the relation for distance between the contact line and a general point on the ellipse. The distance from any point (X,Z) to a line is

$$d = \frac{|AX + CZ + D|}{\sqrt{A^2 + C^2}}$$ (145)

where the normalized from of the line is as in equation 141 and the radical equals unity.

The ellipse point coordinates X and Z of equation 143 may be substituted into equation 145, and the point of maximum deflection my be found by determining the value of the parameter α for which $d'(\alpha) = 0$. The results of this procedure are as follows:

$$X_o = X_\ell \pm K\left(\mu_1 A + \mu_2 C\right)$$
$$Z_o = Z_\ell \pm K\left(\mu_2 A + \mu_3 C\right)$$ (146)

where

$$\mu_1 = a_\ell^2 \cos^2(\theta_n + \theta_\ell) + c_\ell^2 \sin^2(\theta_n + \theta_\ell)$$
$$\mu_2 = \left(c_\ell^2 - a_\ell^2\right) \sin(\theta_n + \theta_\ell) \cos(\theta_n + \theta_\ell)$$
$$\mu_3 = a_\ell^2 \sin^2(\theta_n + \theta_\ell) + c_\ell^2 \cos^2(\theta_n + \theta_\ell)$$ (147)
$$\lambda = \sqrt{\mu_1 A^2 + 2\mu_2 AC + \mu_3 C^2}$$
$$K = 1/\lambda$$

The sign uncertainty in equation 146 results because an ellipse always has two different tangent lines that are parallel to any given line. The two different results for (X_o, Z_o) can be substituted into equation 141, and the resulting sign of F determines whether (X_o, Z_o) is a point of maximum deflection or whether it is the paired point, which is of no interest.

Alternatively, and more simply, the sign may be selected so as to give the largest value of d (distance) from equation 145. Equation 145 yields

$$\delta = d = AX_\ell + CZ_\ell + D \pm \lambda ,$$ (148)

where the sign for λ is the same as selected for equations 146. The value δ

is the relative deflection between the ellipse and the contact line. (Here, λ is the effective semiwidth of the ellipse measured normal to the line and $|\ A\ X_{\varrho} +\ C\ Z_{\varrho} +\ D\ |$ is the distance from the contact line to the ellipse center.)

2.6.4.5 Generalized Forces

The force associated with the deflection δ is determined from the material properties of the contact ellipse and contact line and is known as a function of δ and $\dot{\delta}$:

$$F = f(\delta, \dot{\delta}) \ . \tag{149}$$

The generalized forces associated with this contact force are

$$Q_k = F\frac{\partial \delta}{\partial q_k} , \qquad k = 1, 2, \ldots , \text{NDOF} \tag{150}$$

where NDOF is the number of degrees of freedom resulting from the MVMA 2-D data set. The "lever arm" $\dfrac{\partial \delta}{\partial q_k}$ can be shown to be

$$\frac{\partial \delta}{\partial q_k} = X_{\varrho}\, C\, \frac{\partial \theta_m}{\partial q_k} - Z_{\varrho}\, A\, \frac{\partial \theta_m}{\partial q_k} + A\left[\frac{\partial x_n}{\partial q_k} + (Z_{\varrho} - z_n)\frac{\partial \theta_n}{\partial q_k}\right]$$

$$+ C\left[\frac{\partial z_n}{\partial q_k} - (X_{\varrho} - x_n)\frac{\partial \theta_n}{\partial q_k}\right] - A\frac{\partial x_m}{\partial q_k} - C\frac{\partial z_m}{\partial q_k} \tag{151}$$

$$\pm \frac{1}{\lambda}\left\{\left[\mu_2(A^2 - C^2) + (\mu_3 - \mu_1)AC\right]\left(\frac{\partial \theta_n}{\partial q_k} - \frac{\partial \theta_m}{\partial q_k}\right)\right\}$$

The deflection rate $\dot{\delta}$ is

$$\dot{\delta} = \dot{A} X_\ell + \dot{C} Z_\ell + \dot{D} + A \dot{x}_n + C \dot{z}_n$$

$$+ \left[A(Z_\ell - z_n) - C(X_\ell - x_n) \right] \dot{\theta}_n \qquad (152a)$$

$$\pm \frac{1}{\lambda} \left\{ \left[\mu_2(A^2 - C^2) + (\mu_3 - \mu_1)AC \right] \dot{\theta}_n \right.$$

$$\left. + (\mu_1 A + \mu_2 C)\dot{A} + (\mu_2 A + \mu_3 C)\dot{C} \right\}$$

where

$$\dot{A} = \dot{r} \cos\theta_m + \dot{p} \sin\theta_m + C \dot{\theta}_m$$

$$\dot{C} = -\dot{r} \sin\theta_m + \dot{p} \cos\theta_m - A \dot{\theta}_m \qquad (152b)$$

$$\dot{D} = -\dot{A} x_m - \dot{C} z_m + \dot{s} - A \dot{x}_m - C \dot{z}_m$$

6/28/85

2.6.5 Specified Motion of a Contact Surface Relative to the Vehicle (Occupant Compartment Intrusion)

The motion of any of the contact surfaces relative to vehicle coordinates is specified as input data to the MVMA crash victim simulator by presenting the positions of the two end points at a sequence of time points. Implicit in this type of specification is the ability to change length and orientation as well as position of a contact surface as a function of time.

Figure 31 illustrates this general type of motion in a contact surface specified at three time points. The sample contact surface starts out as a line at t=0, moves to the right and becomes longer by $t=t_1$, and moves further to the right while changing orientation and length by $t=t_2$.

Each of the four coordinates defining the position of the end points are treated as piece-wise linear functions of time. A typical coordinate, the x-coordinate of Point 1, is shown in Figure 32. The coordinate rate is a step function but is made continuous by adding ramps from one level to the next within a small time interval. Values for corner coordinates and coordinate rates determine the $\dot{\xi}_j$ for j= 1-3 used in Equation 148.

2.6.6 Generation of Tangential Contact Forces (Friction)

The force which is generated tangential to a surface when a body element ellipse contacts a vehicle contact surface is modeled by the modified tangential Coulomb friction force, T,

$$\overline{T} = -C\mu F \frac{\dot{\overline{\eta}}}{\dot{\eta}} \tag{153}$$
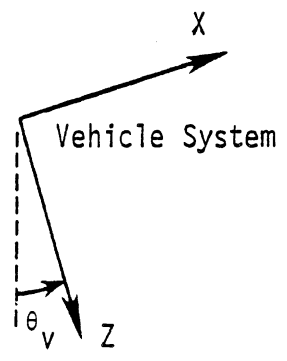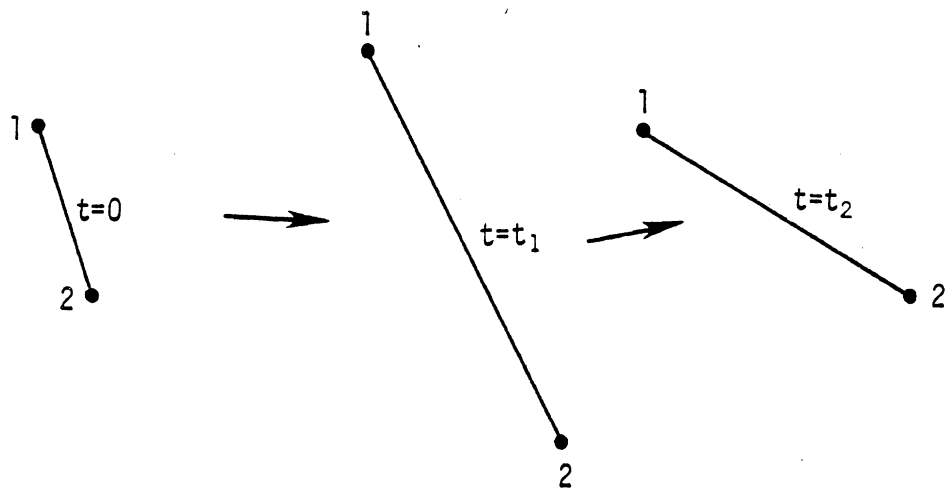
Figure 31. A Moving Contact at Three Time Points
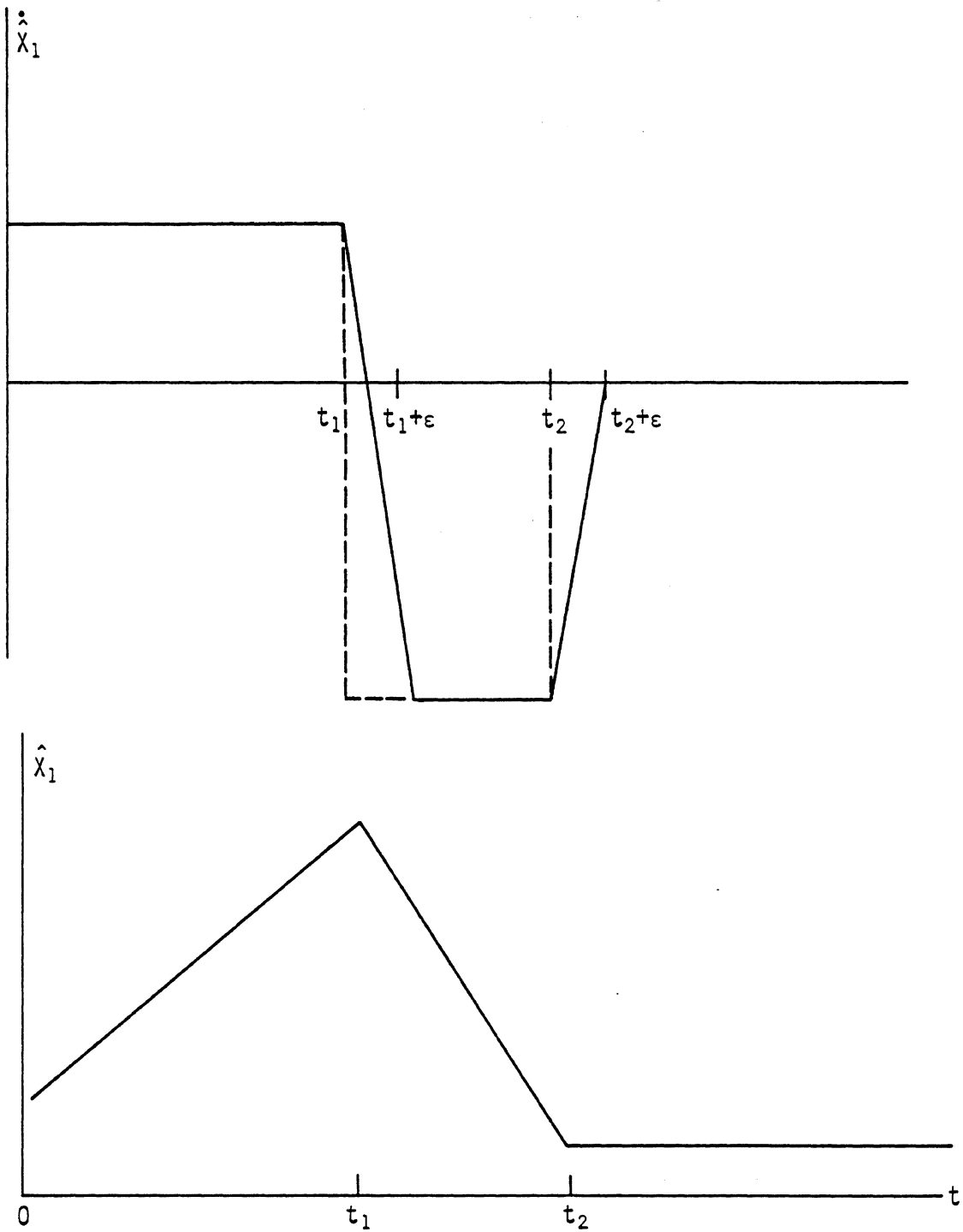
Figure 32. A Corner Coordinate Value and Rate as a Function of Time

where

$\dot{\eta}$ = velocity of contact point over surface ($\dot{\eta}$ inherently zero or positive)

F = normal force

μ = coefficient of friction = $\mu_1 + \mu_2\delta + \mu_3\delta^2$ (154)

C = 1 if $\dot{\eta} > \nu$ and a linear ramp from 0 to 1 if $\dot{\eta} < \nu$

ν = ramp length (in/sec)

μ_1 = Coulomb friction coefficient specified as computer program

    input data.

μ_2 and μ_3 = nonlinear coefficients to represent the effect of

    plowing are computer program input data.

As the tangential forces are chosen to be dissipative in nature, their contribution to the right hand sides of the equations of motion are given in the terms,

$$Q_i = -\frac{\partial}{\partial q_i} \int \vec{T} \cdot \vec{\delta\eta} = -\frac{\partial}{\partial q_i} \int -C\mu F \frac{\vec{\dot\eta}}{\dot\eta} \cdot \vec{\delta\eta}$$

$$= C\mu F \frac{\partial \dot\eta}{\partial \dot{q}_i}$$
(155)

The quantity $\dot{\eta}$ is the speed of the motion of the contact point across the contact surface.

The length of a contact surface with end points (1, 2) is called ℓ. The computations in the program are based on a unit length so that the same logic may be used for each contact. The coordinate of this surface is s (Eq. 133). The speed of the contact point is

$$\dot{\eta} = \left| \ell \dot{s} \right|$$
(155)

The equation 155 may now be written in terms of the individual contact planes as

$$\frac{\partial \dot{\eta}}{\partial \dot{q_i}} = \frac{\ell^2 \dot{s}}{\dot{\eta}} \frac{\partial \dot{s}}{\partial \dot{q_i}} \tag{157}$$

Because $s = s(q_i)$

$$\frac{\partial \dot{s}}{\partial \dot{q_i}} = \frac{\partial s}{\partial q_i} \tag{158}$$

and thus

$$\frac{\partial \dot{\eta}}{\partial \dot{q_i}} = \frac{\ell^2 \dot{s}}{\dot{\eta}} \frac{\partial s}{\partial q_i} \tag{159}$$

Because s is a point on the line for which analytical expressions have already been presented, it is relatively easy from this point to compute the contributions to the right hand sides of the equations of motion resulting from tangential contact forces using formulae similar to those developed in Section 2.6.4.

2.6.6.1   Link Sharing for Hip, Knee, and Elbow Ellipses

A contact interaction feature called "link-sharing" can be specified for ellipses at the hip, knee, or elbow. Use of this feature is optional but recommended. It is set "on" by values in field 8 of Card 220.

"Link-sharing" is important in making more realistic the way that an ellipse at (or near) a joint produces tangential forces with a line segment. Card 219 is used to specify the link of attachment for each ellipse. When the link rotates, the ellipse rotates with it. Consider the case of a circle attached to the lower torso link and positioned with its center exactly at the hip joint. Consider, also, a similar data set in which the circle is attached instead to the upper leg link--and still positioned exactly at the hip joint. It seems desirable that these two data sets produce the same results, but they will not unless link-sharing is requested since for one the hip circle

rotates with the lower torso and for the other it rotates with the upper leg. This means that slip point velocities and therefore also tangential forces will be different. This feature will cause the hip circle to rotate (in essence) as an average of lower torso and upper leg rotations. This is much more realistic than a rotation with either one or the other of the two links associated with the hip, knee, and elbow joints.

The MVMA 2-D model allows specification in field 8 of the 220-Cards (hip, knee, and elbow) of values for the link number of the adjoining link, i.e., the link which "shares" the ellipse with regard to calculation of rotational terms for the slip velocity, deflection and lever arms for ellipse-line contact, etc. For the case described above, for example, where the 219-Card for the hip ellipse has a "4." in field 5, a "5." can be put in field 8 of the 220-Card to turn on link sharing. This feature is most reasonably used when the ellipses are circles (or nearly) and are positioned at or near to the joint.*

In lieu of equations, a description is now given of the method by which "link sharing" is accomplished for hip, knee, and elbow ellipses. At time zero, the inertial position and orientation of the ellipse are determined from input data. From these results, the position and orientation with respect to both the link of attachment and the contiguous link (the shared link) are calculated. These relative positions and orientations are saved. They are constant values which define the attachment coordinates (x, z, and theta) to the two links of, respectively, one user-defined and one derived (conceptual) ellipse.

At all subsequent times the inertial position and orientation of an "average ellipse" are determined as the average of the inertial positions and orientations of the defined ellipse (fixed on the link of attachment)

---

* Allowed link pairs on Cards 219 and 220 for shared attachment are:
  (4.,5.) (5.,4.) (5.,6.) (6.,5.) (7.,8.) (8.,7.) [hip, knee, elbow]

and the derived ellipse (fixed on the shared link). These averaged inertial values are then used throughout the contact algorithm in calculation of deflection, deflection rate, slip position, slip velocity, forces, torques, lever arms, and generalized forces.

Use of this feature except for defining what is, in essence, an averaged contact ellipse at a joint is unreasonable. The concept and its implementation in the model have the most meaning for circles that are centered at the allowed joints. It is not unreasonable to use this feature for ellipses that are not centered at a joint, but an advisory warning message is printed either if the ellipse is not a circle or if it is not located (almost) exactly at the joint connecting the two links. Also, if the secondary attachment specified in field 8 of Card 220 does not define a legitimate link pair for sharing, then a warning is printed and sharing is ignored for that ellipse.

2.6.7 Force Interactions Between Contact Ellipses

Allowance is made in the model for contact interaction between body segment "ellipses."* Regardless of whether the user provides circles or true ellipses, each interaction is modeled as one circle against another.

A user-defined ellipse is replaced either by a circle fixed to the body element or by a circle which can migrate along the major axis of the ellipse to a position of minimum distance from an approaching circle. Whether the fixed circle or the migrating circle is used depends on whether the ellipse does or does not approximate a circle. The definition of this criterion, the selection of circle radii, and definition of the extreme allowed positions on either side of the ellipse center for a migrating circle, or "replacement circle," are discussed in the following text.

---

* A body ellipse may also interact with an elliptically shaped element fixed to the vehicle frame of reference, to the inertial frame of reference, or to a user-defined link.

Since a circle migrating along the major axis essentially reduces an ellipse to parallel lines with a semicircular cap at each end, the approximation is best for ellipses with a>>c.

Figure 33 is a schematic showing the approach of a circle to a contact ellipse.

The parametric equations for line m are

$$x_i = x_{oi} + \lambda_i t \quad , \quad i = 1, 2 \tag{160}$$

where λ_i is yet to be determined but can for now be represented as

$$\lambda_i = x_{1i} - x_{oi} \tag{161}$$

The distance between the center of an approaching circle and points on the line m is given by

$$d^2 = \sum_{i=1}^{2} (x_i - X_i)^2 = \sum_{i=1}^{2} (x_{oi} - X_i + \lambda_i t)^2 \tag{162}$$

The shortest distance is found from

$$\left. \frac{\partial d^2}{\partial t} \right|_{t=\bar{t}} = 0 = \sum_{i=1}^{2} 2(x_{oi} - X_i - \lambda_i \bar{t}) \lambda_i \tag{163}$$

or

$$\sum_{i=1}^{2} \lambda_i (x_{oi} - X_i) + \sum_{i=1}^{2} \lambda_i^2 \bar{t} = 0$$

which gives

$$\bar{t} = \frac{\sum_{i=1}^{2} \lambda_i (X_i - x_{oi})}{\sum_{i=1}^{2} \lambda_i^2} \tag{164}$$

120   6/28/85
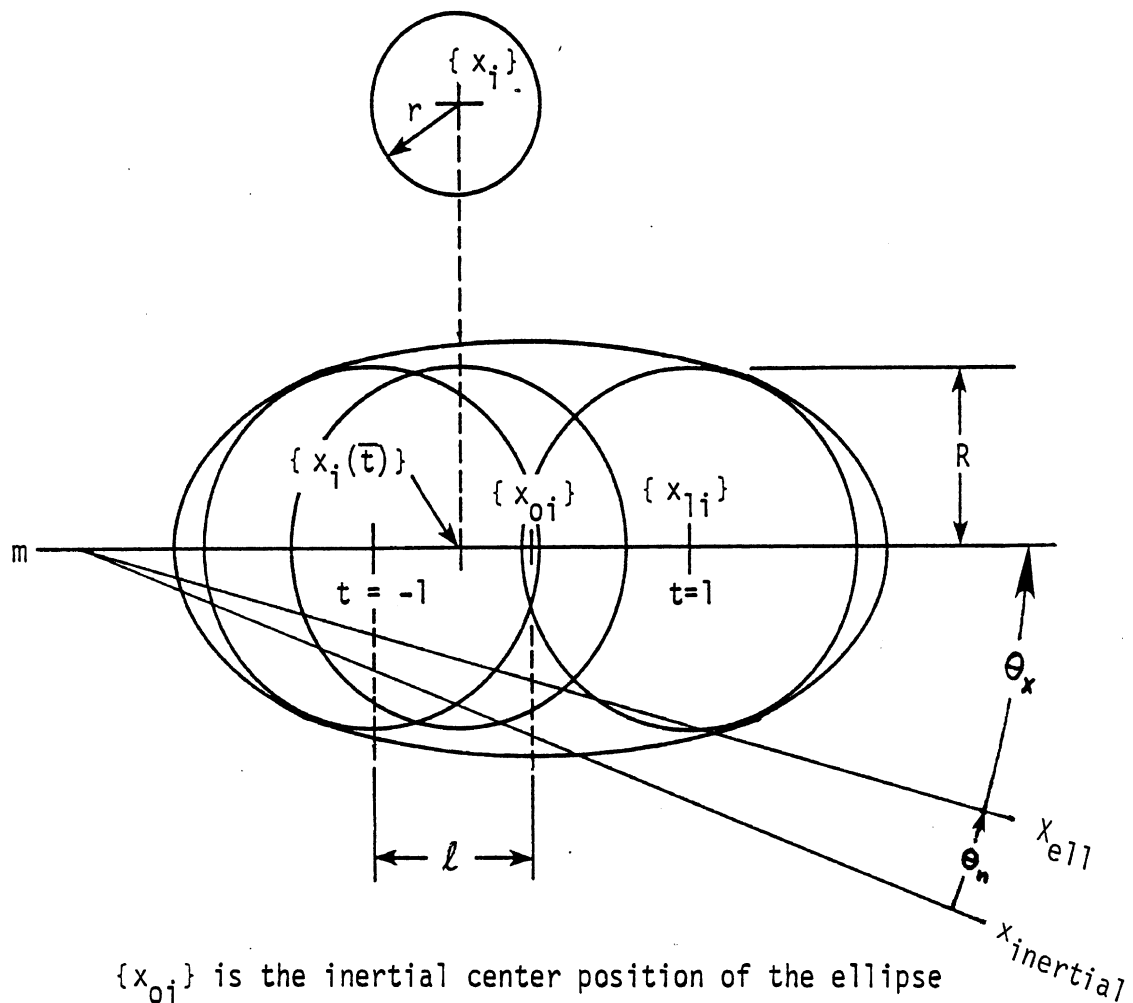
$\{x_{oi}\}$ is the inertial center position of the ellipse

$\{x_{1i}\}$ is the inertial center position of the migrating circle

θ_x = counterclockwise angle from link x-axis to ellipse axis #1
(zero if circle)

ϑ_n = link angle in inertial frame

Figure 33.   Approach of Circle to Ellipse

6/28/85

121

Now, $\{x_i(\bar{t})\}$ is the position of the center of a circle slid along the major axis to a point opposite the approaching circle as long as $-1 \leq \bar{t} \leq 1$. If $|\bar{t}| > 1$, then the circle may be positioned at $\bar{t} = \pm 1$. The ellipse is thus represented by parallel lines with semicircle (radius R) at each end.

If $\bar{t} < -1$, set $\bar{t} = -1$.

If $\bar{t} > 1$, set $\bar{t} = 1$.

Then evaluate

$$(R+r)^2 - \sum_{i=1}^{2} (x_{oi} - X_i + \lambda_i \bar{t})^2$$

If this is positive then the circles intersect and

$$\delta = R + r - \sqrt{\sum_{i=1}^{2} (x_{oi} - X_i + \lambda_i \bar{t})^2} \tag{165}$$

The derivative is

$$\frac{\partial \delta}{\partial q_j} = \frac{\sum_{i=1}^{2} (x_{oi} - X_i + \lambda_i \bar{t}) \left(\frac{\partial x_{oi}}{\partial q_j} - \frac{\partial X_i}{\partial q_j} + \lambda_i \frac{\partial \bar{t}}{\partial q_j} + \bar{t} \frac{\partial \lambda_i}{\partial q_j} \right)}{\delta - (R+r)} \tag{166}$$

Since

$$\sum_{i=1}^{2} 2 (x_{oi} - X_i + \lambda_i \bar{t}) \lambda_i = 0,$$

we have

$$\sum_{i=1}^{2} (x_{oi} - X_i + \lambda_i \bar{t}) \lambda_i \frac{\partial \bar{t}}{\partial q_j} = 0$$

Therefore,

$$\frac{\partial \delta}{\partial q_j} = \frac{\sum_{i=1}^{2} (x_{oi} - X_i + \lambda_i \bar{t}) \left(\frac{\partial x_{oi}}{\partial q_j} - \frac{\partial X_i}{\partial q_j} + \bar{t} \frac{\partial \lambda_i}{\partial q_j} \right)}{\delta - (R+r)} \tag{167}$$

where

$$\frac{\partial X_{oi}}{\partial q_k} = \frac{\partial X_{ni}}{\partial q_k} + X_{em} \frac{\partial T_{1in}}{\partial q_k} + Z_{em} \frac{\partial T_{2in}}{\partial q_k} \quad , i=1,2 \qquad (168)$$

and

$$\left[T_n \right] = \begin{bmatrix} \cos \theta_n & -\sin \theta_n \\ \sin \theta_n & \cos \theta_n \end{bmatrix} \qquad (169)$$

The derivatives of T_{ijn} are non-zero only if they are taken with respect to the generalized coordinate of the member on which the body ellipse is located.

The distance components λ_i (see Equation 161) will now be determined. From Figure 33 we have:

$$X_{o1} \hat{i} + X_{o2} \hat{k} + \ell \cos(\theta_x + \theta_n) \hat{i} - \ell \sin(\theta_x + \theta_n) \hat{k}$$
$$= X_{11} \hat{i} + X_{12} \hat{k} \qquad (171)$$

Thus,

$$X_{11} = X_{o1} + \ell \left(\cos \theta_x \cos \theta_n - \sin \theta_x \sin \theta_n \right)$$
$$X_{12} = X_{o2} - \ell \left(\sin \theta_x \cos \theta_n + \cos \theta_x \sin \theta_n \right) \qquad (172)$$

Therefore, by Equation 161,

$$\lambda_1 = \ell \left(\cos \theta_x \cos \theta_n - \sin \theta_x \sin \theta_n \right) \qquad (173)$$
$$\lambda_2 = -\ell \left(\sin \theta_x \cos \theta_n + \cos \theta_x \sin \theta_n \right)$$

and
$$\frac{\partial \lambda_1}{\partial q_k} = -\ell \left(\cos\theta_x \sin\theta_n + \sin\theta_x \cos\theta_n \right) \frac{\partial \theta_n}{\partial q_k}$$

$$\frac{\partial \lambda_2}{\partial q_k} = \ell \left(\sin\theta_x \sin\theta_n - \cos\theta_x \cos\theta_n \right) \frac{\partial \theta_n}{\partial q_k} \qquad (174)$$

Figure 34 is a schematic showing the approach between two body ellipses. The parametric equations for lines m and n are

$$x_i = x_{oi} + \lambda_i t$$
$$\xi_i = \xi_{oi} + \mu_i s \qquad , \quad i = 1, 2 \qquad (175)$$

where

$$\lambda_i = x_{1i} - x_{oi} \quad , \quad \mu_i = \xi_{1i} - \xi_{oi} \qquad (176)$$

The distance between two points on the lines is

$$d^2 = \sum_{i=1}^{2} (x_i - \xi_i)^2 = \sum_{i=1}^{2} (x_{oi} - \xi_{oi} + \lambda_i t - \mu_i s)^2 \qquad (177)$$

The shortest distance is found by minimizing d with respect to t and s and is

$$\bar{t} = \frac{\left[\sum\limits_{i=1}^{2} \lambda_i(x_{oi} - \xi_{oi})\right]\left[\sum\limits_{i=1}^{2} \mu_i^2\right] - \left[\sum\limits_{i=1}^{2} \mu_i(x_{oi} - \xi_{oi})\right]\left[\sum\limits_{i=1}^{2} \mu_i \lambda_i\right]}{\left[\sum\limits_{i=1}^{2} \mu_i \lambda_i\right]^2 - \left[\sum\limits_{i=1}^{2} \lambda_i^2\right]\left[\sum\limits_{i=1}^{2} \mu_i^2\right]}$$

$$\bar{s} = \frac{\left[\sum\limits_{i=1}^{2} \lambda_i(x_{oi} - \xi_{oi})\right]\left[\sum\limits_{i=1}^{2} \mu_i \lambda_i\right] - \left[\sum\limits_{i=1}^{2} \mu_i(x_{oi} - \xi_{oi})\right]\left[\sum\limits_{i=1}^{2} \lambda_i^2\right]}{\left[\sum\limits_{i=1}^{2} \mu_i \lambda_i\right]^2 - \left[\sum\limits_{i=1}^{2} \lambda_i^2\right]\left[\sum\limits_{i=1}^{2} \mu_i^2\right]} \qquad (178)$$

If $\bar{t} < -1; \ \bar{t} > 1; \ \bar{s} < -1; \ \bar{s} > 1$, then $\bar{t}$ and $\bar{s}$ are set to $\bar{t}=-1; \ \bar{t}=1; \ \bar{s}=-1; \ \bar{s}=1$.

If

$$(R + r)^2 - \sum_{i=1}^{2} (x_{oi} - \xi_{oi} + \lambda_i \bar{t} - \mu_i \bar{s})^2 \qquad (179)$$

124   6/28/85
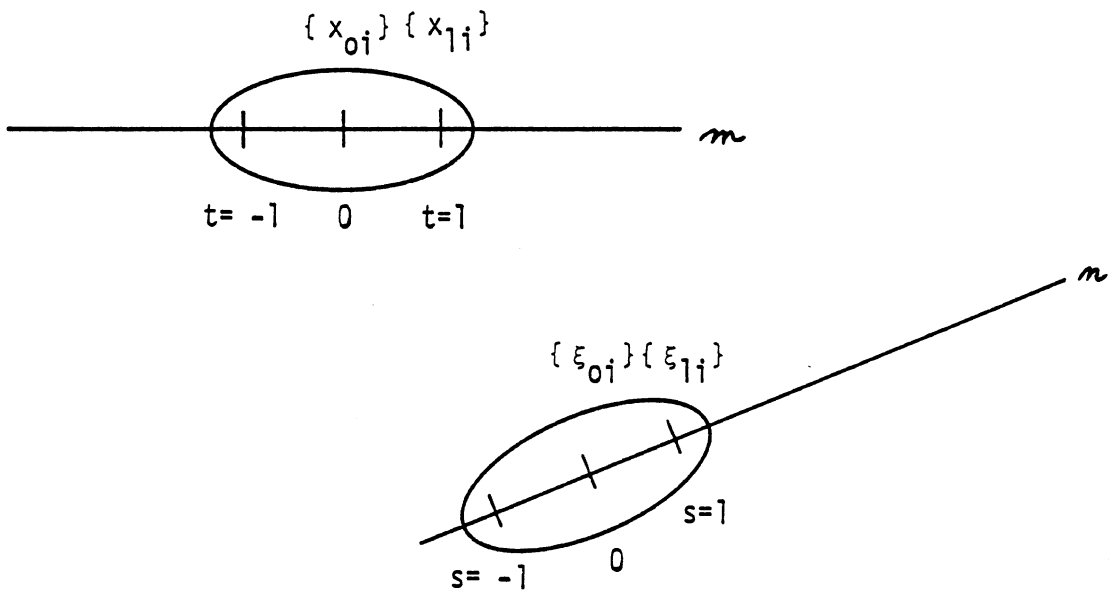
Figure 34. Approach of Ellipse to Ellipse

is positive then

$$\delta = R + r - \sqrt{\sum_{i=1}^{2} \left(x_{oi} - \xi_{oi} + \lambda_i \bar{t} - \mu_i \bar{s} \right)^2} \qquad (180)$$

and its derivative is

$$\frac{\partial \delta}{\partial q_n} = \frac{\sum_{i=1}^{2} \left(x_{oi} - \xi_{oi} + \lambda_i \bar{t} - \mu_i \bar{s} \right) \left(\dfrac{\partial x_{oi}}{\partial q_n} - \dfrac{\partial \xi_{oi}}{\partial q_n} + \bar{t} \dfrac{\partial \lambda_i}{\partial q_n} - \bar{s} \dfrac{\partial \mu_i}{\partial q_n} \right)}{\delta - (R + r)} \qquad (181)$$

The form of the derivative quantities is similar to that for the circle-ellipse contact discussed previously.

If the denominators of Equation 178 are zero, then the major axes of the ellipses are parallel and the problem must be treated as a special case.

A body ellipse is replaced by a circle for the purpose of "ellipse-ellipse" interaction if it is sufficiently like a circle. The criterion is as follows: Where $a \geqslant c$, the ellipse is replaced by a circle if $\frac{c}{a} \geqslant \beta$, where β is an input parameter. If this condition is satisfied, then R=c and the circle will be positioned at the center of the ellipse. Alternative definitions of R, such as R=(a+c)/2 or R=$[(a^2+c^2)/2]^{1/2}$ were considered, but R=c is felt to be the best selection.

If an ellipse fails the circle replacement test just outlined, then a radius must be assigned for a circle which migrates along the major axis. This radius is taken as R=c, where $a \geq c$. This is illustrated in Figure 35.

Given R for the migrating circle, how should ℓ be selected? The following form is used:

$$\ell = \gamma \, (a - R)$$

Here, $\gamma \leq 1$ is an input parameter. Note that γ=1 puts the circle flush to the end of the ellipse. At the user's option specific "ellipse-ellipse" interactions are either allowed or disallowed.

Ellipse replacement
circles at the extreme
allowed positions

$R = c$

$$I = \gamma (a-R)$$

Ellipse with $\dfrac{c}{a} < \beta$
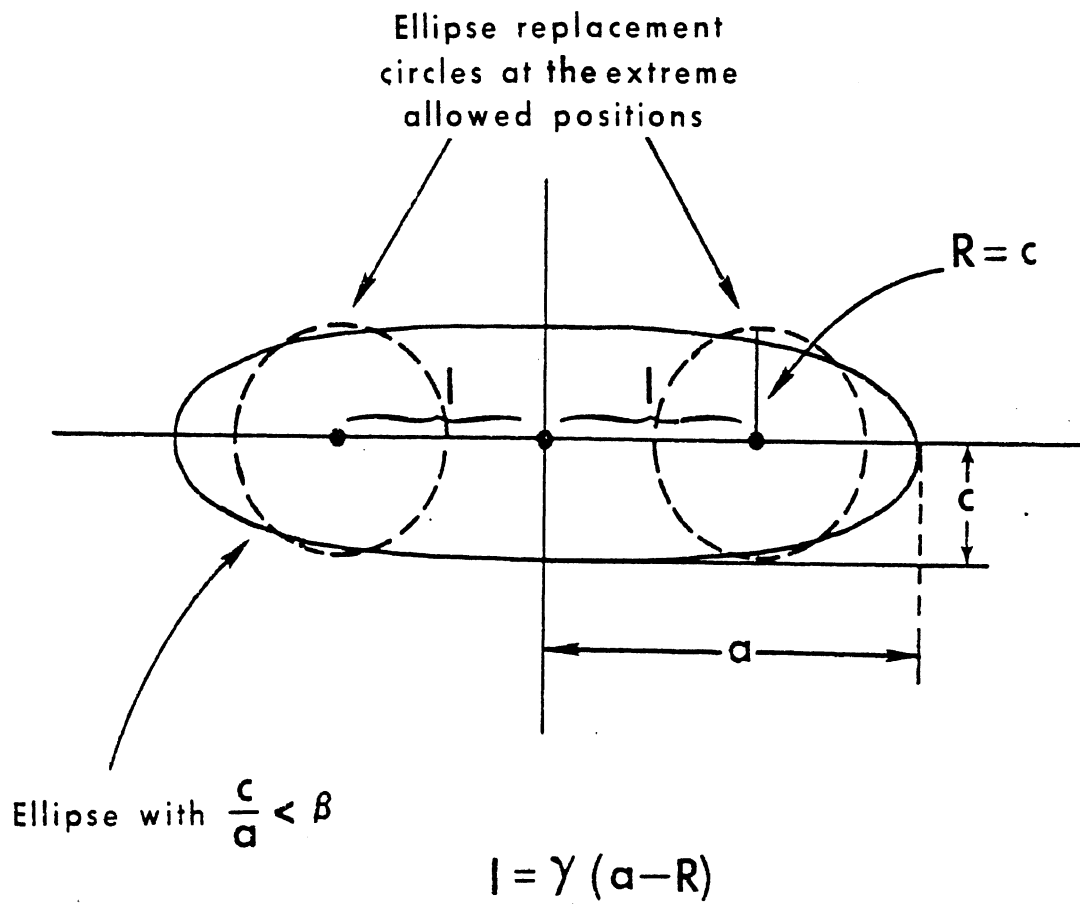
FIGURE 35   Approximation of an Ellipse by a Replacement Circle
of Varying Position

127

Sections 2.6.8-2.6.10

Sections 2.6.8 through 2.6.10 (pages 128-148) are obsolete and have been removed from Volume 1.

6/30/88

2.7 INFLATABLE OCCUPANT RESTRAINT SYSTEM SUBMODEL (also see Section 2.11)

Available as an option is a submodel of an inflatable occupant restraint device (airbag). The airbag is intended to contact both the occupant and vehicle interior while restraining forces due to the internal pressure and skin tension are generated when the bag is fully inflated. The shape of the bag is allowed to conform to that of the occupant and the vehicle interior with free sections of the perimeter defined as circular segments. When the pressure in the bag reaches a specified level, gas is allowed to flow out of the bag through defined orifices.

2.7.1 Airbag Enclosure

The airbag expands within a closed area illustrated in Figure 45.   The area is defined by: a) five inputted straight line segments attached, respectively, to the upper torso, middle torso, lower torso, upper legs, and lower legs (see Figure 46) ; b) calculated straight line segments joining the endpoints of the five primary line segments; c) two calculated straight line segments approximating the front of the head; d) from one to five inputted frontal interior line segments (special entries on standard 411 cards); e) a roof line extending to above and behind the head; f) and two calculated line segments which close the area (a-b and 10-A in Figure 45).

In Figure 45 the bag source, or "attachment point," is (X_A, Z_A). This point is inputted in vehicle coordinates on the 901 and 902 cards and is fixed in the vehicle. For the example frontal interior for airbag contact in the figure six entries on 411 cards define the points A, B, C, D, E, F and thus the lines AB, BC, CD, DE, EF. All vehicle interior line segment endpoints can be prescribed as functions of time, and the airbag will sense any collapse of the lines AB, BC, DE, and EF about it. These lines are sensitive
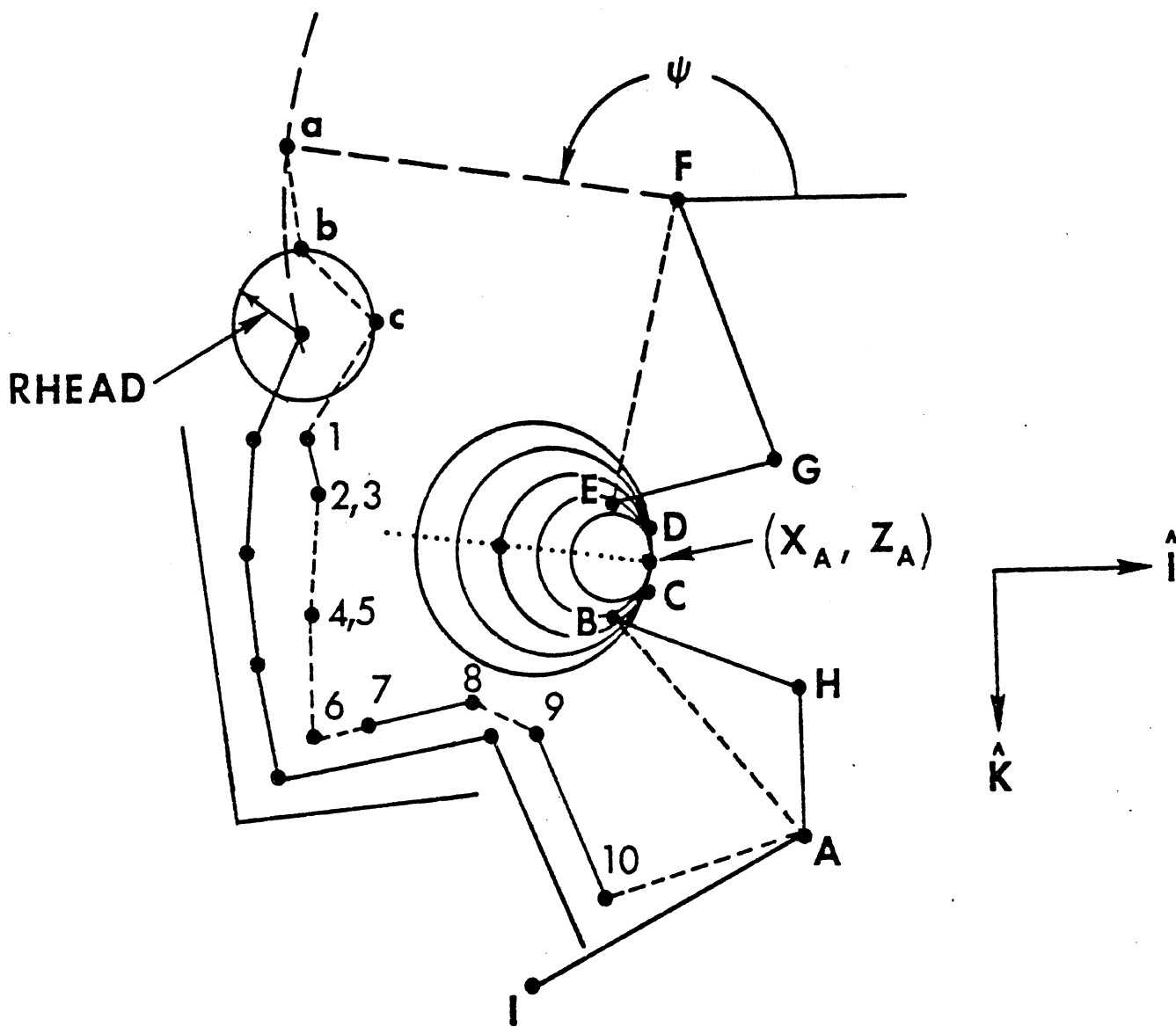
FIGURE 45   MVMA 2-D Airbag Model
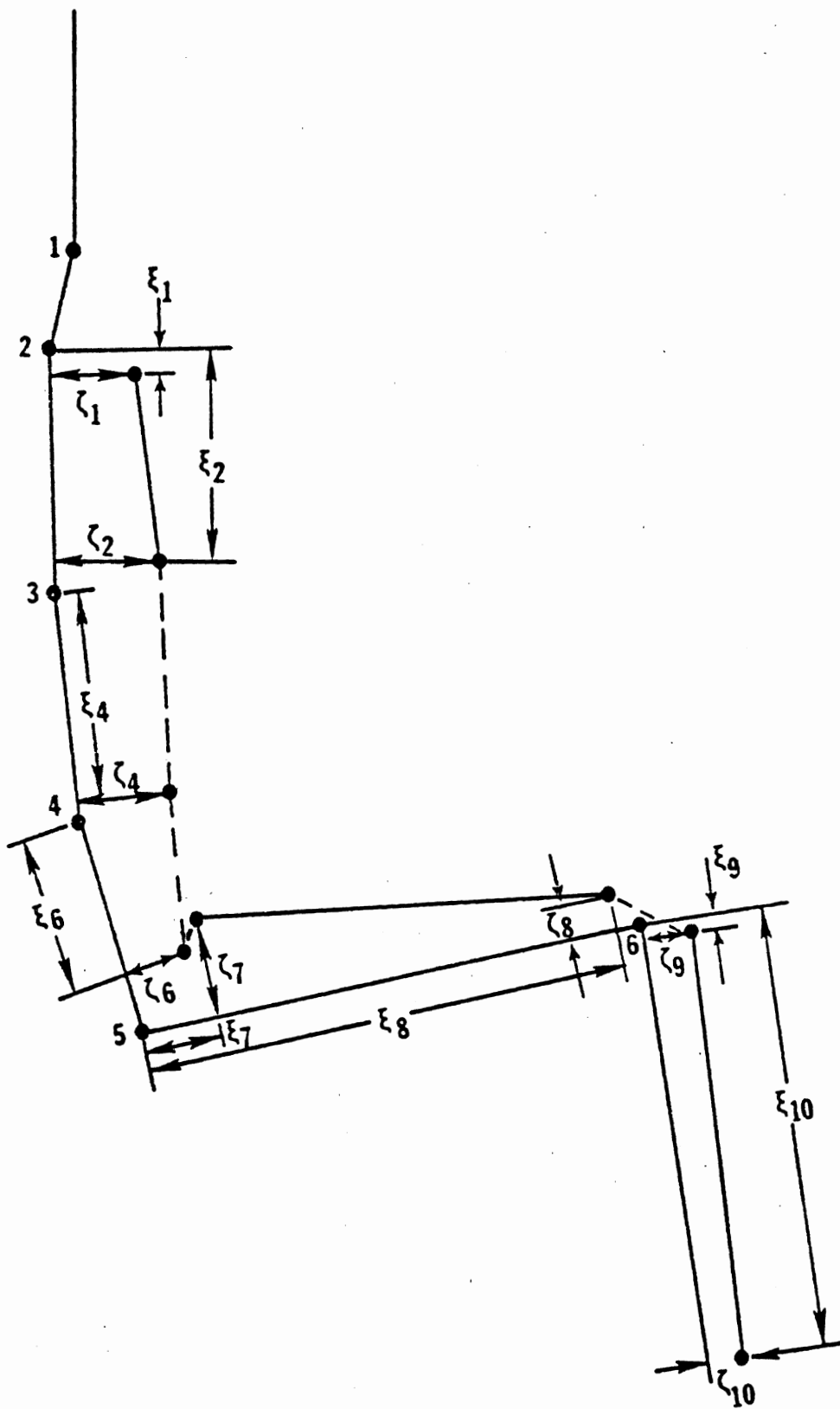
FIGURE 46   Airbag Contact Lines on Occupant

only to airbag contact while the example vehicle interior configuration defined by FGEDCBHAI is sensitive only to interaction with contact ellipses. Airbag forces and moments are applied to the occupant at segments C-1, 1-2, 3-4, 5-6, 7-8.

2.7.2 Assumptions

The approach chosen for developing a mathematical submodel for the simulation of inflatable occupant restraints was to produce the simplest model that would provide acceptable agreement with experimental data. This approach was taken to minimize the time and effort required to develop the model and to moderate the computer time required to run the simulation. Assumptions made in the formulation of the mathematical model were based upon both analysis of the physical processes involved and observation of high-speed movies of tests of prototype inflatable safety restraints. User experience with the model may suggest alteration of some of the assumptions or generalization of some of the algorithms used to cover a wider variety of physical situations. Observation of high-speed movies of tests led to four assumptions:

1. No restraint force is exerted upon the occupant until the bag is fully expanded. This is equivalent to stating that the mass of the bag and its contents can be neglected.

2. The skin of the bag does not stretch.

3. The perimeter of the bag cross section in the plane of motion conforms to the shape of the automobile interior or to the occupant wherever they touch. Elsewhere the perimeter is described by circular arcs.

4. The bag slips freely over the occupant surface after contact, i.e., frictional forces are small compared with normal forces.

Four other assumptions were made to simplify the model.

1. Thermodynamic properties of the gas in the bag are calculated using adiabatic expansion of ideal nitrogen, neglecting potential energy of the gas. Flow of gas through the deflation membranes is calculated assuming unchoked flow through a converging nozzle.

2. The gas generator inflating the bag delivers gas at a predetermined rate . This implies that the area of the cross section of the bag increases at a predetermined rate until the bag is filled.

3. The point at which the bag attaches to the automobile interior is fixed with respect to the interior. This means that the bag may not be attached to a collapsible steering column.

4. Restraint force due to tension in the skin of the bag, caused primarily by the bag wrapping around the sides of the occupant, is approximated by a simple algorithm which takes into account the most important variables: pressure in the bag, width of the occupant and depth of penetration into the bag.

2.7.3 Simulation Description

The differential equations for occupant motion require values for forces and moments, from all sources, acting on the occupant. At each step of the numerical integration a central routine calls the airbag submodel, presents it with an updated occupant and vehicle position and receives in return updated forces and moments on the occupant due to the airbag. Basic organization of the airbag simulation is shown in Figure 47.

The bag may be arbitrarily positioned within the passenger compartment; for example, on the instrument panel. A vector heading must be specified to define an axis along which the bag center progresses as the bag becomes an ever-expanding circle. This heading remains constant before contact

153
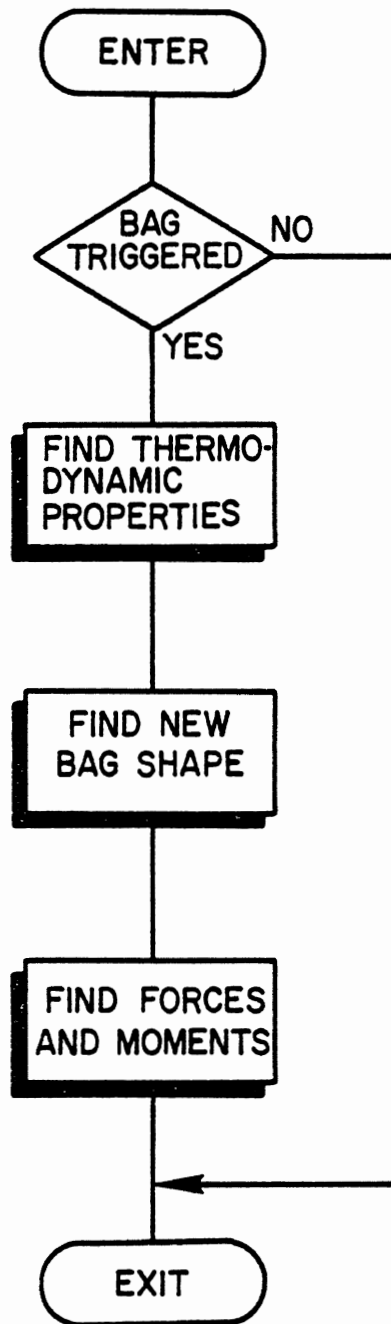
Figure 47. General Organization of the Airbag Simulation.

154

occurs with the line segments described in Section 2.7.1. In each integration step the radius of the undeformed portion of the bag is computed. Next, a radial search vector of this length originating at the bag center is allowed to sweep through a circle in three degree increments. If this search vector intersects any of the line segments used to constrain the bag, the bag outline coincides with the line segment up to the point of the sweep vector intersection. If no intersection occurs, the bag shape conforms to the undeformed circle. In this procedure, the summation of the bag perimeter components is checked and the radius of the undeformed portion adjusted so that the perimeter requirements are met. Before maximum inflation, the perimeter of the bag depends on the instantaneous volume of the bag, which is determined from the gas thermodynamics and the mass rate of the bag inflation. After full inflation the bag perimeter is maintained at the given input value. The instantaneous perimeter is deemed acceptable if its increase is less than 5% in the adjustment step even though the perimeter requirements are not met. This procedure is included to permit undeformed bag arc segments adjacent to the occupant and interior contact areas.

Bag shape is calculated in three ways corresponding to three different situations:

1. If the bag is neither fully inflated nor in contact with the occupant, the shape is assumed to be circular. The bag becomes "full" when the gas volume becomes as large as $\pi r^2 \cdot w$, where w is the inputted bag width and r is the filled-bag radius, as determined from the inputted filled-bag perimeter.

2. If the bag is not fully inflated but has contacted the occupant, the shape is calculated to enclose the known volume of gas thus far supplied by the source. The bag becomes "full" when the calculated perimeter of the deformed bag becomes as large as the inputted filled-bag perimeter.

155

3. If the bag is full, the shape is calculated to fit the inputted perimeter for the fully inflated bag. Whether or not the fully inflated bag is contacted by the occupant, its volume is calculated from its geometry, and the corresponding pressure can then be found. (After the pressure exceeds an inputted bound, the deflation membranes burst and the flow rate through them must also be calculated.) If the bag is contacted by the occupant, then the volume is lessened additionally by the intrusion of the occupant. Here, an assumption is made that the deformed section has half the width of the bag.

Forces on the bag are caused by contact with the occupant and the interior. It is assumed that forces in the vehicle x-direction caused by contact with the occupant are balanced by forces caused by contact with the interior. This assumption is viable if the bag is squeezed between the instrument panel and the occupant. In the z-direction the forces on the bag are balanced by changing the angle of the line along which the bag center moves during bag expansion.

Forces on the occupant are calculated as a sum of incremental forces caused by incremental areas of contact between bag and occupant as shown in Figure 48. Forces are accumulated for each of the body segments representing head, torso and upper legs. Moments on each segment are calculated in the same process. Each incremental force is made up of two parts: one caused by pressure inside the bag and the other by tension in the bag skin. The first of these is calculated from the incremental length, the width of the occupant at that point and the pressure in the bag. The skin tension force results from the tendency of the bag to wrap around the sides of the occupant. Since this simulation only calculates the shape of the bag in the

156
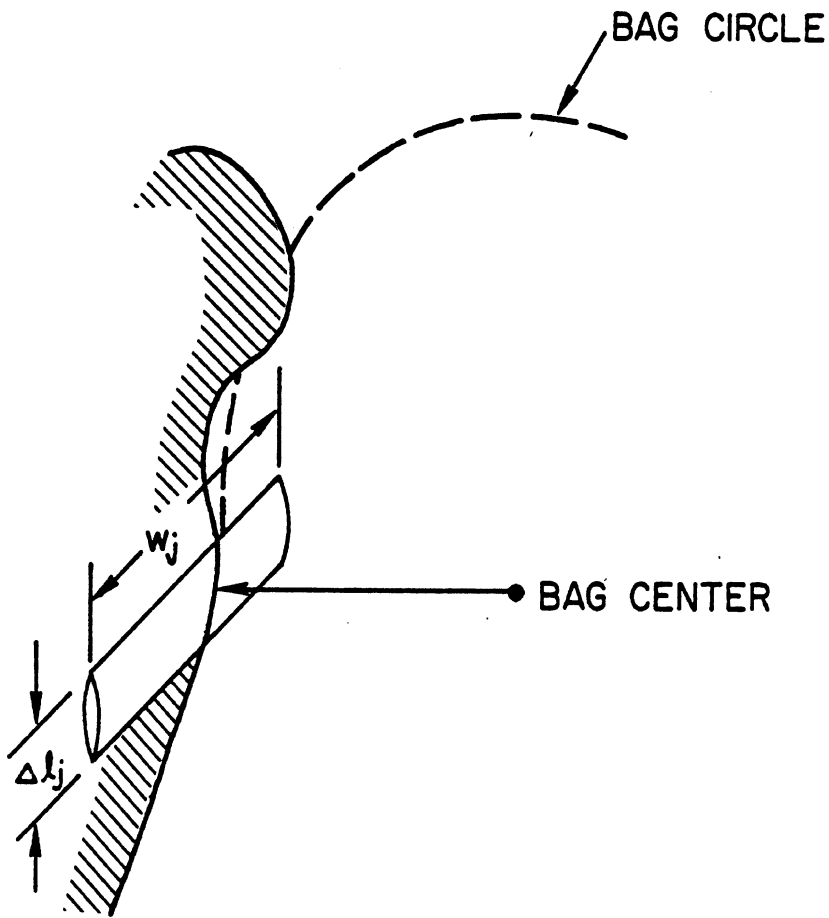
Δl_j = Incremental length of contact in plane of motion.

w_j = Width of occupant at this increment.
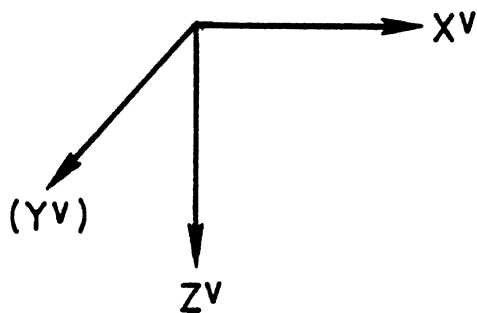
Figure 48. Incremental Force Generation.

plane of motion, skin tension force can only be roughly approximated. The variables of strongest influence on skin tension force are pressure inside the bag, width of the occupant at each increment and the distance the occupant has penetrated into the bag at that increment. The approximation used is an attempt to take all three of these factors into account without unduly increasing the complexity of the program. The equations for forces on the occupant are derived in Section 2.7.6.

2.7.4 Notation

In the analysis section 2.7.5 the following notation will be used

m	mass, lbm
h	specific enthalpy, BTU/lbm
$\bar{v}$	RMS velocity, ft/sec
W	work, ft-lb
U	internal energy, BTU
u	specific internal energy, BTU/lbm
T	temperature, °R
C_p	constant pressure specific heat, BTU/lbm-°R
V	volume, ft^3
P	pressure, lb/ft^2
$()_s$	supply cylinder
$()_n$	nozzle exit
$()_{ex}$	exhaust
$()$	(no subscript) bag
A	area, ft^2
γ	ratio of specific heats (C_p/C_v)
n	subscript indicating "nozzle"
s	subscript indicating "source" or "supply"

$()_s$, $()_n$, $()_{ex}$ see Figure 49

158
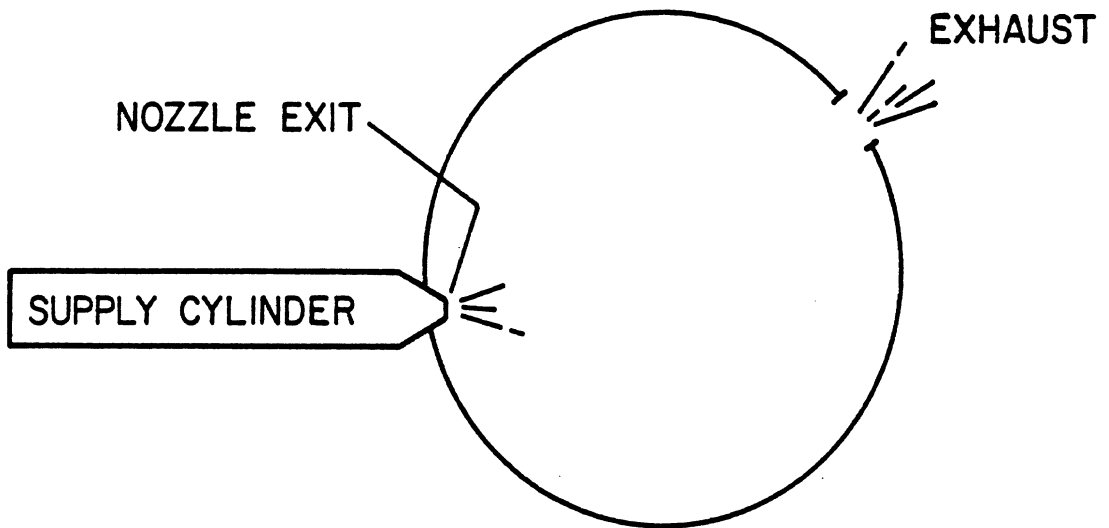
Figure 49. Supply Cylinder and Bag.

$()_i$ quantity evaluated at the ith integration increment

$()_{i-1}$ quantity evaluated at the (i-1)st integration increment

Δt integration increment, sec

t   time, sec

Units and Constants

The units used are British engineering units as suggested by Reference 22.

temperature	°R
mass	lbm
force	lb
heat	BTU
length	feet

In this unit system the gas constant and work equivalent of heat are:

$$R \quad \frac{ft\text{-}lb}{lbm\text{-}°R} \qquad 55.15 \text{ for nitrogen}$$

$$J \quad \frac{ft\text{-}lb}{BTU} \qquad 778$$

Newton's law in this unit system is:

$$F = ma/g_0 \text{ where } g_0 = 32.2 \frac{lbm\text{-}ft}{lb\text{-}sec^2}$$

It is noted here that while the MVMA 2-D computer model can be run in either English or metric units (internal units in-lb-sec or m-N-sec), all calculations within the package of airbag submodel subroutines are in English units.

2.7.5 Thermodynamic Model

The thermodynamic model consists of a set of differential equations to be numerically integrated along with the other system equations.

Equations for the thermodynamic model are:

$$\dot{T} = \frac{\dot{m}_n c_p (T_s - T) + (\dot{m}_n - \dot{m}_{ex})\frac{RT}{J} - \frac{\dot{W}}{J}}{m(c_p - R/J)}$$

$$\dot{m}_{ex} = \frac{A_{ex} P}{R} \sqrt{2 g_o J \left(\frac{c_p}{T} \left\{ \left(\frac{P_{ex}}{P}\right)^{2/\gamma} - \left(\frac{P_{ex}}{P}\right)^{(\gamma+1)/\gamma} \right\} \right)}^{1/2}$$

$$\dot{W} = \frac{P_{i-1} + P_i}{2 \Delta t} \left(|V_{i-1} - V_i| \right) \tag{206}$$

Volume during inflation is

$$V = \frac{mRT}{P} \tag{207}$$

Pressure during compression is

$$P = \frac{mRT}{V} \tag{208}$$

The basic assumptions used are:

1. The gas is ideal nitrogen.

2. The process is adiabatic.

3. Change in potential energy due to changes in elevation is negligible.

2.7.5.1 Thermodynamics During Inflation

Assume: 1. Steady flow through the nozzle of the supply cylinder

2. The gas in the supply cylinder is at rest.

With these assumptions the first law of thermodynamics for an adiabatic open system reduces to:

$$h_s = h_n + \frac{\bar{V}_n^2}{2g_0 J} \qquad (209)$$

For an ideal gas the specific enthalpy is a function only of temperature. For temperature below 810°R, constant pressure specific heat and therefore specific enthalpy varies less than 10% (Reference 23, Table 1) so assume it is constant. In this case,

$$h_s - h_n = C_p (T_s - T_n) \qquad (210)$$

Hence, the temperature at the nozzle exit is

$$T_n = T_s - \frac{\bar{V}_n^2}{2g_0 J C_p} \qquad (211)$$

Now, consider the expanding bag as an open system with $\delta m_{ex} = 0$ (i.e., before rupture of the deflation membranes). In this case, the first law of thermodynamics is:

$$\delta m_n \left(h_n + \frac{\bar{V}_n^2}{2g_0 J} \right) = \frac{\delta W}{J} + d \left(U + \frac{m \bar{V}^2}{2g_0 J} \right) \qquad (212)$$

The work term is $\delta W = P \delta V$. Assume that in the expanding bag the pressure is constant (at 1 atmosphere), that h_n and $\bar{V}_n$ are constants, and that kinetic energy of gas inside the bag is negligible. Then, since $\delta m = \delta m_n - \delta m_{ex}$, the above equation yields:

$$m \left(h_n + \frac{\bar{V}_n^2}{2g_0 J} \right) = \frac{PV}{J} + U \qquad (213)$$

From the equation of state PV = mRT; the definition of enthalpy $U = m(h - \frac{RT}{J})$; the relation $h_n - h = C_p(T_n - T)$; equation 211 for T_n; equation

213 reduces to:

$$T = T_s \tag{214}$$

That is, given the aforementioned assumptions, the temperature of the gas in the expanding bag approximates the supply temperature before bursting of the deflation membranes.

2.7.5.2 Thermodynamics During Exhaust

Start with the derivative form of the first law of thermodynamics for an adiabatic open system.

$$\dot{m}_n \left(h_n + \frac{\overline{V}_n^2}{2g_0 J} \right) = \frac{\dot{W}}{J} + \dot{m}_{ex} \left(h_{ex} + \frac{\overline{V}_{ex}^2}{2g_0 J} \right) + \frac{d}{dt} \left(U + \frac{m \overline{V}^2}{2g_0 J} \right) \tag{215}$$

Assume: 1. Kinetic energy of the exhaust gas is small. In this case the exhaust is an isenthalpic throttling.

2. Kinetic energy of gas inside the bag is small.

3. The work term is solely due to the moving boundary of the system (expansion or compression of the bag).

4. C_p is constant.

For an ideal gas:

1. $U = m(h - \frac{RT}{J})$ definition of enthalpy

2. $\dot{h} = C_p \dot{T}$

With T_n from (211) in $h_n - h = C_p(T_n - T)$ and from $\dot{m} = \dot{m}_n - \dot{m}_{ex}$, equation 215 may be reduced to solve for the rate of change of temperature of the gas in the bag.

$$\dot{T} = \frac{\dot{m}_n (T_s - T) C_p + (\dot{m}_n - \dot{m}_{ex}) \frac{RT}{J} - \frac{\dot{W}}{J}}{m (C_p - R/J)} \tag{216}$$

Inlet mass flow rate is a tabular input to the simulation. The exhaust mass flow rate is calculated from the equation for unchoked flow through an orifice with no losses (i.e., a value of 1 for the orifice discharge coefficient, C_D).

$$\dot{m}_{ex} = \frac{A_{ex} P C_D}{R} \sqrt{2 g_o J} \left(\frac{C_p}{T} \left\{ \left(\frac{P_{ex}}{P} \right)^{2/\gamma} - \left(\frac{P_{ex}}{P} \right)^{(\gamma+1)/\gamma} \right\} \right)^{1/2} \qquad (217)$$

Rate of work at the moving boundary is determined in the program by numerical differentiation using stored values of the bag pressure and volume calculated for the previous integration time increment (See Figure 50).

2.7.6 Restraint Force Calculation

Restraint forces are assumed to exist only when the bag is fully inflated and in contact with the occupant. Restraint forces are calculated at the same time that the bag shape is being determined.

A radial search vector (see Section 2.7.3) begins at an angle $\alpha_1 = \theta_R$ and rotates by three degree increments through the full circle. The search vector is equal in length to the current bag radius. The intercepted length for bag contact is R_n. When the bag is fully inflated, restraint forces are present whenever the vector intersects the occupant. There are two contributions to restraint force: pressure over the contact area and skin tension force. The contributions for each three degree increment are determined in the direction of the search vector and the component normal to the contacted line segment is then resolved to components in the inertial frame of reference.

164
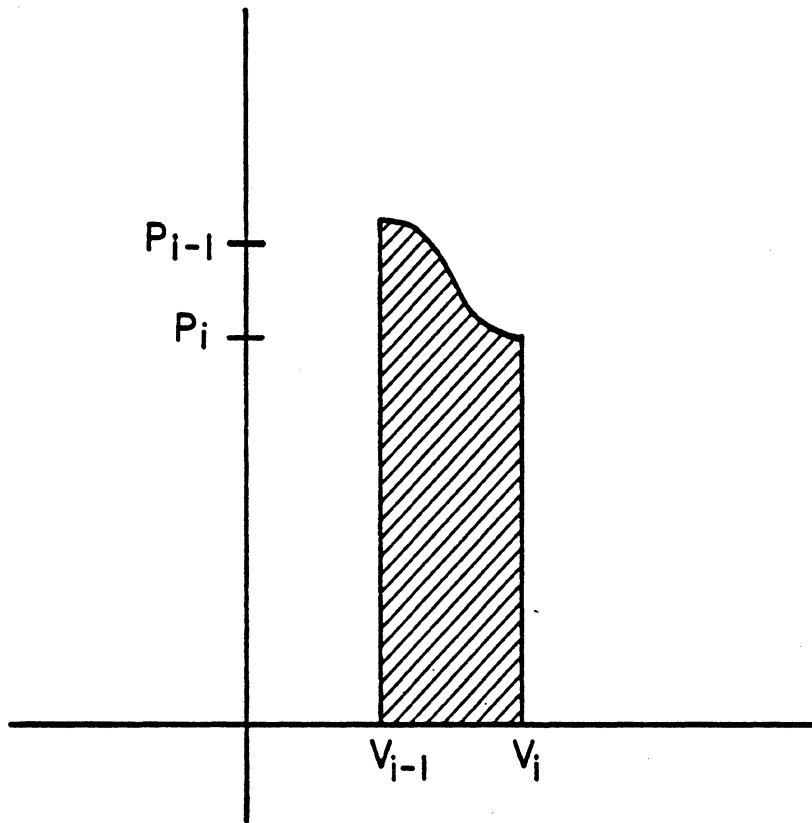
$$\dot{W} \approx \frac{(P_{i-1} + P_i)}{2 \Delta t} \left| V_{i-1} - V_i \right|$$

Figure 50.   Rate of Work of Moving Boundary.

6/30/88
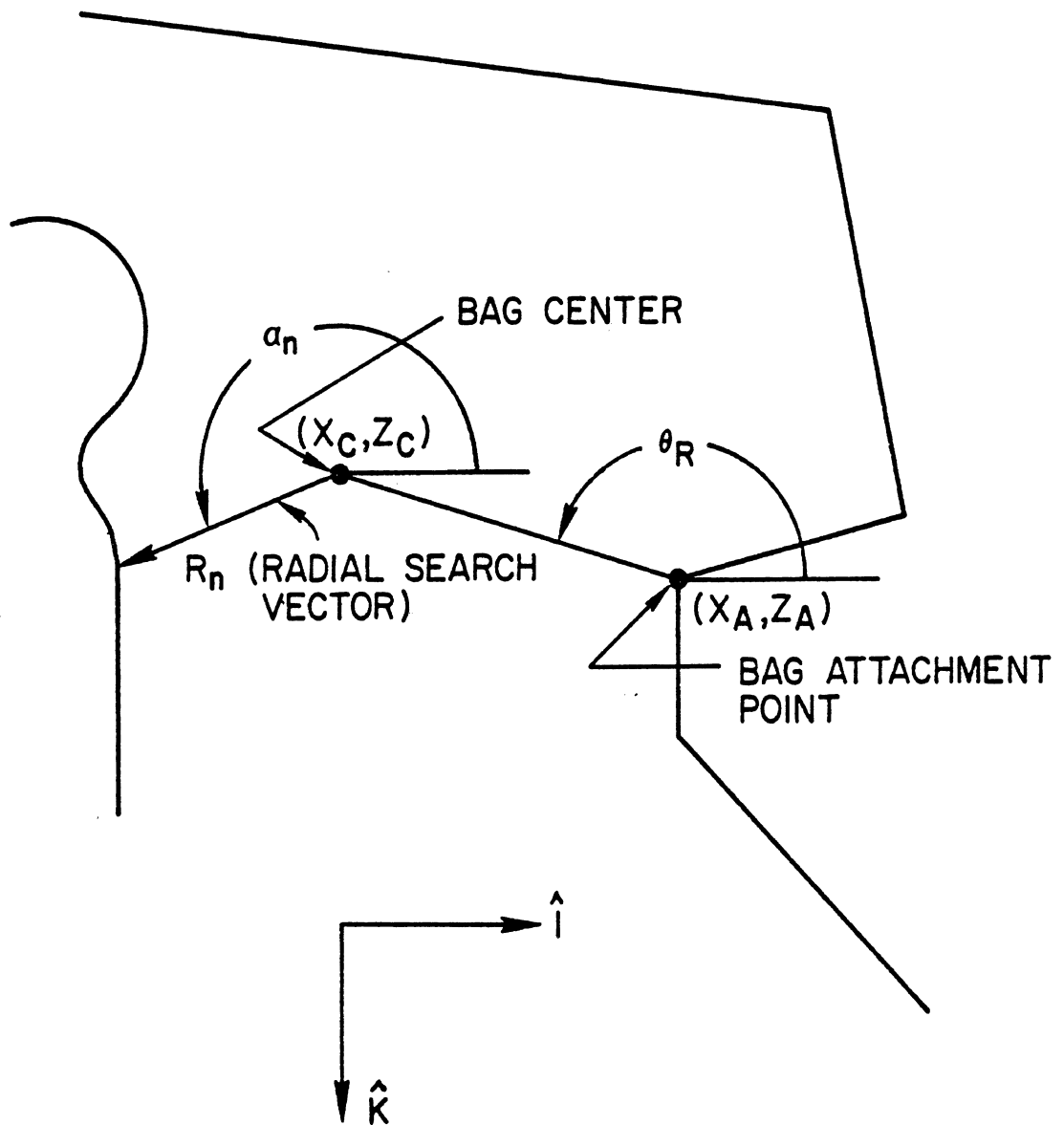
Figure 51. Radial Search Vector.

2.7.6.1 Pressure Force

As the radius vector rotates by $\Delta\alpha$, its tip sweeps out an increment of length $\Delta\ell = R_n \Delta\alpha$. Assuming that the jth segment of the occupant has constant width w_j leads to a contact area increment of $\Delta A = w_j \Delta\ell$. The pressure force contribution in the direction of the search vector is then

$$F_p = \left(P - P_a\right)\Delta A = \left(P - P_a\right)w_j R_n \Delta\alpha \, , \tag{218}$$

where P is absolute bag pressure and P_a is atmospheric pressure.

2.7.6.2 Skin Tension Force

The component of restraint force caused by tension in the bag skin can only be approximated in a two-dimensional simulation. The variables that influence skin tension force are pressure in the bag, width of the portion of the occupant contacting the bag, and the distance the occupant has penetrated into the bag. A horizontal slice through the bag before and after contact is illustrated in Figure 52.

It is assumed that the tension force in the skin of the bag contacted by the occupant is caused by pressure on the ends of the bag. Because restraint forces are calculated as a sum of incremental forces, the tension force must be divided up. This is equivalent to regarding the skin of the bag as being made up of a series of bands connecting the ends. Each of the bands is in tension but is supporting only its geometrical share of the total tension (See Figure 53).

The tension per unit length of bag skin is

$$\lambda = \frac{\left(P - P_a\right)A_E}{\not p} \, , \tag{219}$$

BEFORE OCCUPANT CONTACT:

|←—PLANE OF SIMULATION
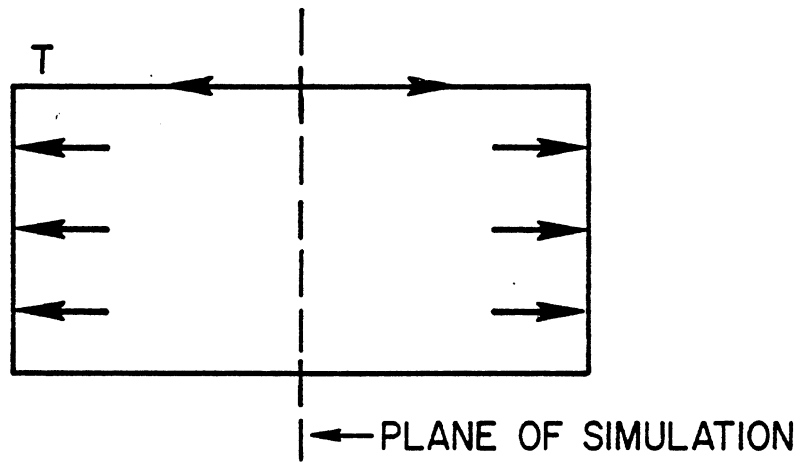
AFTER OCCUPANT CONTACT:
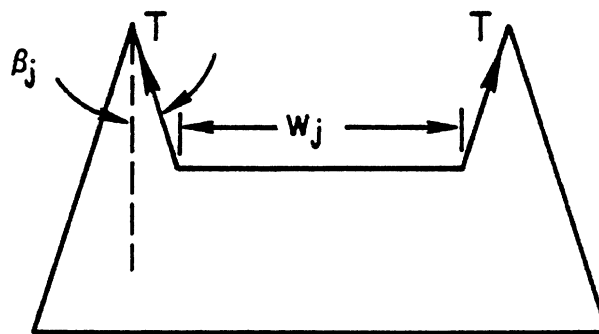
T = Skin Tension Force

w_j = Occupant Width at This Station

Figure 52.   Skin Tension Force.
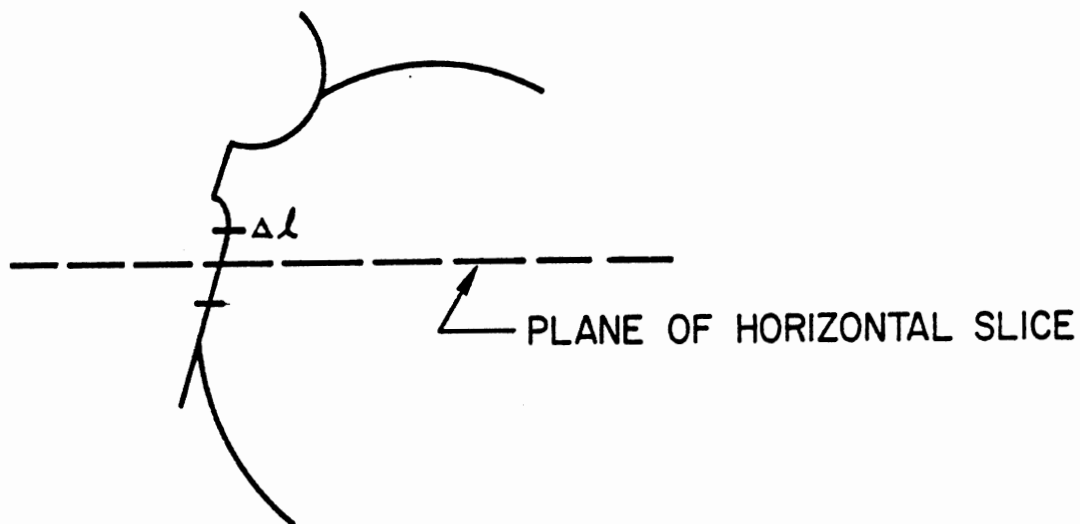
Figure 53.   Occupant-Bag Contact.

169
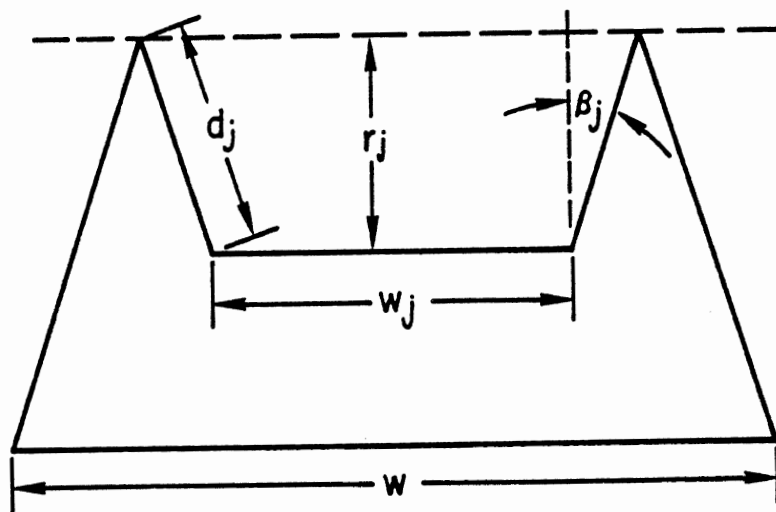
Figure 54.   Bag Penetration by Occupant.

where A_E is the area of the end of the bag and p is the total bag perimeter in the plane of simulation. The incremental skin tension force T is calculated assuming that the bag is composed of independent strips of width $\Delta\ell(=R_n \Delta\alpha)$:

$$T = \lambda\Delta\ell .\tag{220}$$

From Figure 52 it is clear that the total component of force restraining the occupant is

$$F_T = 2T \cos \beta_j.\tag{221}$$

The factor $\cos \beta_j$ is found from Figure 54. If it is assumed that the bag skin does not stretch, then $w = w_j + 2d_j$, where w is the bag width and w_j is the occupant width. Hence,

$$d_j = \frac{w-w_j}{2}\tag{222}$$

Then, where r_j is penetration into the bag, β_j is seen to be $\cos^{-1} (r_j/d_j)$, or

$$\cos \beta_j = 2r_j/(w-w_j).\tag{223}$$

Hence, the incremental skin tension force contribution in the direction of the search vector is

$$F_T = \frac{4 (P-P_a)A_E}{p} \frac{r_j R_n \Delta\alpha}{(w - w_j)} .\tag{224}$$

171

2.8 ENERGY ABSORBING STEERING COLUMN

Section 2.8 (pages 173-210) is obsolete and has been removed from Volume 1.

6/30/88

2.9 VEHICLE MOTIONS

Vehicle dynamics are constrained and specified by input to the computer program. The occupant compartment angular acceleration or angular position is described as a tabular function of time. Four basic options are available for specification of translational motion. 1) The two inertial components of linear acceleration at the defined vehicle origin point (i.e., origin of the vehicle-fixed coordinate frame) may be described as tabular functions of time. 2) Inertial horizontal and vertical positions may be defined for the vehicle origin. 3) Two linear accelerations along the vehicle-fixed axes, for a user-specified accelerometer location (a,c) in the vehicle, may be prescribed. (See Figure 63.) 4) Finally, the user may specify the vehicle x-axis component of acceleration at an accelerometer location together with motion of a "pivot point" for vehicle pitching. The usefulness of this last option is suggested from examination of film of crash tests. Here, the word "pivot" is used for a point for which position is constrained in one inertial coordinate (z), not both x and z. (x motion of the pivot point is unconstrained only in the sense that it is not explicitly prescribed.) Consider first a point (the pivot point) fixed with respect to the vehicle frame, i.e., a point with constant coordinates (p,q) in the vehicle system. (See Figure 63.) Suppose this point on the vehicle is constrained to move parallel to the inertial x-axis regardless of vehicle pitching motion, i.e., its inertial z coordinate is held constant. Such a point is the simplest type of pivot point that the user can define with the fourth option for specification of translational motion. For the general case, the user may prescribe a time varying inertial z position, $P_z(A)$, for the pivot point. Additionally, the pivot point need

Inertial reference frame
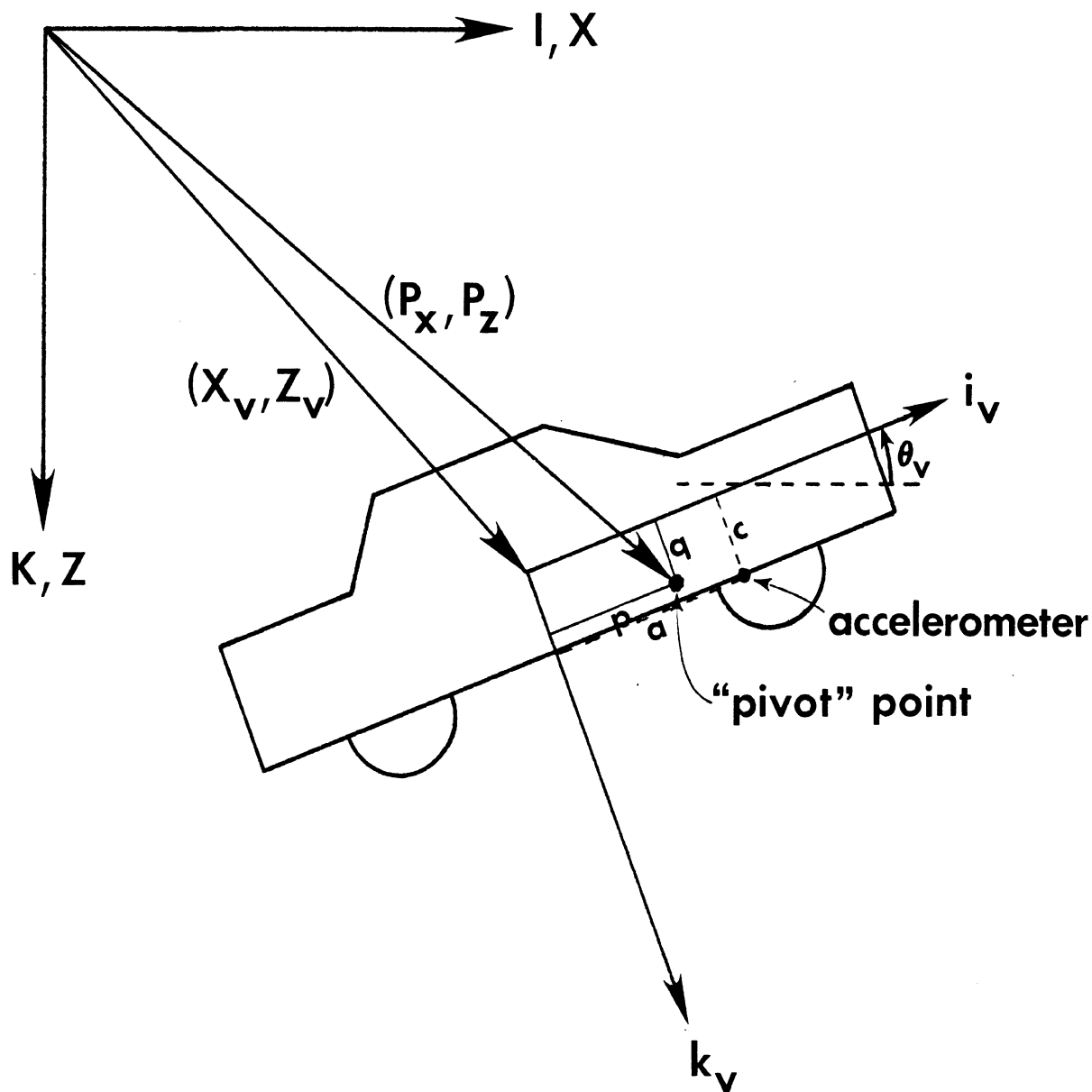
Figure 63.   Accelerometer Location and Pivot Point

not be fixed with respect to the vehicle coordinate frame, i.e., the co-ordinates p and q may also be specified as functions of time. For all cases, x motion of the pivot point, while not prescribed by the user, is determined from the x-accelerometer data, the pivot point z-motion, and the vehicle angular motion.

The vehicle translational degrees of freedom used in the equations of motion for the occupant are the inertial coordinates of the vehicle origin point. The positions of all contact panels, belt anchors, etc., are described with respect to that point. It is necessary, therefore, to determine the components of the inertial acceleration vector for the vehicle origin from whatever translational motion data have been speci-fied by the user. Velocities and positions are obtained from integration of the accelerations. The pertinent equations will now be developed.

Consider the general three-dimensional case of relative motion. Let a point in the vehicle be defined by its position vector $\vec{R}$ in the vehicle frame. The inertial velocity vector of such a point, in a trans-lating and rotating frame of reference, is given by the vector equation:

$$\vec{V} = \vec{V}_o + \dot{\vec{R}} \quad , \tag{308}$$

where $\vec{V}_o$ is the velocity of the origin of the rotating frame relative to the inertial frame of reference, i.e., the vehicle origin.

Where $\dot{\vec{R}}$ is the time rate of change as seen from the inertial frame of $\underline{any}$ vector $\vec{R}$ defined in the rotating frame, $\dot{\vec{R}}$ is found as

$$\dot{\vec{R}} = \frac{d\vec{R}}{dt} + \vec{\omega} \times \vec{R} \quad , \tag{308.1}$$

where:

$\vec{R}$ is the vector in the rotating frame

$\frac{d\vec{R}}{dt}$ is the time rate of change relative to the rotating frame of reference

$\vec{\omega}$ is the rotational velocity vector of the rotating frame relative to the inertial frame.

If $\vec{R}$ is the position vector of a point relative to the rotating frame, the acceleration of the point relative to the inertial reference frame is, from equation 308,

$$\vec{A} \equiv \dot{\vec{V}} = \dot{\vec{V}}_o + \ddot{\vec{R}} \ ,$$

or by carrying out the differentiation as indicated by equation 308.1,

$$\vec{A} = \dot{\vec{V}}_o + \left(\frac{d\dot{\vec{R}}}{dt}\right) + \dot{\vec{\omega}} \times \vec{R} + \vec{\omega} \times \dot{\vec{R}}$$

$$= \dot{\vec{V}}_o + \left[\frac{d^2\vec{R}}{dt^2} + \vec{\omega} \times \frac{d\vec{R}}{dt}\right] + \dot{\vec{\omega}} \times \vec{R}$$

$$+ \left[\vec{\omega} \times \left(\frac{d\vec{R}}{dt} + \vec{\omega} \times \vec{R}\right)\right]$$

This is

$$\vec{A} = \dot{\vec{V}}_o + \frac{d^2\vec{R}}{dt^2} + 2\vec{\omega} \times \frac{d\vec{R}}{dt} + \vec{\omega} \times (\vec{\omega} \times \vec{R}) + \dot{\vec{\omega}} \times \vec{R} \qquad (309)$$

Now, in particular, let $\vec{R}$ be the position vector for the biaxial accelerometer (Figure 63), i.e.,

$$\vec{R} = a\,\hat{\imath}_v + c\,\hat{k}_v \ . \qquad (309.1)$$

Also, in terms of their components, the other vectors in equation 309 are:

$$\vec{A} = a_x \hat{\imath}_v + a_z \hat{k}_v$$

$$\dot{\vec{V}}_o = \ddot{X}_v \hat{I} + \ddot{Z}_v \hat{K}$$

$$\frac{d\vec{R}}{dt} = \dot{a}\hat{\imath}_v + \dot{c}\hat{k}_v \qquad (309.2)$$

$$\frac{d^2\vec{R}}{dt^2} = \ddot{a}\hat{\imath}_v + \ddot{c}\hat{k}_v$$

$$\vec{\omega} = \dot{\theta}_v \hat{J} = \dot{\theta}_v \hat{\jmath}_v$$

Since the accelerometer location (a,c) is assumed fixed relative to the vehicle, $\dot{a}$, $\dot{c}$, $\ddot{a}$, and $\ddot{c}$ are all zero and equation (309) reduces to

$$a_x \hat{\imath}_v + a_z \hat{k}_v = \ddot{X}_v \hat{I} + \ddot{Z}_v \hat{K}$$
$$+ \dot{\theta}_v^2 \hat{\jmath}_v \times [\hat{\jmath}_v \times (a\hat{\imath}_v + c\hat{k}_v)]$$
$$+ \ddot{\theta}_v \hat{\jmath}_v \times (a\hat{\imath}_v + c\hat{k}_v), \qquad (310)$$

where $a_x(t)$ and $a_z(t)$ are accelerometer data. Since

$$\hat{I} = \hat{\imath}_v \cos\theta_v - \hat{k}_v \sin\theta_v$$

$$\hat{K} = \hat{\imath}_v \sin\theta_v + \hat{k}_v \cos\theta_v, \qquad (311)$$

we may write the component equations of equation (310) as

$$a_x = \ddot{X}^v - a\dot{\theta}^2 + c\ddot{\theta} \qquad (312.1)$$

$$a_z = \ddot{Z}^v - c\dot{\theta}^2 - a\ddot{\theta}, \qquad (312.2)$$

212.1   2/2/81

where $\ddot{x}^V$ and $\ddot{z}^V$ are the components of $(\ddot{X}_V, \ddot{Z}_V)$ -- the vehicle origin inertial acceleration -- expressed in the vehicle reference frame, i.e., the inverse relationships to

$$\ddot{X}_V = \ddot{x}^V \cos\theta_V + \ddot{z}^V \sin\theta_V \tag{313.1}$$

$$\ddot{Z}_V = -\ddot{x}^V \sin\theta_V + \ddot{z}^V \cos\theta_V \tag{313.2}$$

None of the foregoing equations are needed if the user supplies $\ddot{X}_V$ and $\ddot{Z}_V$ directly. However, if accelerometer data $a_x(t)$ and $a_z(t)$ are specified, equations (312) may be solved for $\ddot{x}^V$ and $\ddot{z}^V$ and then equations (313) yield $\ddot{X}_V$ and $\ddot{Z}_V$.

Consider next the case where $a_x(t)$ data and pivot point data are specified for the vehicle translational motion, i.e., the case of option 4 discussed previously. The user specifies pivot data $P_z(t)$, $p(t)$, and $q(t)$ in tabular form, from which time derivatives are found by the program. From Figure 63 , it is seen that

$$Z_V = P_z + p \sin\theta_V - q \cos\theta_V \tag{314.1}$$

Therefore,

$$\dot{Z}_V = \dot{P}_z + \dot{p} \sin\theta_V - \dot{q} \cos\theta_V + \dot{\theta}_V \left(p \cos\theta_V + q \sin\theta_V \right) \tag{314.2}$$

and

$$\ddot{Z}_V = \ddot{P}_z + \dddot{p}\,\sin\theta_V - \dddot{q}\,\cos\theta_V$$
$$+ \ddot{\theta}_V\left(\dot{p}\,\cos\theta_V + \dot{q}\,\sin\theta_V\right)$$
$$- \dot{\theta}_V^2\left(\dot{p}\,\sin\theta_V - \dot{q}\,\cos\theta_V\right) \qquad (314.3)$$
$$+ 2\,\dot{\theta}_V\left(\ddot{p}\,\cos\theta_V + \ddot{q}\,\sin\theta_V\right)$$

Now, $\ddot{x}^V$ may be determined from equation (312.1) as

$$\ddot{x}^V = a_x + a\,\dot{\theta}_V^2 - c\,\ddot{\theta}_V \qquad (315.1)$$

and, since (314.3) yields $\ddot{Z}_V$, equation (313.2) establishes $\ddot{z}^V$ as

$$\ddot{z}^V = \frac{\ddot{Z}_V + \ddot{x}^V\,\sin\theta_V}{\cos\theta_V} \;. \qquad (315.2)$$

$\ddot{X}_V$ may then be found from equation (313.1) and solution for the inertial acceleration vector $(\ddot{X}_V, \ddot{Z}_V)$ for the vehicle origin is complete. Integration (or table look-up if numerical differentiation was involved) yields velocities and displacement.

NOTE: For input of pivot data, z-accelerometer printout calculated by the program will be "jumpy" (although not necessarily inaccurate) unless all of the following are smooth: a) x-accelerometer input; b) angular acceleration (from direct entry or numerical differentiation of tabular $\theta_V(t)$; c) inertial Z-acceleration of pivot point (second derivative of Z input). Even when z-accelerometer calculations are unreliable, vehicle inertial velocities and displacements will be good, and only these terms enter the equations of motion.

2.9.1 Specifying Vehicle Motion With Pitching

The user has several options in relation to specification of vehicle motion. [See pages 211, 211.1, 211.2, and 277 (Card 601)]. It is recommended that the "pivot point" option be used whenever it is desired to model vehicle pitch, which normally occurs in barrier crash tests.

This option is easy to use. Any point for which motion with respect to both the inertial and vehicle coordinate systems is known is suitable for a "pivot point." A point on the header might be used for barrier tests. Such a point is easily targeted for determination of motion in the inertial system, and its motion in the vehicle coordinate system is simple—it is fixed. Model input data specifications for this example would be: vehicle x-accelerometer data, location of the fixed point ("pivot") on the vehicle, z-displacement time history in the inertial frame for the fixed point, and the vehicle pitch angle displacement time history. (Note: It is not necessary to use a fixed point on the vehicle as the pivot, but it is easier than using a moving point, which requires specification of motion of the point in both the inertial and vehicle systems.)

To use a fixed point on the vehicle as the "pivot point" (or "constraint point")—say, a point on the header—follow these steps:

1. Select the pivot point option by entering "-1." in field 9 of Card 601.

2. Specify x-accelerometer data by using Card 602 and associated unnumbered cards.

3. Specify pivot point option parameters on Card 603 as illustrated in the example below. The values on the card may be interpreted as follows:

    field 1: 49. (example) — the number or time points that will be given for the inertial z-displacement of the point on the header

    field 2: 0. — position data for the pivot point are in centimeters

213.1

field 3:   2.   — two time points will be given for the (fixed)
                   x position in the vehicle frame of the header
                   point, viz., equal values for t=0 and t=240, the
                   beginning and end times for the crash history

field 4:   2.   — two time points will be given for the z
                   position (fixed) in the vehicle frame of the
                   header point

field 5:   .25   (example) — typical value for control parameter,
                   but see note 7 for Card 602 for method to
                   calculate value

field 6:   12700. — recommended control value, not critical

field 7:   5080. — recommended control value, not critical

4. Follow Card 603 with as many unnumbered cards as necessary (13
    for this example) to specify the time history for inertial
    z-displacement of the header point. Follow these cards by one
    unnumbered card that has the two time point values for the fixed
    x-position of the header point and then a similar card for the
    z-position of the header point.

5. Specify vehicle pitch motion by using Card 604 and associated
    unnumbered cards. Motion may be given in terms of either
    angular accelerations or angular displacements. Displacement
    data is easier to obtain in most cases. The example 604-Card
    below is for displacement data.

EXAMPLE VEHICLE MOTION SPECIFICATION BY USE OF THE PIVOT
POINT OPTION FOR A FIXED POINT ON THE VEHICLE

```
0.      13.72   0.     0.      0.     0.       -190.   -12.   -1.    601
241.    1.                                                           602
(61 unnumbered cards with time history for x-accelerometer data)
49.     0.      2.     2.      .25    12700.  5080.                  603
0.      -147.5  11.    -147.5  20.    -148.4  25.     -146.9
32.     -146.4  .      .       .      .       .       .
.       .       .      (13 unnumbered cards for inertial   .    .
.       .       .      z-displacement of header point)     .    .
.       .       .      .       .      .       .       .    .    .
240.    -141.5
0.      -282.   240.   -282.          (x position in vehicle)
0.      -147.5  240.   -147.5         (z position in vehicle)
26.     2.      .13    5000.                                        604
(7 unnumbered cards with time history for pitch angle)
```

2.10 NON-BODY LINKS AND ELLIPSE CONTACT PROFILES

2.10.1 Non-Body Links

The MVMA 2-D occupant linkage is discussed in Sections 2.1 through 2.3. It is comprised of eight body-segment links which have mass and moment of inertia attributes (and two non-mass, extensible links -- the neck and the shoulder). These eight links are called "body links." In this section, user-defined mass segments not included in the body linkage are discussed. They are called "non-body links."

Non-body links are single-mass elements with three degrees of freedom. They can move translationally (x and z) and angularly (theta) within any specified coordinate system. They are independent from the body linkage except for possible interaction through external contact or viscoelastic connections that can be defined with a body link. Non-body links cannot be coupled to each other directly (e.g., at "joints"), although they can interact through standard contact forces.

General uses that can be made of non-body links are discussed below. There are two types of model elements that can be represented: 1) internal organs; 2) external masses not related to the occupant linkage.

2.10.1.1 Internal Organs

For each user-defined, non-body link, the MVMA 2-D model allows specification of numerous parameters. Appropriate specifications make possible a simple, deformable mass model of an internal organ. As an example, consider the heart. Parameters on Cards 219, 220, 249-254, and 305 might be specified as follows.

a. A non-body link (the heart) is defined, referenced to the upper torso link.

b. The equilibrium position and orientation of the link with respect to upper torso coordinate system are specified.

c. Viscoelastic (nonlinear spring-damper) coefficients are defined for resistance to motion away from the equilibrium location. These coefficients can be prescribed as functions of the circumferential direction of radial displacement away from the equilibrium position. This means that it is not necessary to confine the organ mass within a cavity of uniform resistance in all directions.

d. An elliptical profile (or more than one) is attached to the link so that the heart can interact with external contact-sensing elements that might intrude into the body.

e. Material properties for possible interaction with intruding elements are specified.

Even a simple model such as this allows study of potential injury to internal organs. Deformations, accelerations, and force and moment loadings for any organ of interest can be determined. (The MVMA 2-D model can also be used in ride comfort studies, for heavy equipment, in which motion of internal organs is a criterion.)

Similar links can be attached viscoelastically to the vehicle system or to the inertial system, instead of to body links, for special user applications.

2.10.1.2 External Masses

There are various ways that non-body links not related to the body linkage might be used. Such links might be attached viscoelastically to a designated reference system, or they might be physically unattached, i.e., "free."

One example is definition of a simple model of an infant held on a parent's lap. One or more contact-sensing ellipses can be attached to the infant link and appropriate material assignments can be made to the ellipse profiles. In addition, contact-sensing straight-line segments could be attached to the link as they can be attached to any reference system by use of the 401, 402, and 409-411 cards. Interactions of the infant's profile with both the adult occupant's profile and the vehicle interior are determined. An

example of a simple infant model is given in Volume 2 following the 219-Card layout.

Another type of use that might be made of non-organ, non-body links is in representing vehicle-interior elements which have mass and degrees of freedom. Non-body links can be attached to the vehicle through user-specified material properties so that forces generated by occupant impact will include both inertia and quasi-static deformation contributions. Straight-line contact surfaces can be used for constraining (guiding) the motion of mass elements and for providing resistance to their motion. Such an application might be made in modeling a steering column assembly, for example.

2.10.2 Ellipse Contact Profiles

2.10.2.1 Contact Profiles on Non-Body Links

Usually it is desired that a non-body link be "coupled" to other elements in the system through direct contact interactions in addition to "connection" interactions of a simple spring-mass-damper type. Contact interaction forces can be determined only if profiles for the interacting elements are specified, together with material properties relating to deformation of the elements.

Therefore, the user is allowed to attach any number of ellipse profiles to any non-body link in just the same manner that they can be attached to any body link. The dimensions and fixed position and orientation of the ellipse on the link can be specified. Ellipse contact-sensing profiles are discussed in Section 2.6.

"Regions" of contact-sensing straight lines (for interaction with ellipses) can also be attached to non-body links just as to any other primary reference system in an MVMA 2-D simulation. The purpose of this would usually be for allowing "impact contact" with ellipse profiles attached to other elements of the system. It is also possible to define a system of attached

contact line segments (as a box) on one link with a trapped contact ellipse on
a second link which will fasten the two links together. Such use of the model
must be done with great care, but there is no other way to couple together two
non-body links, i.e., they cannot be constrained at a true joint pivot of the
sort that is on the body linkage.

2.10.2.2 Contact Profiles on Body Links and on the Vehicle and Inertial
         Reference Systems

There is no fundamental difference between attaching a contact ellipse to
a non-body link and to a body link -- or to the vehicle or inertial reference
systems. All links and the vehicle and the inertial frame have their own
fixed reference frames, and the user can specify attachment of an ellipse to
any reference system through use of the 219 and 220 Cards (and 249 for
user-defined non-body links). Similarly, contact regions of straight-line
segments can be attached to any reference system.

While the standard manner of defining vehicle-interior profiles is to
model straight-line segment panels, the accuracy of representation of the
geometry of the vehicle interior can sometimes be improved by using curved
panels. Such panels should normally used together with straight-line segment
panels. Curved vehicle-interior panels can interact with either straight-line
or elliptically shaped elements of the occupant profile.

One special application of elliptical elements in the vehicle-interior
profile is in representation of the vertex point of two vehicle-interior
elements which meet in an acute angle. This can be accomplished through use
of an elliptical element of small radius of curvature. Edge constants (for
straight-line elements) probably become less significant in such simulations.

2.10.3 Summary of Allowed Non-Body Link Specifications

Imaginative use of non-body links together with other features of the MVMA 2-D model make possible the investigation of a variety of dynamic systems not related to an occupant or a vehicle interior. The MVMA 2-D features listed below are pertinent to standard and non-standard applications of non-body links. Data cards used for these features are Cards 219, 220, 249 through 254, and 305. In addition standard material card subsets described in Volume 2 are used to specify material properties relating to some of the features. (These are Cards 403-408, 221-226, 704-709, or 812-817.)

● A non-body link can be defined with respect to the coordinate system (reference system) of any body link, the vehicle, or the inertial frame.

● Mass and moment of inertia are specified for each non-body link. Initial position and velocity conditions are also specified by the user.

● A non-body link can be a free body, not connected physically to any other element of the system. Alternatively, it can be connected to its reference system through material or viscoelastic properties which provide:

   a. force resistance to radial motion from a specified equilibrium point

   b. torsion resistance to angular motion from a specified equilibrium orientation

   c. tangential resistance to circumferential motion

   Nonlinear spring-like resistances and damping resistances to radial motions can be defined as functions of circumferential heading.

● Contact ellipses profiles can be attached to any link (or other) coordinate system. They can be assigned standard material properties for determination of interaction forces with other ellipses or straight-line segments.

2.10.4 Allowed/Disallowed Interactions for Ellipses and Regions

The user can specify allowed or disallowed interactions for any ellipse or region. This is done by setting switches on the 102-Card and by making declarations for allowed or disallowed ellipse vs. ellipse and ellipse vs. region pairs on 106-Cards. The following rules apply, however, and will

override any inappropriate user 106-Card specifications. A warning is given for any "allowed interaction" specification that is overridden.

The general nature of the rules is to restrict interactions to those that might reasonably occur in any real mechanical system. For example, ellipse profiles fixed to the same link system are not allowed to produce an interaction force even though they may overlap. Also, "organ" links are not allowed to interact with other organ links even if the ellipses or regions which define their profiles are referenced to different body link systems since user-assigned radial stiffness/damping properties for entrapment of an organ are defined specifically to account for such interaction. In general, however, the user has considerable latitude in his specification of interactions, and he should make his 106-Card declarations with some care.

Table 5-1 describes the implicit conditions that relate to allowance of interaction between two ellipses or between an ellipse and a region. The following definitions apply to ellipses and to regions alike:

- Fixed -- rigidly attached to any reference system 1-10 (body links, vehicle system, and inertial system, respectively)

- Organ -- attached to a user-defined link referenced to system 1-8 and with at least one Card 250-252 included in the data deck (for radial stiffness connection)

- Free -- attached to a user-defined link referenced to a system 9, 10,..., or if referenced to a system 1-8, then without any associated Cards 250-252 (i.e., not radially connected)

TABLE 5-1. Allowed Ellipse-Ellipse or Ellipse-Region Interactions

Ellipse or Region Type

		FIXED	ORGAN	FREE
	FIXED	unless on same segment	unless on same segment	always
Ellipse Type	ORGAN	unless on same segment	never	always
	FREE	always	always	unless on same segment

2.11 ADVANCED AIRBAG SYSTEM (OVERVIEW)

2.11.1 Description of the Advanced Airbag System Submodel and Documentation

The Advanced Airbag System Submodel is documented in a separate manual. The submodel itself, however, is included in the MVMA 2-D program code. The Advanced Airbag System is a submodel of considerable complexity and flexibility. Its features include those listed below.

1. Representation of an arbitrary number of airbags, external and/or internal to each other.

2. Bag slap forces.

3. Pressure forces.

4. Membrane forces.

5. Deflation through vents and/or porous bag fabric.

6. Yielding of vehicle interior components in response to bag forces.

7. Tabularly-specified mass influx and source gas temperature as functions of time and fabric porosity as a function of pressure differential.

8. User-specified bag profiles during inflation, i.e., an arbitrary number of profiles in a time-history and arbitrary polygonal shape for each profile.

9. User-defined vehicle and occupant profiles for interaction with bags.

10. Analytical features and user inputs which take into account three-dimensional aspects of bag behavior even though the MVMA 2-D CVS is a planar model.

The Advanced Airbag System Submodel manual contains sections which parallel and supplement the three volumes of the Version 3 manuals.

2.11.2 General Description of Submodel Function

The flow diagram shown here as Figure 63-1 serves to illustrate the primary aspects of the Advanced Airbag System. Also, reference may be made to Volume 2, where data requirements are described for Cards 910-929.

Subroutine ADVBAG

(1) Establish the geometry of the enclosure for airbags   ENCLOS

n = 1

n = n + 1

(2) Investigate nth airbag   beginning of loop on airbags

(3) Determine whether airbag interacts with enclosure and determine profile of cross section of deformed bag   PROFLE

(4) Determine area of occupant-plane cross section of airbag   AREA1 AREA2

(5b) Use improved estimate of pressure for continuing the iteration

(5) Estimate pressure using pressure-volume relationship and user prescribed volume-area relationship   pressure-volume iteration

(5a) Has iteration for pressure converged?

no

yes

Figure 63-1 Flow Diagram for Advanced Airbag System Submodel (page 1)

```
                    ┌──────────────────────┐
                    │ Determine time       │
                    │ rate of change of    │
         (6)        │ gas temperature      │        THERMO
                    │ and mass for         │
                    │ integration          │
                    └──────────────────────┘

                    ┌──────────────────────┐
                    │ Determine width      │
         (7)        │ of bag contact       │        WIDTH
                    │ with vehicle         │
                    │ interior             │
                    └──────────────────────┘

                    ┌──────────────────────┐
                    │ Determine occupant-  │
         (8)        │ plane flotation      │        FLOTW
                    │ forces               │
                    └──────────────────────┘

                    ┌──────────────────────┐
                    │ Determine off-       │
         (9)        │ occupant plane       │        FLOTE
                    │ flotation forces     │
                    └──────────────────────┘

    (10b)         (10) ┌──────────────────┐
 ┌────────────────┐    │ Determine sum of │
 │ Determine angular   │ moments on       │
 │ position of         │ airbag           │
 │ bag in direction    └──────────────────┘
 │ consistent with
 │ the imbalance     ┌──────────────────┐
 └────────────────┘  │ Is the moment    │
              no     │ imbalance        │
            (10a)    │ acceptable?      │
                     └──────────────────┘
                              │ yes
```
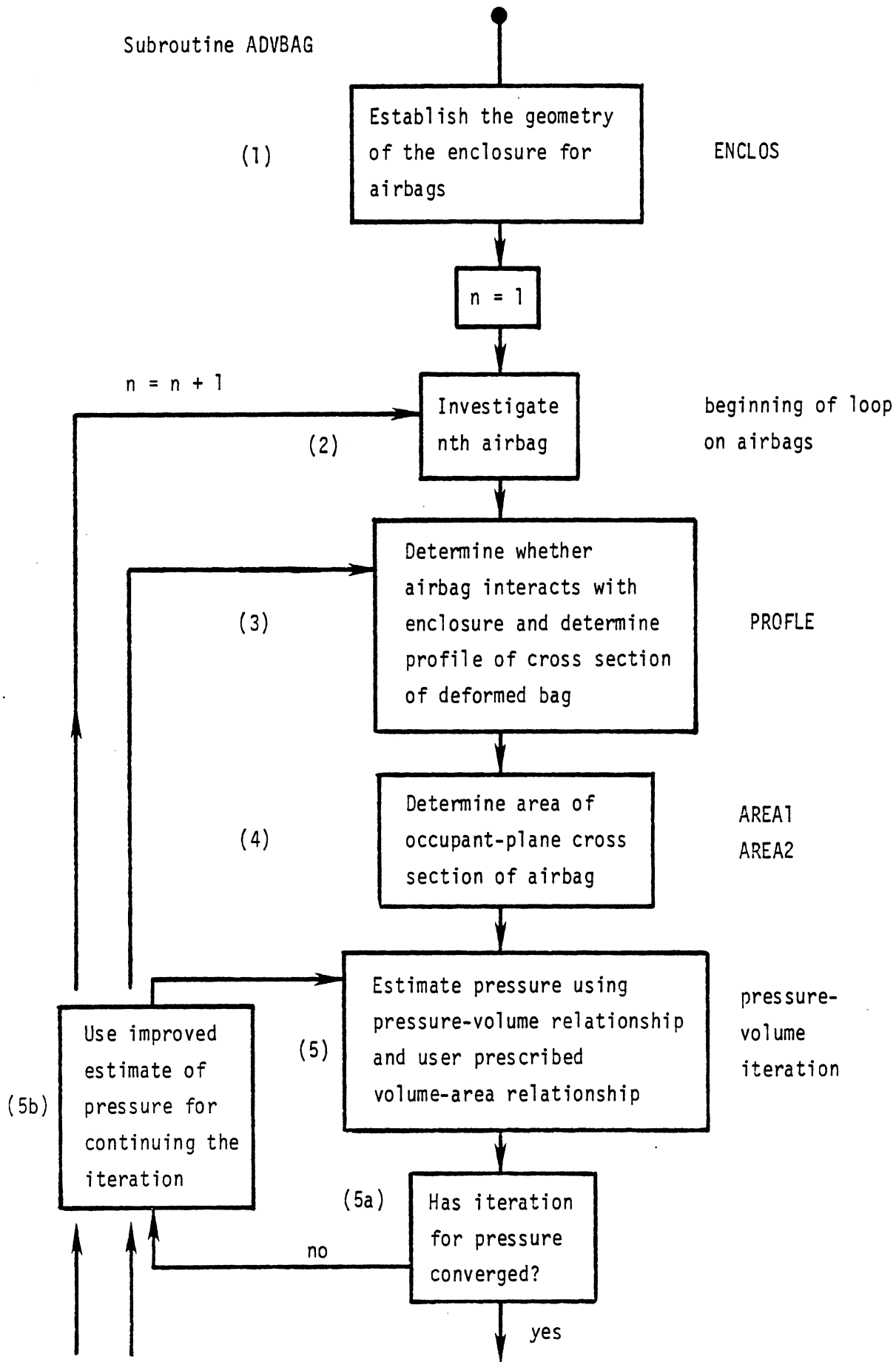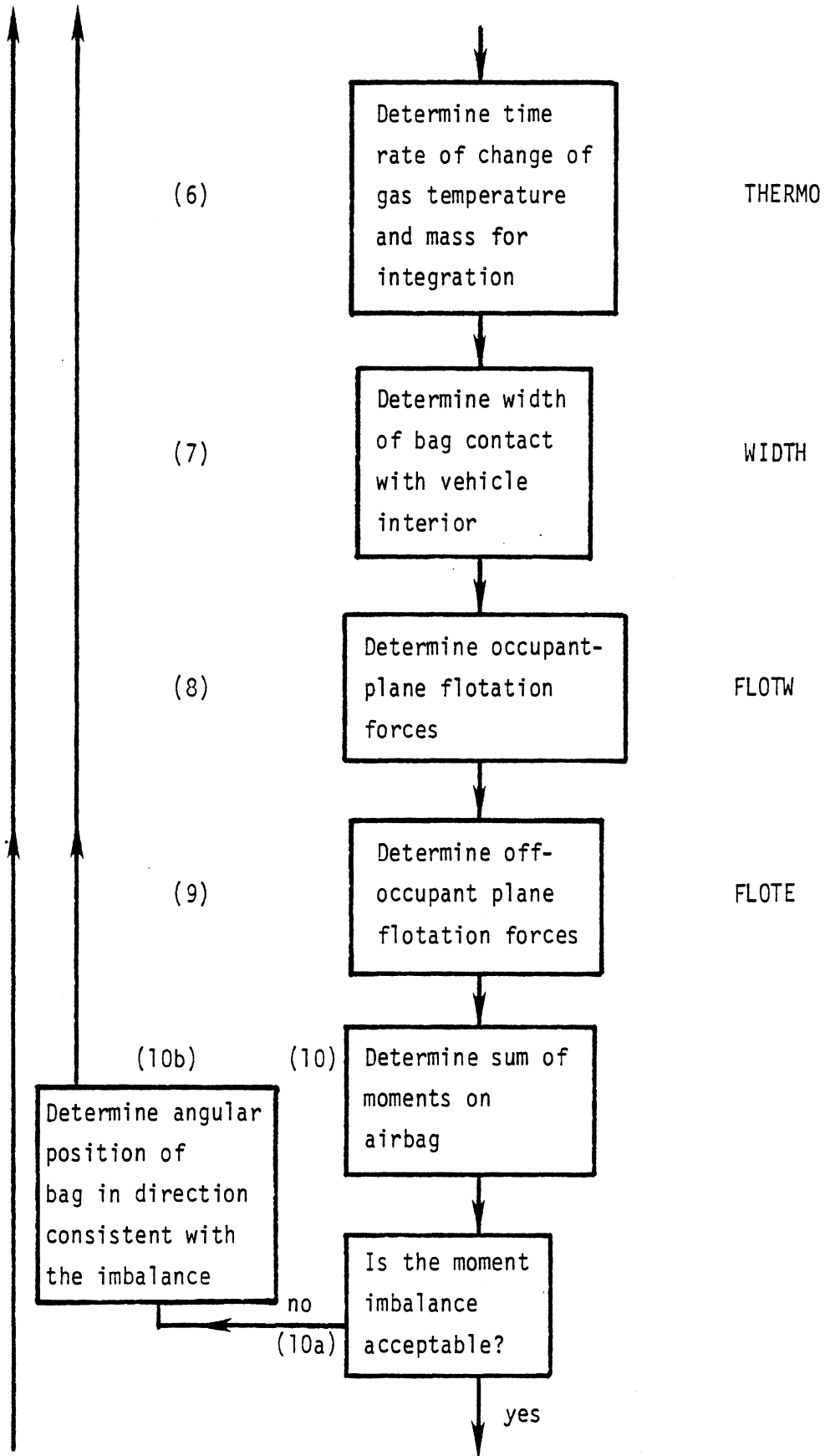
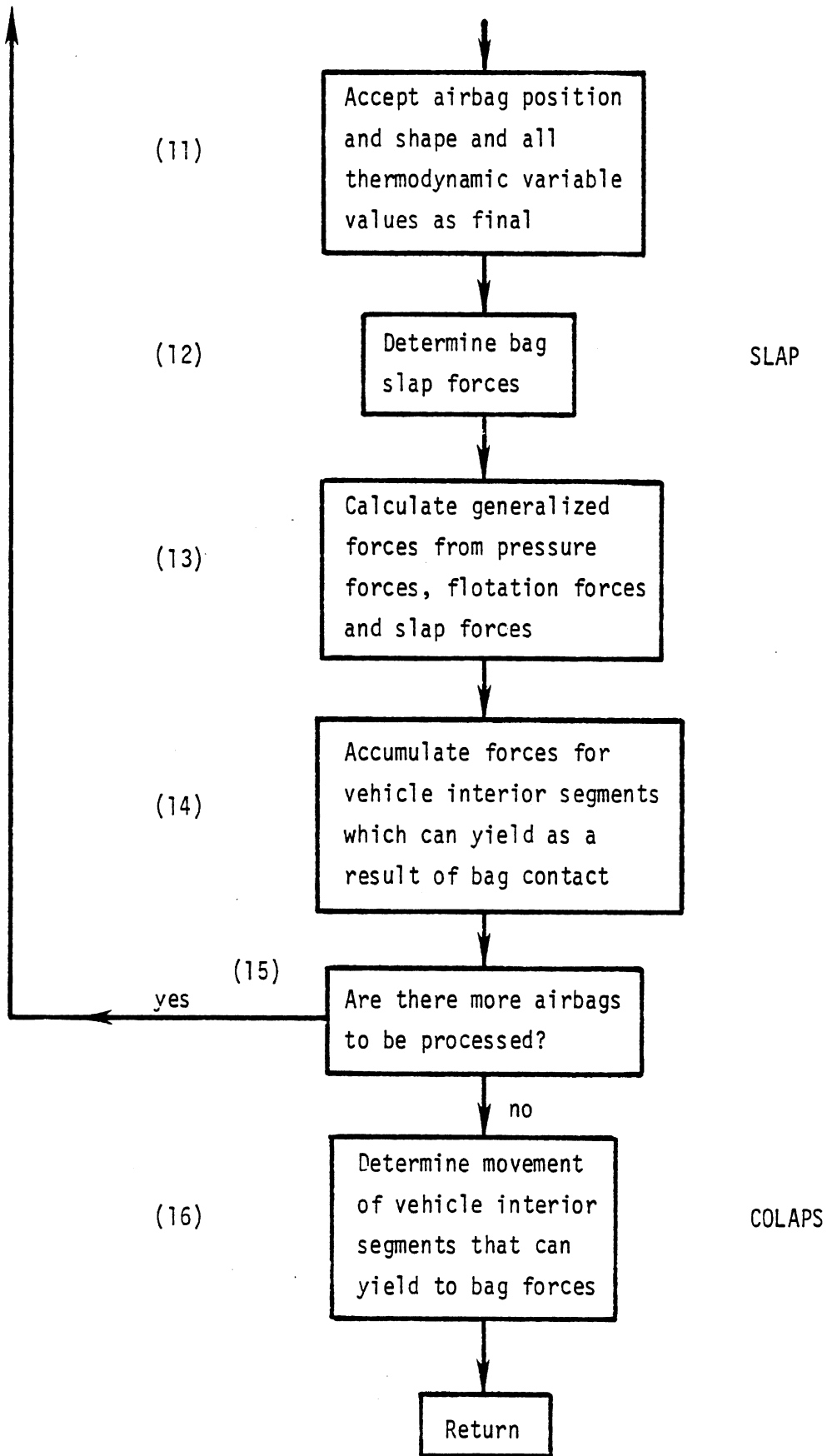Figure 63-1 Flow Diagram for Advanced Airbag System Submodel (page 2)

Figure 63-1 Flow Diagram for Advanced Airbag System Submodel (page 3)